The septin cage:
a novel mechanism of host defence to restrict bacterial replication

Andrea Sirianni

Imperial College London

Faculty of Medicine

Submitted for the degree of Doctor of Philosophy

2016

Fatti non foste per viver come bruti,
ma per seguire virtute e conoscenze

Consider your origin: you were not made to live as brutes,
but to follow virtues and knowledge

– Dante Alighieri, *L'Inferno*

ABSTRACT

Autophagy is a highly conserved intracellular degradation process crucial for cell-autonomous immunity against bacterial infection. However, some bacteria may subvert the host cytoskeleton to escape recognition from autophagy. In the cytosol, *Shigella flexneri* and *Listeria monocytogenes* use actin-based motility to avoid cell-autonomous immunity and spread from cell-to-cell.

The host cytoskeleton plays a key role in autophagy and its ability to restrict or promote bacterial replication. Septins, a cytoskeletal component that interacts with cellular membranes and actin filaments, are GTP-binding proteins that polymerize into non-polar filaments and rings. Our lab has discovered that septin cage-like structures entrap actin-polymerising *Shigella* targeted to autophagy. The septin cage is recognized as a mechanism of host defence mechanism, however the precise fate of septin cage entrapped *Shigella* remains unknown.

Evidence has suggested that mitochondria provide membrane for the biogenesis of autophagosomes during starvation. The role of the mitochondria during the autophagy of *Shigella* is unknown. Mitochondria are highly dynamic organelles characterised by events of membrane fission and fusion. Work has previously established a role for the host cell division machinery, i.e. actin and myosin, in the regulation of mitochondrial dynamics (a process called

'mitokinesis'). Whether septins are also involved in mitochondrial dynamics has not yet been tested.

For my thesis, the entrapment of *Shigella* by septin cages was used as a paradigm to better understand host defence against bacterial infection and to discover new septin biology. Results have shown that mitochondria mediate the assembly of septins into cage that target *Shigella* to degradation by autophagy. We have also discovered that septins regulate mitochondrial fission. Finally, we have revealed a new link between septins, autophagy, and host cell metabolism. Together these results suggest that a more complete understanding of septin biology during bacterial infection can enable its manipulation for therapeutic purposes.

DECLARATION REGARDING AUTORSHIP

The data presented in this thesis are solely my own work with the exception of results done in collaboration and appropriately referenced in the text.

September, 2016

Andrea Sirianni

DECLARATION REGARDING COPYRIGHT

PUBLICATIONS

1. Sirianni, A., Krokowski, S., Lobato-Marquez, D., Buranyi, S., Pfanzelter, J., Galea, D., Willis, A., Culley, S., Henriques, R., Larrouy-Maumus, G., Hollinshead, M., Sancho-Shimizu, V., Way, M., Mostowy, S. (2016). **Mitochondria mediate septin cage assembly to promote autophagy of *Shigella*.** EMBO Reports (2016 Jun 03)

2. Sirianni, A., Mostowy, S. (2014). **Autophagy in the infected cell: insights from pathogenic bacteria**. In Autophagy, Infection, and the Immune Response 143-157(John Wiley & Sons, Inc, 2014 Dic 03).

3. Mostowy S., Boucontet L., Mazon Moya MJ., Sirianni A., Boudinot P., Hollinshead M., Cossart P., Herbomel P., Levraud J-P., Colucci-Guyon E. (2013). **The zebrafish as a new model for the *in vivo* study of *Shigella flexneri* interaction with phagocytes and bacterial autophagy**. PLoS Pathogens (2013 Sep 05)

ACKNOWLEDGMENTS

Firstly, I would like to thank my supervisor Serge Mostowy. Thanks for the guidance, scientific advice and the set of skills you helped me develop throughout my PhD. Having been the first PhD student of the Mostowy lab was not an easy journey, but I feel very honoured to have contributed to the development of what is now a very successful lab here at Imperial College London.

I wish to thank all my collaborators for any contribution to this work, and to other projects outside my PhD thesis. A special acknowledgment goes to Dr. Michael Hollinshead for sharing his expertise in electron microscopy with the Mostowy lab, and for always delivering top-quality results in time-limited situations.

I would like to show my gratitude to the members of the Mostowy lab, along with friends and colleagues from the MRC-CMBI department, who shared memorable moments with me during my stay. From those, I would like to thank a few that were especially important for me since the start of my PhD:

Maria, I like to think in the past few years we were like brother and sister helping our little family getting bigger and stronger. I will never forget those memorable moments spent with you and Juan outside the lab. Grzegorz, I never met such a genuine person like you and thank you for being a fantastic

colleague and friend to me. All our discussions on every kind of topic but science really helped to cheer me up and to get away from the vicious cycle of our lab life. So, thank you.

I big acknowledgment goes to all my friends I met outside the lab: the “Biotech family” from Bologna, which has always been my driving force for succeeding in science, the “evergreen” material scientists and people from the RSD course, where the Imperial crew was born. From those, thanks to the four musketeers Claudio, Gil, Giorgio and Giovanni, great friends and comrades in many of the adventures we have experienced over these years in London.

Finally, I would like to express my full gratitude to my family and the people dearest to me. To Emma, my muse, friend and partner, who inspired me with motivation and support during this important phase of my life. You filled me with love and energy, and together we shared unforgettable moments that go far beyond just having coffee breaks in the foyer. Un ringraziamento particolare va a Paolo ed Alki, per il supporto emozionale, ed a Nostradamus per avermi insegnato I termini della filosofia di vita moderna. Grazie per non avermi fatto mollare mai.

Ultimi, ma non per importanza, i miei genitori Ugo e Giovanna. Siete stati il pilastro portante di tutto il mio ciclo educativo, che termina ora con il dottorato. A voi dedico tutto questo grande sforzo e traguardo. Grazie di cuore per gli anni di supporto, investimenti (non solo economici) e fiducia che avete posto in me. È ora di mettere via l’arco e godervi la scena, perché la vostra freccia è andata a buon segno.

CONTENTS

LIST OF FIGURES

LIST OF TABLES

ABBREVIATIONS

AA	Amino acid
Arp2/3	Actin-related protein 2/3
ATG	Autophagy related protein
ATP	Adenosine triphosphate
Co-IP	Co-immunoprecipitation
DFCP1	Double SYVE-containing protein 1
DMEM	Dulbecco modified eagle medium
Drp1	Dynamin-related protein 1
EBSS	Earle's Balanced Salt Solution
ER	Endoplasmic reticulum
FBS	Fetal bovine serum
GABARAP	Ɣ-aminobutyric acid receptor-associated protein
GFP	Green fluorescence protein
GO	Gene ontology
GTP	Guanosine triphosphate
IF	Intermediate filament
IPTG	Isopropyl β-D-1-thiogalactopyranoside
LAP	LC3-associated phagocytosis
LC-MS AMRT	Liquid chromatography mass-spectrometry accurate mass retention time
LC3	Light chain 3 protein
LIR	LC3-interacting region
LLO	Listeriolysin O
LRSAM1	Leucine-rich repeat sterile alpha motif-containing protein 1
Mfn	Mitofusin
minpi	Minutes post infection
MOI	Moltiplicity of infection
MT	Microtubule
mTOR	Mammalian target of rapamycin

NBR1	Neighbor of BRCA1 gene 1
NDP52	Nuclear domain 10 protein 52
NLR	Nucleotide-binding oligomerization domain (NOD) -like receptors
OPA1	Optic astrophy 1
OPTN	Optineurin
p62	Sequestosome1 or SQSTM1
PAMPS	Pathogen-associated molecular patterns
PAS	Phagophore assembly site
PCV	Pathogen-containing vacuole
PE	Phosphatidylethanolamine
PI(3)P	Phosphatidylinositol-3-phosphate
PI3K	Class III phosphatidylinositol-3-phosphate
PRR	Pattern recognition receptors
qPCR	Quantitative PCR
RLR	RIG-I-like receptors
s.e.m.	Standard error of the mean
SCV	*Salmonella*-containing vacuole
SEPT	Septin
siRNA	Small interfering RNA
SLAP	Spacious *Listeria*-containing vacuole
SLRs	Sequestosome 1/p62-like receptors
STX17	Syntaxinx17
SUE	Septin unique element
T3SS	Type III secretion system
TEM	Transmission electron microscopy
TLR	Toll-like receptors
Ub	Ubiquitin
ULK	UNC-51-like kinases
ULK	Unc-51-like kinase
VPS	Vacuolar protein sorting
WIPI	WD-repeat domain phosphoinositide-interacting protein

CHAPTER 1: INTRODUCTION

Cell-autonomous immunity is a first line of host defence against invading bacterial pathogens (Randow et al., 2013). Upon invasion of host cells, bacteria are enclosed in a membrane-bound vacuole (also called phagosome) that acidifies after fusing with lysosomes (Haas, 2007). However, some pathogens have mechanisms that allow them to survive inside the phagocytic vacuole or escape to the host cell cytosol (Ray et al., 2009). Vacuolar bacteria, including *Mycobacterium* spp. and *Salmonella* spp., replicate inside their phagocytic vacuole by preventing fusion with the lysosome (Cemma and Brumell, 2012). In contrast, cytosolic bacteria can escape from the phagocytic vacuole before fusion with the lysosome. These pathogens rely on their type III secretion system (T3SS) (e.g. *Shigella flexneri*) or express lytic enzymes (e.g. *Listeria monocytogenes*) to find a gateway to the cytosol (Pizarro-Cerda et al., 2016).

Host cells use multiple sensors to detect bacterial invasion and activate cell-autonomous immunity. Specifically, pattern recognition receptors (PRRs) localized on the cell surface or in the cytosol recognise pathogen-associated molecular patterns (PAMPS) expressed by invading bacteria (Deretic et al., 2013). Examples of PPRs include Toll-like receptors (TLRs), nucleotide-binding oligomerization domain (NOD) -like receptors (NLRs), RIG-I-like receptors (RLRs) or sequestosome 1/p62-like receptors (SLRs), which activate immune signalling pathways to control infection (Deretic, 2012). In the

case of SLRs, these adaptor proteins initiate clearance of bacteria by autophagy (Mostowy, 2013).

Autophagy (from Latin “to eat oneself”) is an evolutionarily conserved degradation pathway targeting and eliminating bacteria, viruses and parasites (Mizushima et al., 2008, Levine et al., 2011b, Randow, 2011). On the other hand, several bacterial pathogens, such as *Shigella*, *Listeria* or *Salmonella*, have mechanisms to evade or benefit from autophagy (Deretic and Levine, 2009, Mostowy, 2013). Interestingly, studies have shown important roles for the cytoskeleton in determining the autophagic response to bacterial pathogens (Mostowy and Shenoy, 2015).

This chapter will review how the host cell uses autophagy to protect itself against invasive bacteria. The first section will focus on autophagy pathways and the mechanisms of selective autophagy. The second section is dedicated to the role of autophagy in host defence against bacteria. The third section will introduce the mitochondria, and describe parallels between the autophagy of mitochondria and the autophagy of bacteria. The final section will summarize the cytoskeleton and its links to autophagy, followed by the aims of my PhD project.

1.1. Autophagy

1.1.1. ATGs and the multi-step process of autophagy

Autophagy is a process of cellular self-eating in which portions of the cytosol are isolated into vesicles for lysosomal degradation. The best-described autophagy pathways are chaperone-mediated autophagy, microautophagy and macroautophagy, which differ in how the cytosolic material is delivered into lysosomes (Levine et al., 2011a, Mostowy, 2014). Macroautophagy (hereafter referred as autophagy) involves the sequestration of cytosolic material into a double membrane vesicle, known as the autophagosome, which ultimately fuses with the lysosome for degradation (Ohsumi, 2001, Khaminets et al., 2016, Mostowy, 2013).

Autophagy was discovered as a non-selective mechanism for bulk degradation of cytosolic components in response to nutrient deprivation (Levine et al., 2011a, Mizushima and Komatsu, 2011). Since then, multiple studies have shown that autophagy can also selectively target and eliminate substrates including misfolded proteins, damaged organelles and intracellular pathogens (Boyle and Randow, 2013, Randow and Münz, 2012, Khaminets et al., 2016). Autophagy has an important role for several cellular functions including development, programmed cell death, tumour suppression and host defence (Rubinsztein et al., 2011, Wang et al., 2012, Harris and Rubinsztein, 2012, Levine et al., 2011b, Boyle and Randow, 2013).

Autophagosome formation occurs in three main steps: initiation, elongation and maturation (Wen and Klionsky, 2016). During the initiation (also called

nucleation) step, an isolation membrane (also called phagophore) forms and targets cargo in the cytosol. The phagophore elongates and seals to sequester the cytosolic material into a double-membrane vesicle known as the autophagosome. Subsequently, the autophagosome fuses with the lysosome to form an autolysosome (**Figure 1.1**).

Genetic studies using budding yeast *Saccharomyces cerevisiae* have shown that autophagosome formation is mediated by a group of highly conserved proteins known as the autophagy-related (ATG) proteins. At least 38 ATG proteins have been identified (Xie et al., 2015, Araki et al., 2013). 18 ATGs are required for efficient autophagy and are classified in five main groups: the ULK complex, the VPS34-PI3K complex, the ATG2-WIPI complex, the ATG12-conjugation system, and the LC3-conjugation system (Araki et al., 2013). These five groups are localized on the phagophore assembly site (PAS) in yeast, and cooperate to generate the phagophore. Although no clear equivalent of the yeast PAS has been found in mammalian cells, at least half of the yeast ATGs have orthologues in humans (**Table 1.1**) (Xie et al., 2015, Feng et al., 2014).

Table 1.1: Autophagy-related (ATG) proteins.
Mammalian ATGs and their yeast counterparts are shown. Specific mammalian factors required for autophagosome biogenesis are also indicated. Adapted from (Bento e*t al.*, 2016)

Complex	Mammals	Yeast	Characteristics	Function
ULK-complex	ULK1,2	Atg1	Ser/Thr kinase; ULK1,2 are phosphorylated by mTORC1	Negatively regulated by (m)TORC1.
	ATG13	Atg13	Target of the mTOR signaling pathway	
	FIP200	Atg17	Scaffold for ULK1,2 and ATG13	
	ATG101	nd	Interacts with ATG13	
VPS34-PI3K complex	hVPS34	Vps34	PI3-kinase	Produces PI3P at the site of autophagosome formation. Bcl-2 inhibits autophagy by sequestering Beclin1 from the PI3K complex
	VPS15	Vps15	Ser/Thr kinase	
	Becltin1	Atg6	Beclin1 interacts with Bcl-2	
	ATG14L	Atg14	Autophagy-specific subunit	
ATG2-WIPI complex	ATG2A,B	Atg2	Important for ATG9 recruitment to expanding autophagosomes	ATG9 and WIPIs are present on autophagosomal membrane. WIPIs interact with phosphoinositides to allow expansion of the nascent autophagosome
	mATG9	Atg9	Transmembrane protein postulated to be a carrier for membrane during phagophore expansion	
	WIPI-1,2,3,4	Atg18	Important for ATG9 recruitment to autophagosome	
	DECP1	nd	PI3P-binding protein	
ATG12-conjugation system	ATG5	Atg5	Acting as an E3-like enzyme in LC3 lipidation	The complex ATG12-ATG5-ATG16L1 is essential for elongation step, and it is important for LC3-PE conjugation
	ATG7	Atg7	E1-like enzyme in LC3 and ATG12 conjugation	
	ATG10	Atg10	E2-like enzyme in ATG12 conjugation	
	ATG12	Atg12	Ubiquitin-like protein that conjugates to ATG5	
	ATG16L1,2	Atg16	Binds to ATG5-ATG12 and is postulated to specify LC3 lipidation sites in autophagic membranes	
LC3 conjugation system	ATG3	Atg3	E2-like enzyme in LC3 lipidation	LC3-PE conjugation is essential for isolation membrane elongation and closure. LC3 is present on both outer and inner membrane of autophagosomes. Required for selective autophagy in yeast and mammals.
	ATG4A,B,C,D	Atg4	Cysteine protease involved in LC3 activation and delipidation	
	ATG7	Atg7	E1-like enzyme in LC3 and ATG12 conjugation	
	LC3A, B, C; GABARAPs; GATE-16	Atg8	Ubiquitin-like proteins that conjugate to PE and are used as autophagosome markers	

1.1.2. Molecular events of autophagy

The events of autophagosome formation are regulated by the ATG1-UNC-51-like kinases (ULK) complex together with the class III phosphatidylinositol (PtdIns) 3-kinase (PI3K) complex (Johansen and Lamark, 2011, Moreau et al., 2013). Under nutrient-rich conditions, the serine/threonine kinase mammalian target of rapamycin (mTOR) complex 1 (mTORC1) negatively regulates activity of ULK complex (Ravikumar et al., 2004). Following amino acid deprivation, the ULK complex dissociates from mTORC1 and interacts with the PI3K complex, vacuolar protein sorting 34 (VPS34) complex and Beclin 1 (Zhong et al., 2009, Ganley et al., 2009, Hosokawa et al., 2009, Jung et al., 2009).

The VSP34 complex produces phosphatidylinositol-3-phosphate (PI(3)P), which recruits the double SYVE-containing protein 1 (DFCP1) and WD-repeat domain phosphoinositide-interacting (WIPI) family proteins, which respectively provide a platform for expansion of the isolation membrane and promote the formation of the autophagosomes (Axe et al., 2008, Polson et al., 2010).

The steps of elongation and autophagosome closure are regulated by the ATG12-ATG5 ubiquitin-like conjugation system and the ATG8 lipidation system (Ichimura et al., 2000, Kabeya et al., 2000). The ATG12-ATG5 complex interacts with ATG16L1 to form an ATG12-ATG5-ATG16L1 complex essential for autophagosome biogenesis (Mizushima et al., 2003). Recruitment of ATG12-ATG5-ATG16L1 to the phagophore requires the generation of PI(3)P, as it recruits ATG8/LC3 family members to the isolation membrane. ATG12-ATG5-ATG16L1 dissociates upon completion of

autophagosome biogenesis (Itakura and Mizushima, 2010, Mizushima et al., 2001, Mizushima et al., 2003).

The conjugation of ATG8 to phosphatidylethanolamine (PE) is required to mediate closure of the autophagosome (Kabeya et al., 2000, Mostowy, 2014). The ATG8 lipidation system has six ATG8 orthologues belonging to the light chain 3 (LC3) or Y-aminobutyric acid receptor-associated (GABARAP) proteins subfamilies (Mizushima et al., 2011). LC3 is synthesized as a precursor in the cytosol, and upon induction of autophagy the ATG12-ATG5-ATG16L1 complex conjugates a glycine (Gly) exposed at the C-terminal of LC3 to PE (LC3-PE) (Kabeya et al., 2004, Fujita et al., 2008). LC3-PE is found in the inner and outer membranes of the pre-autophagosomes. Upon autophagosome closure, ATG4 cleaves LC3 from the outer membrane of the autophagosome, thus only LC3 associated to the inner membrane is degraded by autophagy (Ichimura et al., 2000, Kirisako et al., 2000). This feature makes LC3 valuable as a marker for the entire process of autophagy (Itakura and Mizushima, 2010).

Fusion of autophagosomes with the lysosomal compartment is mediated by TECPR1 in a step regulated by ATG14 (Chen et al., 2012b, Diao et al., 2015). During this process, ATG14 binds to syntaxinx17 (STX17) and SNAP29 to form a stable STX17-SNAP29 binary t-SNARE complex, which then interacts with VAMP8 to promote fusion (Diao et al., 2015, Itakura et al., 2012). Autophagosome clearance is mediated by the interaction between STX17 and the homotypic fusion and vacuole protein sorting (HOPS) tethering complex (**Figure 1.1**) (Takáts et al., 2014).

Evidence has recently shown that some ATGs have a role outside of canonical autophagy, in a process called 'non-canonical autophagy' (Mostowy, 2013, Huang and Brumell, 2014). During this non-canonical autophagy, a subset of ATG proteins are recruited to a pre-existing membrane without following the hierarchy of events required for autophagy.

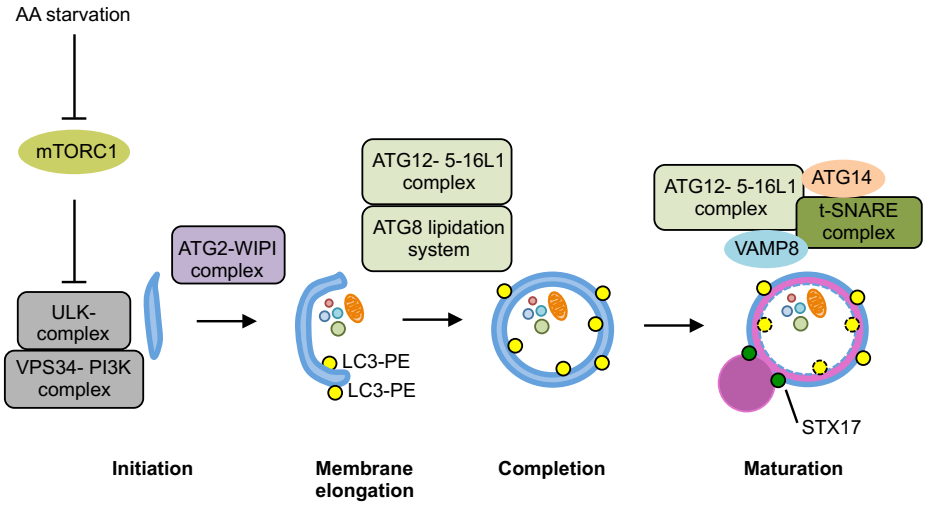

Figure 1.1: Molecular mechanism of canonical autophagy
Upon starvation, the ULK- and VPS34-PI3K -complexes contribute to the generation of a double membrane (phagophore), which targets the cargo from the cytosol. The ATG2-WIPI complex promotes the elongation of the phagophore to form a double membrane vacuole (autophagosome), in a step completed by the ATG12-ATG5-ATG16L1 complex and the ATG8 lipidation system. The maturation of the autophagosome occurs with fusion with lysosomes to form the autolysosome, in a process mediated by ATG12-ATG5-16L1, ATG14, VAMP8 and the t-SNARE complex. Finally, the material enclosed in the autolysosome is degraded due to fusion with lysosomes and acidification of the vacuole.

1.1.3. Membrane dynamics and origin of the autophagosomal membrane

The precise source of membrane for autophagosome biogenesis remains to be established (Tooze and Yoshimori, 2010). Early observations suggested that autophagosomal membranes are synthesised *de novo* from a Golgi-ER-lysosome compartment (Fengsrud et al., 2000). By contrast, more recent research has suggested that the phagophore can arise from pre-existing membranes (Orsi et al., 2010) .

Autophagosome formation can be observed at various sites in mammalian cells, suggesting different sources of autophagosomal membrane. It was originally suggested that endoplasmic reticulum (ER) contributes to the autophagosomal membrane during starvation (Axe et al., 2008, Hayashi-Nishino et al., 2009). However, whether ER can provide membrane for the expansion of the phagophore at early stage of autophagy under non-starvation conditions (e.g. selective autophagy) still remains unclear. Evidence has also suggested that mitochondria contribute membrane to the growing autophagosome (Hailey et al., 2010). However, further investigation is required to determine the precise contribution of mitochondria to autophagosome biogenesis. The plasma membrane may also contribute to early autophagosomal structures (Ravikumar et al., 2010). In this case, it was proposed the plasma membrane can act as a reservoir for autophagosome biogenesis during periods of increased autophagy (Ravikumar et al., 2010).

Collectively, further studies are needed to determine to what extent different membrane sources contribute to autophagosome formation. If and how

multiple membrane sources act cooperatively, or whether they contribute differently, to specialised forms of autophagy remains to be fully elucidated.

1.1.4. Selective autophagy against bacterial infection

Mounting evidence has implicated autophagy as a selective process (Lazarou et al., 2015, Khaminets et al., 2016). A variety of selective autophagy pathways have been described and named after the cellular target, including protein inclusions caused by aggregate-prone or misfolded proteins (aggrephagy), peroxisomes (pexophagy), ribosomes (ribophagy), endoplasmic reticulum (ER-phagy), nuclear envelope (nuclear-phagy), liposomes (lipophagy), ferritin (ferritinophagy), lysosomes (lysophagy), mitochondria (mitophagy), and intracellular bacterial pathogens (xenophagy) (Khaminets et al., 2016) (**Table1.2**).

Xenophagy is a key component of innate immunity to infection (Mostowy, 2013). While the exact mechanism of bacterial recognition by autophagy remains unknown, the most-characterized process involves ubiquitination and the recruitment of SLRs including p62 (sequestosome1 or SQSTM1), NDP52 (nuclear domain 10 protein 52), NBR1 (neighbor of BRCA1 gene 1) and OPTN (optineurin) (Deretic et al., 2013). The binding of SLRs to both ubiquitin (via a ubiquitin binding domain) and to LC3 family members (via a LC3-interacting region) directs the autophagy machinery to the bacteria (Birgisdottir et al., 2013). In addition to binding ubiquitin, NDP52 uniquely recognizes cargo labelled with Galectin-8, a marker of membrane damage exposed to the cytosol after rupture of a phagocytic vacuole (Thurston et al., 2012).

Table 1.2: Overview of receptors and substrates in selective autophagy pathways.
Ub-dependent and Ub-independent receptors are indicated. Adapted from Khaminets e*t al.*, 2016

Pathway	Receptor	Target
	Ub-dependent	
Aggrephagy	p62, NBR1, OPTN, Cue5,TOLLIP	Protein aggregates
Mitophagy	OPTN, NDP52, p62, Tax1BP1	Mitochondria
Xenophagy	p62, NDP52, OPTN	Bacteria
Pexophagy	NBR1	Peroxisomes
Zymophagy	p62	Zymogen
Proteaphagy	RPN10	Proteasomes
Midbody disposal	p62, NBR1	Midbody
Nucleic acid disposal	p62, NDP52	Nucleic acids
	Ub-independent	
Mitophagy	NIX, BNIP3, FUNDC1, Atg32	Mitochondria
ER-phagy	FAM134B, Atg40	ER
Nucleophagy	Atg39	Nuclear envelope
Ferritinophagy	NCOA4	Ferritin
Pexophagy	NBR1, Atg30, Atg36	Peroxisomes
Glycophagy	Stbd1	Glycogen
Signalophagy	c-Cbl	Src
Cvt targeting	Atg19, Atg34	Ape1,Arns1
Lysophagy	Galectin-8	Lysosomes
Xenophagy	Galectin-8	Bacteria
Virophagy	TRIM5a, SMURF1	Viral components
Fatty scid synthase (FAS) disposal	FAS	FAS

1.1.5. The role p62 and NDP52 in bacterial autophagy

The precise targets of ubiquitination underlying bacterial autophagy remain to be discovered (Khaminets et al., 2016). E3 ligase proteins are involved in the poly-ubiquitination process of cytosolic bacteria (Morimoto et al., 2015). Recently, LRSAM1 and Parkin have been identified as important E3 ligases during autophagy of *Salmonella* and *M. tubercolosis* respectively (Huett et al., 2012, Manzanillo et al., 2013).

The recruitment of p62 and / or NDP52 to bacterial autophagy has been reported for a wide variety of bacterial pathogens, including *Salmonella* Typhimurium*,* Mycobacteria *spp, Listeria monocytogenes,* and *Shigella flexneri* (Mostowy et al., 2011b, Yoshikawa et al., 2009, Thurston et al., 2012, Dupont et al., 2009, Pilli et al., 2012). Specific examples of bacterial autophagy will be described in full in the sections below.

1.1.6. Non-canonical autophagy: a pro-bacterial process?

Non-canonical autophagy is characterised by the recruitment of some ATGs to pre-existing membranes (Huang and Brumell, 2014, Florey and Overholtzer, 2012). In a process known as LC3-associated phagocytosis (LAP), non-canonical autophagy bypasses double-membrane autophagosome biogenesis, and facilitates lysosome fusion to single membranes and the degradation of internalized cargos (Florey et al., 2011). Examples of LAP were first reported during infection of host cells with *Escherichia coli*, where Beclin1 and LC3 are recruited to the phagocytic vacuole after bacterial internalization mediated by TLR signalling pathways (Sanjuan et al., 2007). LAP has since been reported to restrict the replication of some bacterial pathogens including

Salmonella and *Burkholderia pseudomallei* (Lam et al., 2013, Martinez et al., 2015). In contrast, non-canonical autophagy has also been described to promote the replication of some bacterial pathogens (**Figure 1.2**)(Mostowy, 2013). For example, *Staphylococcus aureus* and *Brucella abortus* are two Gram-positive bacteria that have been shown to exploit non-canonical autophagy pathways for intracellular replication (Mestre et al., 2010, Starr et al., 2012).

After escaping from the phagocytic vacuole, *Listeria* is known to avoid canonical autophagy by expressing the cell surface ActA. A subpopulation of *Listeria* has also been described to exploit the autophagy machinery by forming replicative niches inside spacious *Listeria*-containing phagosomes (SLAPs) (Birmingham et al., 2008). The formations of SLAPs depend on LAP pathways together with the activity of *Listeria* Listeriolysin O (LLO), a pore-forming toxin, to damage membranes (Cemma and Brumell, 2012). Surprisingly, recent work has also shown that intracellular growth of *Salmonella* is impaired in ATG5 or ATG16L depleted cells, suggesting a pro-bacterial role for these components of the autophagy machinery (Yu et al., 2014).

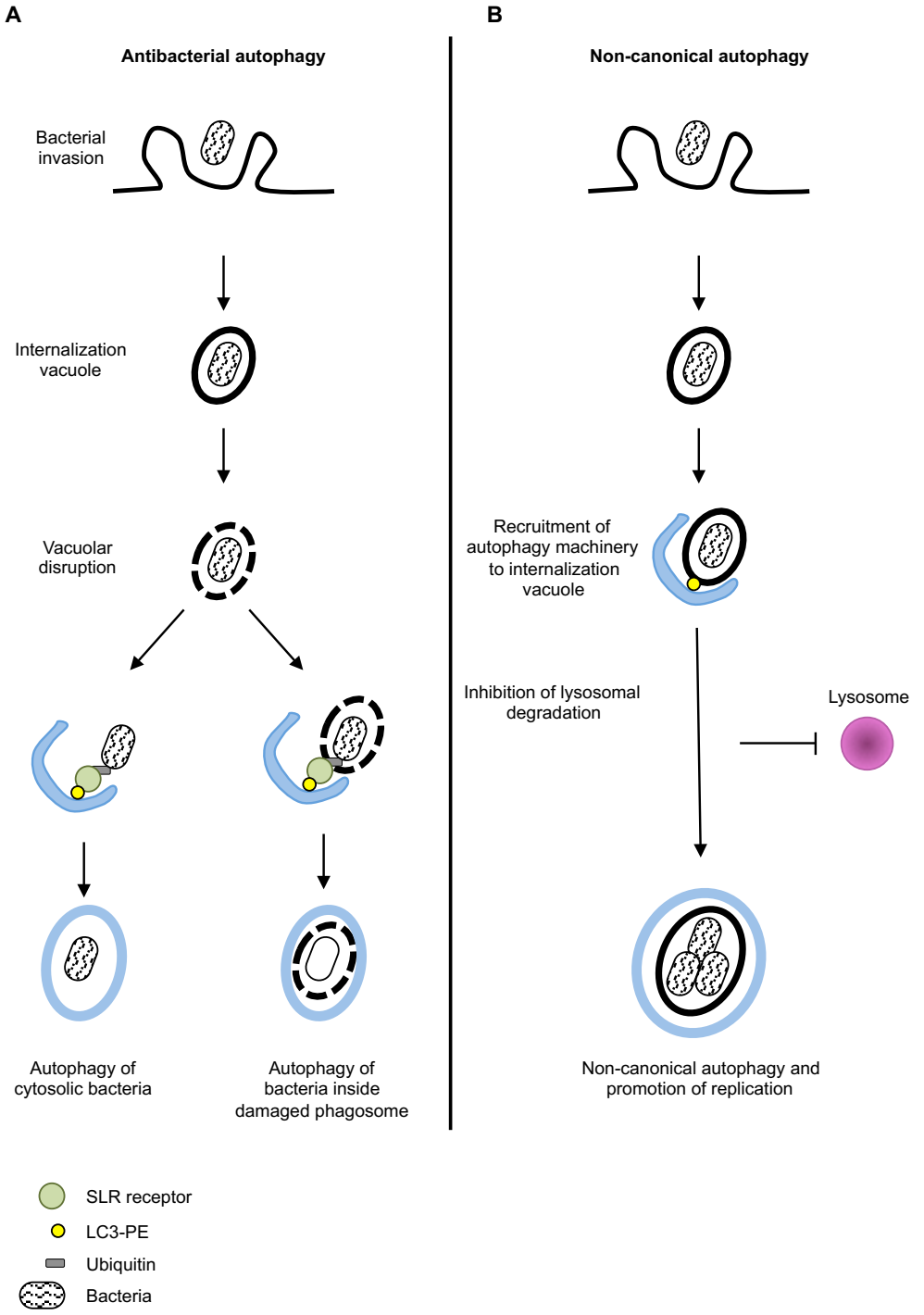

Figure 1.2: Different autophagy pathways triggered by bacterial invasion.
A Antibacterial autophagy. After entry into host cells, bacteria are localized inside an internalization vacuole. Upon vacuolar disruption, autophagy may recognize ubiquitination signals and intracellular pathogens located (left) in the cytosol (e.g. *S. flexneri*, *S.* Typhimurium) and (right) inside a damaged internalization vacuole (e.g. *M. tuberculosis*). In both cases, the enclosed bacterium is delivered to the lysosome for degradation.

B Pro-bacterial autophagy. Some internalized bacteria may recruit a subset of the autophagy machinery and create a replicative niche inside an autophagosome-like vacuole. These bacteria subvert the autophagy machinery to avoid degradation in a lysosomal compartment and support bacterial replication. Ub, ubiquitin; SLR, autophagy receptor (e.g. p62, NDP52); LC3, ATG8 family proteins.
Adapted from Mostowy 2013

1.2. Autophagy-bacteria interactions

A theme emerging, mostly from studies using *Salmonella*, is that anti-bacterial autophagy efficiently clears pathogens that are unintentionally exposed to the host cytosol (Randow and Münz, 2012, Mostowy, 2013). By contrast, cytosolic pathogens (e.g. *Listeria* and *Shigella*) that intentionally access the host cytosol have mechanisms to avoid autophagic degradation (Killackey et al., 2016). In this section, I will focus on bacteria that have served as paradigms of bacterial autophagy, namely *Salmonella*, *Listeria* and *Shigella*.

1.2.1. *Salmonella* Typhimurium

Salmonella enterica serovar Typhimurium (or *Salmonella*) is a Gram-negative foodbourne bacterial pathogen (Perrin et al., 2004). Most bacteria replicate inside a membranous compartment, the *Salmonella* containing vacuole (SCV), though ~25% of intracellular *Salmonella* can escape to the cytosol (Mesquita et al., 2012, Shahnazari et al., 2010). As a result, *Salmonella* has been very useful to study autophagy-bacteria interactions (Sirianni and Mostowy, 2014).

Pioneering studies first established the links between *Salmonella* infection and selective autophagy showing that p62, NDP52 and OPTN are SLRs crucial for *Salmonella* recognition and degradation by autophagy (Zheng et al., 2009, Thurston et al., 2009, Wild et al., 2011). During *Salmonella* infection, the E3 ligase LRSAM1 ubiquitinates and recruits NDP52 to *Salmonella* (Huett et al., 2012). Interestingly, *Salmonella* has mechanisms to counteract ubiquitination. The bacterial effector SseL deubiquitinates cytosolic aggregates and prevents the recruitment of p62 and LC3 (Pruneda et al., 2016, Mesquita et al., 2012).

Membranes damaged upon invasion of *Salmonella* are bound by Galectin 8 and recognised by NDP52 that preferentially binds to LC3C on the autophagosome (Thurston et al., 2012). LC3C is a rarely studied ATG8 family member, and the preference of NDP52-LC3C interaction over LC3B suggests a layer of specificity for antibacterial autophagy (von Muhlinen et al., 2012). To prevent the escape of *Salmonella* to the cytosol, membrane rupture activates TBK1 and recruits the PI(3)P- binding protein WIPI2 for antibacterial autophagy (Thurston et al., 2016). Membrane damage caused by *Salmonella* also induces amino acid (AA) starvation (Tattoli et al., 2012). This starvation pathway is tightly regulated by mTOR, and *Salmonella* is able to recruit mTOR to the SCV to escape from autophagy-mediated degradation (Tattoli et al., 2012). Although AA starvation has gained recognition as an immune response to cytosolic bacteria (Tattoli et al., 2012), the role of host cell nutritional status on pathogen survival remains unclear.

1.2.2. *Listeria monocytogenes*

L. monocytogenes is a Gram-positive, foodborne pathogen that grows inside phagocytic and non-phagocytic human cells (Cossart, 2011). Following infection, *Listeria* may escape from the vacuole using LLO and phospholipases (Meyer-Morse et al., 2010). In macrophages, *L. monocytogenes* may replicate inside SLAPS. In this case, *Listeria* has been shown to colocalize with LAP-related proteins after 1 h post infection, but not with ubiquitin or ubiquitin-binding proteins (Lam et al., 2013). Thus, *Listeria* inside SLAPs avoid exposure to the cytosol and avoid the recognition by ubiquitination, p62 and selective autophagy (Lam et al., 2013).

Following escape to the cytosol, p62 and NDP52 are able to recognise the membrane damage caused by LLO (Meyer-Morse et al., 2010, Thurston et al., 2012). Experiments using *Drosophila* have shown that autophagy mediated by LLO restricts *Listeria* replication *in vivo* (Yano et al., 2008). In support of this, both mice and *Drosophila* without Parkin are susceptible to *Listeria* infection (Manzanillo et al., 2013). However, *Listeria* can also avoid autophagy in the cytosol. Expression of the *Listeria* effector ActA prevents ubiquitination and recruitment of p62 and NDP52 (Mostowy et al., 2011b), and mimics N-WASP to recruit the Arp2/3 complex to polymerize actin tails and spread from cell-to-cell (Haglund and Welch, 2011).

1.2.3. *Shigella flexneri*

S. flexneri is a Gram-negative enteroinvasive pathogen that infects intestinal epithelial cells in the human gut, causing inflammation and diarrhoea (Lima et al., 2015). *Shigella* possesses a large virulence plasmid that encodes genes required for host cell invasion and vacuolar escape (Phalipon and Sansonetti, 2007).

Shigella entry triggers an inflammatory response by recruiting the PRRs NOD1 and NOD2 at the plasma membrane (Travassos et al., 2010). However, NLRs detect *Shigella* peptidoglycan and trigger a pro-inflammatory signalling cascade to restrict bacterial survival (Philpott et al., 2014). The inflammation response driven by NLRs can additionally be suppressed by recruiting ATG16L1 (which stimulates phagophore biogenesis) to the phagocytic cup (Travassos et al., 2010, Sorbara et al., 2013).

The membrane damage caused by *Shigella* invasion can generate ubiquitinated remnants around the pathogen that is recognised by p62 and NDP52. Similar to *Salmonella*, membrane damage caused by *Shigella* can trigger the galectin8-NDP52-LC3C autophagy pathway in an ubiquitin-independent manner (Thurston et al., 2012).

The bacterial effector IcsA is expressed on the surface of *Shigella* and directly recruits the Arp2/3 complex to form actin tails (Haglund and Welch, 2011). However, ATG5 recognises IcsA (Ogawa et al., 2011, Chen et al., 2012a). *Shigella* avoids ATG5 recognition by expressing IcsB, a T3SS effector, which binds and masks IcsA (Leung et al., 2008, Baxt and Goldberg, 2014). IcsB also acts in synergy with the *Shigella* effector VirA to facilitate *Shigella* escape from LC3-positive vacuoles during entry and cell-to-cell spread (Campbell-Valois et al., 2015). VirA, a guanosine triphosphate (GTP)ase-activating-like protein, is a *Shigella* T3SS effector that inhibits autophagy via inactivation of Rab1 GTPase pathways (Dong et al., 2012). The importance of IcsB for *Shigella* survival is highlighted by results showing that *Shigella* lacking IcsB are recognised by the E3 ubiquitin ligase LRSAM1 and susceptible to autophagy (Ogawa et al., 2011, Huett et al., 2012).

As described above for *Salmonella*, host membrane damage by *Shigella* also triggers amino acid starvation, which then induces autophagic response (Tattoli et al., 2012). As a consequence, nutrient starvation pathways are activated and thought to initiate an immune response against *Shigella* (Tattoli et al., 2012).

1.3. Mitochondria

1.3.1. The powerhouse of the cell

Mitochondria are an ancient endomembrane organelle. They are considered the powerhouse of eukaryotic cells because they regulate the production of ATP through respiration (Nunnari and Suomalainen, 2012, Lydia and Benjamin, 2013). Mitochondria form a dynamic network, which is continuously remodelled by fission (in which one mitochondrion splits in two) and fusion (in which two mitochondria merge into one). Mitochondrial fission and fusion are crucial to maintain healthy mitochondria, and to prevent the outcome of disease associated with defective organelle (Archer, 2014, Wai and Langer, 2016). The mechanisms underlying mitochondrial dynamics have been extensively studied (Mishra and Chan, 2014, Chan, 2012). The fission and fusion process relies on GTP-hydrolysing proteins of the dynamin superfamily. Mitochondrial fission is mediated by dynamin-related protein 1 (Drp1), a cytosolic protein that self-assembles on the mitochondrial outer membrane for constriction and abscission (Ishihara et al., 2009, Lackner and Nunnari, 2009, Archer, 2014). Drp1 activity is regulated by the phosphorylation of specific serine residues (Chang and Blackstone, 2007). Phosphorylation of Drp1 on serine 616 is required for mitochondrial fission (Chang and Blackstone, 2010, Rambold et al., 2011), while phosphorylation of serine 637 inhibits its fission activity (Rambold et al., 2011).

Mitochondrial fusion is mainly controlled by transmembrane proteins mitofusin1 (Mfn1), mitofusin2 (Mfn2) and optic astrophy 1 (OPA1). Mfn1 and Mfn2 are two essential transmembrane proteins that drive fusion of mitochondrial outer membrane (Meeusen et al., 2006, Song et al., 2009).

Mitochondrial inner membrane fusion is led by OPA1, which is dispensable for mitochondrial outer membrane fusion (Song et al., 2009).

New data has highlighted a key role for the cytoskeleton in the regulation of mitochondrial dynamics. In particular, work has shown that actin is crucial for the fission process (Hatch et al., 2014, Korobova et al., 2013, Manor et al., 2015).

1.3.2. The emerging field of "mitokinesis"

How is the recruitment of Drp1 to the mitochondria regulated? Work has shown that ER provides force for pre-constriction by wrapping around mitochondria at fission sites (Friedman et al., 2011, Korobova et al., 2014, Korobova et al., 2013, Murley et al., 2013). Time-lapse microscopy confirmed ER-mediated constriction as an essential step for the recruitment of Drp1 to mitochondrial membrane (Friedman et al., 2011).

During cytokinesis, actin filaments and non-muscle myosin II are essential components of a contractile (actomyosin) ring that leads to furrow ingression at the site of cell division (Mendes Pinto et al., 2012). Actomyosin also is localized at the sites of contact between ER and mitochondria, and enables the recruitment of Drp1 on mitochondrial membrane for subsequent fission (Korobova et al., 2014, Korobova et al., 2013, Hatch et al., 2014). Due to its similarities to models for cytokinesis, the process of actin-mediated mitochondrial fission is than proposed in a model called "mitokinesis" (Korobova et al., 2014).

What is the role of the cytoskeleton in mitokinesis? A cytoskeleton-mediated pre-constriction site would allow Drp1 to oligomerize around the actomyosin ring (**Figure 1.3**) (Macdonald et al., 2014, Fröhlich et al., 2013). The GTPase

activity of Drp1 would then increase mitochondrial constriction until the organelle is completely separated (Bui and Shaw, 2013, Mears et al., 2011, Koirala et al., 2013). Although this model suggests that actomyosin-mediated membrane constriction facilitates Drp1 recruitment to sites of mitochondrial fission, more work is required to fully test this hypothesis.

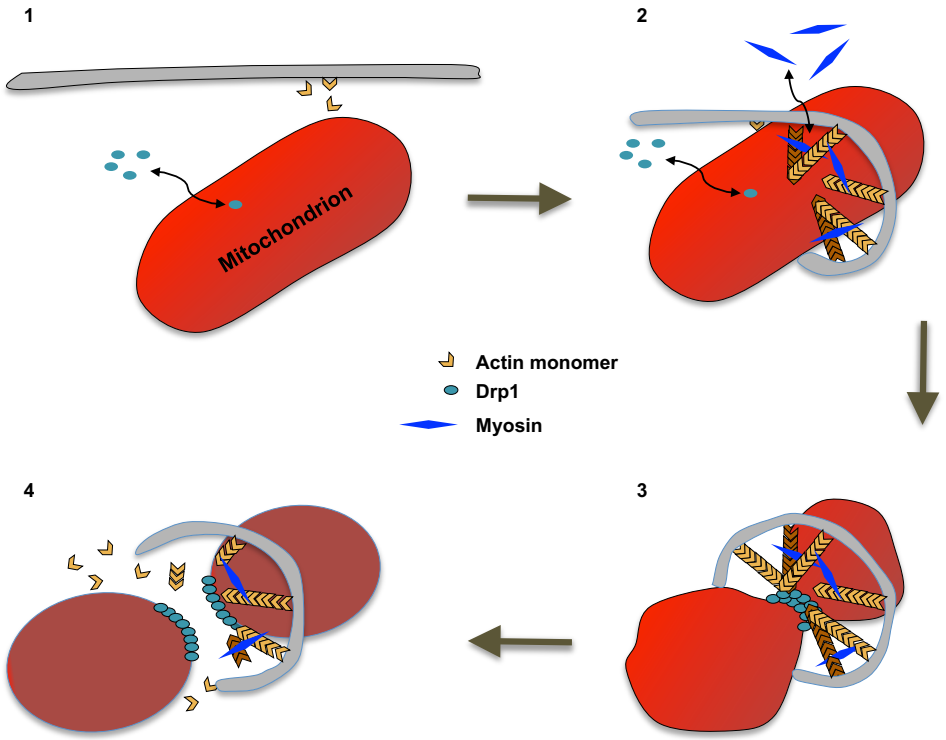

Figure 1.3: Model depicting the molecular events of mitokinesis.
Step 1: ER (grey) and mitochondrion (red) are not in contact. Drp1 is not tightly associated with the mitochondrion.
Step 2: ER-mitochondrial interaction enables the polymerization of actin filaments at the
interface between the two organelles. Myosin II is recruited to these filaments, and myosin II motor activity causes initial constriction of the mitochondrion.
Step 3: Drp1 is recruited to this constriction site, oligomerizes into a ring, and Drp1 GTPase
activity causes constriction of this ring to drive mitochondrial fission.
Step 4: Upon fission, ER detaches from mitochondrion and actin depolymerizes.
This is but one possible model from the available data. Adapted from Korobova *et al*, 2014.

1.3.3. Mitochondrial dynamics and bacterial infection

Mitochondria play a key role during host-pathogen interactions (Lobet et al., 2015). During infection of host cells, intracellular pathogens including *Listeria* and *Shigella* can affect mitochondria function and dynamics (Walker et al., 2014, Saint-Georges-Chaumet and Edeas, 2016). In the case of *Listeria*, LLO causes global mitochondrial damage and network disruption (Stavru et al., 2011). By contrast, mitochondrial fragmentation caused by *Shigella* is localised around bacteria, and is not caused by bacterial toxins (Stavru et al., 2011). Interestingly, *Shigella* can exploit Drp1-mediated mitochondrial fission for intracellular survival (Carneiro et al., 2009, Lum and Morona, 2014, Sirianni et al., 2016), although the underlying mechanisms remain to be established.

Mitochondria regulate cellular metabolism and produce energy (Walker et al., 2014, Palikaras et al., 2015). In addition to providing adenosine triphosphate (ATP), mitochondria produce nutrients (i.e. amino acids, lipids, and nucleotides) and are a centre for host immune regulation (Stehling et al., 2014, Miller, 2013).

1.3.4. Mitophagy and bacterial autophagy

Mitochondria can be selectively eliminated by autophagy in a process called mitophagy (Heo et al., 2015). The selective elimination of mitochondria can be due to damage, differentiation of tissues or declined metabolic demand (Friedman and Nunnari, 2014). Recent work has shown striking parallels between bacterial autophagy and mitophagy (Randow and Youle, 2014, Manzanillo et al., 2013). Damaged mitochondria are recognised and phospho-ubiquitinated by the mitochondrial kinase PINK1 (Lazarou et al.,

2015, Friedman and Nunnari, 2014). PINK1 then recruits and activates Parkin, which mediates ubiquitin chain amplifications for the recognition by p62, NDP52 and OPTN (Lazarou et al., 2015, Zhong et al., 2016). The role of Parkin-mediated ubiquitination in host defence has recently been observed in studies using mycobacteria both *in vitro* and *in vivo* (Manzanillo et al., 2013). Parkin generates ubiquitin signals around *M. tuberculosis* when it is still in the phagocytic vacuole (Manzanillo et al., 2013). How Parkin is recruited to *M. tuberculosis* still remains unclear.

1.4. The eukaryotic cytoskeleton

The main components of the cytoskeleton found in eukaryotes include actin, microtubules, intermediate filaments and septins (**Figure1.4**)(Mostowy and Cossart, 2012b). These cytoskeletal components can interact with each other, and have important roles in numerous cellular processes including cell division and host-pathogen interactions (Mostowy and Shenoy, 2015).

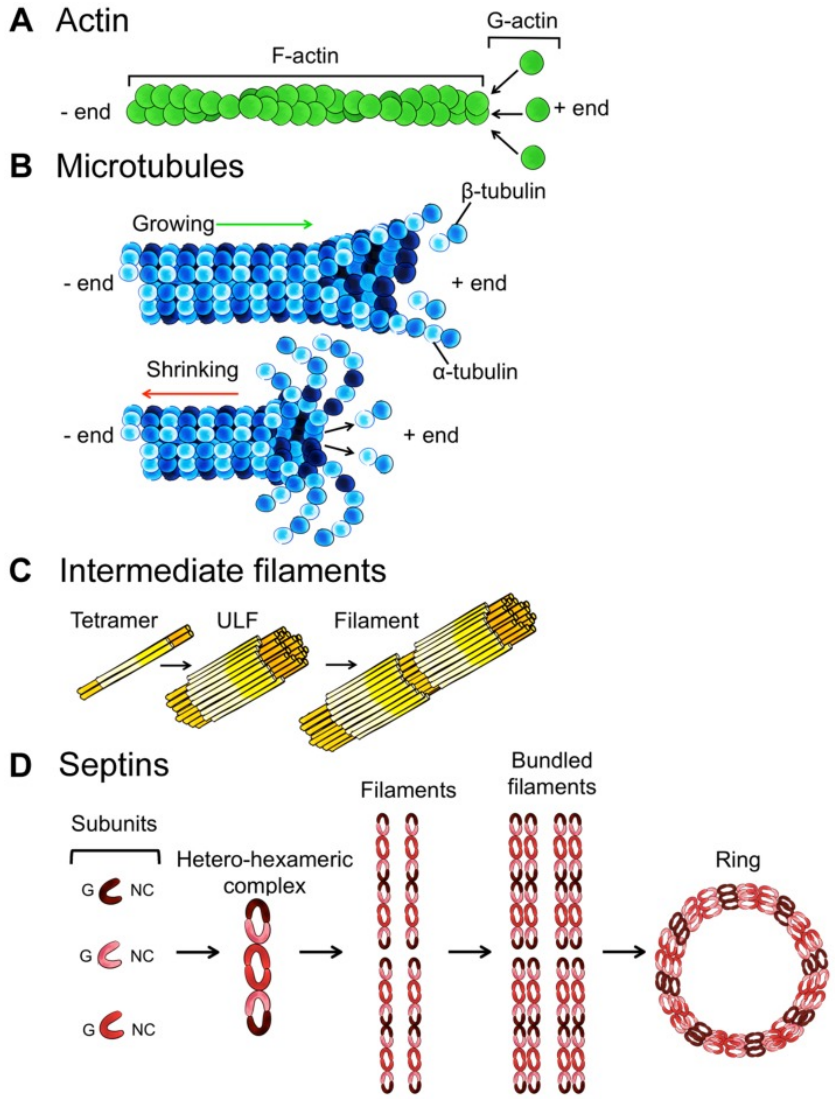

Figure 1.4: The four components of the cytoskeleton

A. Actin filaments (F-actin) consist of a polar structure formed by G-actin monomers. F-actin is assembled into a helix with a diameter of 7nm, with a barbed end growing faster (also called plus end) then the other (also called minus end).

B. Microtubules (MT) are cylindrical structures composed of basic subunits of α- and β-tubulin. MTs nucleate into polar filaments characterised by a fast growing state that switches into a rapid shrinking at the ends of a microtubule. This phenomenon is known as dynamic instability.

C. Intermediate filaments (IFs) are composed of basic tetrameric subunits that assemble in an antiparallel fashion to form unit length filaments (ULFs). ULFs join end to end to form short filaments that anneal to each other longitudinally to form non-polar filaments.

D. Septin subunits interact via a GTP-binding domain (G) and the carboxy-terminal and amino-terminal (NC) regions to form a heteromeric complex. These structures join end-to-end to form non-polar filaments, which can then form bundles and higher order assemblies, including rings.

1.4.1. Actin

Actin (G-actin) is a 40 kDa globular protein that polymerizes into polar filaments (F-actin) (Pollard and Cooper, 2009). The process of nucleation is initiated by the binding of actin to an ATP, which is hydrolysed into adenosine diphosphate (ADP).

The actin cytoskeleton can form bundles of filaments and networks that support the plasma membrane and define cellular shape (Blanchoin et al., 2014). The polymerization of actin filaments also drives cellular plasticity and motility. Eukaryotic cells possess several accessory proteins that help to maintain the stability and activity of the actin network (Blanchoin et al., 2014).

The Arp2/3 complex is the best-characterised actin nucleator (Skau and Waterman, 2015). Examples of Arp2/3-meidated actin polymerization are observed in the formation of lamellopodia, during the process of endocytosis, and at cell-to-cell junctions (Mooren et al., 2012). As described above, some pathogenic bacteria are known to recruit the Arp2/3 complex to polymerize actin tails for intracellular motility (Welch and Way, 2013).

1.4.2. Microtubules

Microtubules are cylindrical structures, nucleated by dedicated organelles called microtubule-organizing centres (MTOCs) into polar filaments with a diameter of ~25 nm (Coles and Bradke, 2015).

Microtubules are characterised by dynamic instability, a fast growing state that switches into a rapid shrinking state at the microtubule ends (Desai and Mitchison, 1997). Dynamic instability allows rapid reorganization of the microtubule network (Pellegrini et al., 2016).

1.4.3. Intermediated filaments

Intermediate filaments include keratin, vimentin and lamins (Margiotta and Bucci, 2016). There are approximately 70 genes coding for intermediate filament proteins, which are categorized into six types based on sequence and structure (Margiotta and Bucci, 2016). Basic tetrameric subunits assemble in an antiparallel fashion to form unit length filaments. Unit length filaments join end to end to form short filaments that anneal to each other longitudinally, and form longer filaments with a diameter of ~11nm (Herrmann et al., 2007). Intermediate filaments are non-polar because of the antiparallel orientation of the tetrameric subunits, and unlike actin and microtubules, their assembly does not require any nucleotide hydrolysis (Herrmann et al., 2009).

A main function of intermediate filaments is to resist mechanical stresses. Intermediate filaments are more stable then actin and microtubules, and are viewed to support the majority of the structural roles in human cells (Kornreich et al., 2015).

1.4.4. The septin cytoskeleton

1.4.4.1. Septins: the fourth component of the cytoskeleton

Septins are guanosine triphosphate (GTP)-binding proteins and polymerise to form non-polar filaments. They associate with actin, microtubules and cellular membrane and therefore can be regarded as a cytoskeleton component (Mostowy and Cossart, 2012b). First discovered in *S. cerevisiae* 40 years ago by Lee Hartwell (Hartwell, 1971), septins are a highly conserved family of proteins. Humans have 13 functional genes (*Sept1-Sept12 and Sept14*) that encode septin proteins (30–65 kDa), which can be classified into four groups (SEPT2, SEPT3, SEPT6 and SEPT7 groups) based on their amino acid sequence homology (Nishihama et al., 2011, Mostowy and Cossart, 2012b). All septins possess a GTP-binding domain, a septin unique element (SUE) comprised of 53 highly conserved amino acids whose function is still unknown, and a polybasic region that binds directly to phosphoinositides on the plasma membrane (**Figure 1.5**)(Cao et al., 2007, Pan et al., 2007). One septin of each group may interact through their GTP-binding domain (G interface) and their N- and C-terminal regions (NC interface) and form basic hetero-oligomeric structures (**Figure 1.4D)**. These form rod-shaped complexes (32-40nm in length) (Sellin et al., 2011, Kim et al., 2011), and may assemble to form higher order structures including rings (~0.6 μm in diameter). Septins are stable cytoskeletal components do not undergo rapid dynamic turnover unlike actin and microtubules (Hu et al., 2008, Hagiwara et al., 2011). Hydrolysis of GTP by septins is thought to induce conformational changes in the G and NC interfaces to regulate septin-septin interaction and function (Sirajuddin et al., 2007, Sirajuddin et al., 2009).

Biochemical studies *in vitro* have shown that septin assembly is membrane-facilitated (Kinoshita et al., 2002, Bridges et al., 2016). Evidence from budding yeast has shown that purified septin complexes polymerize into filaments on phosphatidylinositol-4,5-biphosphate (PIdIn4,5P_2)-containing lipid monolayers (Bertin et al., 2012). Recent studies in mammalian cells have shown that septins preferentially bind to lipid bilayers with micron-scale curvature (Bridges et al., 2016).

Septins are best known for their role during cytokinesis (Kinoshita et al., 2002). Here, septins form filaments alongside actin microfilaments, and regulate constriction of the actomyosin ring (Mostowy et al., 2010, Glotzer, 2005). However, the role of septins in non-dividing cells remains to be fully defined.

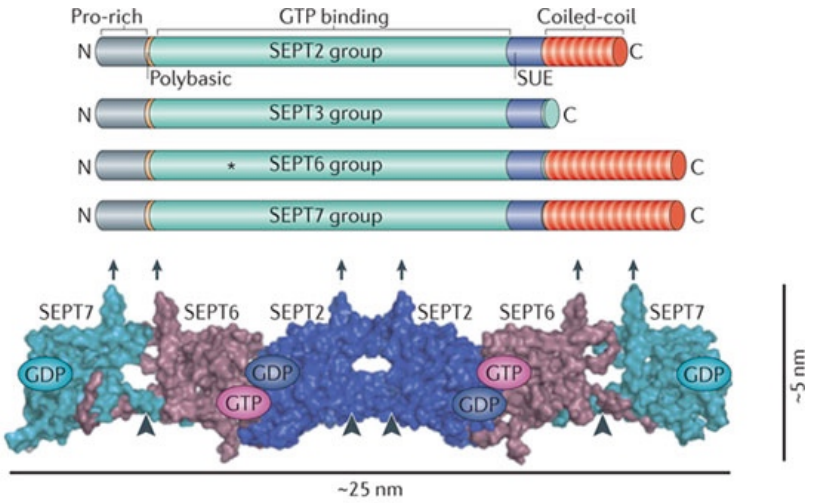

Figure 1.5: Septins: the fourth component of the cytoskeleton.
The schematic shows the classification of septin into 4 subgroups, based on sequence homology. Below, the basic structure of the hetero-hexameric complex shows the interaction between SEPT2-SEPT6-SEPT7.

1.4.4.2. Cellular functions of septins

Septins have been implicated in a variety of cellular processes acting as scaffolds or diffusion barriers. Septin scaffolds accumulate proteins at specific locations in the cell and promote their functional interactions (Mostowy and Cossart, 2012b). Septin filaments with scaffolding features have also been observed in non-dividing cells at the plasma membrane. Here, they play a role during clathrin-mediated endocytosis and regulate the distribution of surface receptors (Mostowy et al., 2011a, Mostowy and Cossart, 2009). In support of this, work has shown a role for SEPT2 and SEPT11 in the anchoring of the receptor tyrosine kinase Met to the plasma membrane (Mostowy et al., 2011a). Septins form stable filaments, and their localization at the plasma membrane may confer structural rigidity and help to define cell shape. Indeed, studies using atomic force microscopy have shown that the loss of SEPT2 or SEPT11 reduces cortical rigidity and plasticity (Tooley et al., 2009, Mostowy et al., 2013). In agreement with this, septins have recently been found to scaffold the axon/myelin unit, important for myelination of the axons structures (Patzig et al., 2016).

Septins have been shown to play important roles as membrane diffusion barriers, acting as a physical impediment for transmembrane proteins, and compartmentalize membranes into domains (Caudron and Barral, 2009). The best examples come from yeast, where selective compartmentalization by septins have been characterised at the level of the ER, plasma membrane and nuclear envelope (Clay et al., 2014, Shcheprova et al., 2008).

Given their role in many essential cellular processes, it is not surprising that septins have been implicated in a variety of human diseases including cancer, neuropathies, ciliogenesis and infection (Mostowy and Cossart, 2012b, Hagiwara et al., 2011).

1.4.4.3. Septins assemble into cage-like structures to prevent bacterial dissemination

Septins form cage-like structures to restrict actin-based motility and autophagy escape (Mostowy et al., 2011a, Mostowy et al., 2010). Septins are recruited to sites of bacterial actin polymerization together with ubiquitinated proteins, p62 and NDP52 (Mostowy et al., 2010, Mostowy et al., 2011b).

Rearrangements of the septin cytoskeleton have been observed in response to actin polymerization from studies using *Listeria* or *Shigella*. Experiments performed at the site of bacterial entry first established that septin recruitment is dependent on actin (Mostowy et al., 2009a, Mostowy et al., 2010). Here, septins were shown to form collar-like structures with actin at the phagocytic cup of invading bacteria. The inhibition of actin polymerization with cytochalasin D impaired the recruitment of both actin and septin to the site of bacterial entry (Mostowy et al., 2009a).

In the cytosol, septins were observed to form rings of ~0.6nm in diameter surrounding some actin tails polymerized by *Listeria* or *Shigella* (Mostowy and Cossart, 2012b). Studies on bacterial motility have shown that the inhibition of septins did not affect the speed of movement of already motile bacteria (Mostowy et al., 2010). The precise role of septin rings surrounding actin tails remains to be determined.

Septins form cage-like structures around intracellular *Shigella* and *M. marinum* and restrict bacterial dissemination. For this reason, the septin cage can be viewed as a mechanism of host defence (Mostowy et al., 2010). Experiments using a *Shigella*-zebrafish (*Danio rerio*) infection model revealed septin caging *in vivo*, demonstrating that septin cages are not an artefact of tissue culture cells (Mostowy et al., 2013).

1.4.5. The roles of the cytoskeleton in autophagy

Studies using infection have helped to understand mechanisms underlying both infection and cytoskeleton biology (Brumell et al., 2002). Results have shown important roles for actin, microtubules, intermediate filaments and septins in cell-autonomous immunity against bacterial pathogens (Mostowy and Shenoy, 2015).

1.4.5.1. Actin assembly mediates different steps of autophagy

A role for actin in autophagosome biogenesis has been described. Upon starvation-induced autophagy, actin is recruited to structures enriched in PI(3)P, important for phagophore formation (Aguilera et al., 2012). Consistent with this, actin polymerization has been observed to promote trafficking of ATG9 (Hohfeld, 2016). However, in the case of selective degradation of protein aggregates, actin has been shown to mediate formation of the autolysosome (**Figure 1.6A**) (Zavodszky et al., 2014) (Lee et al., 2010).

As described above, cytosolic *Shigella* and *Listeria* are well known to exploit the actin-polymerizing machinery for actin-based motility (Welch and Way, 2013). It was recently discovered that the host factor Toca-1 is a key regulator

of actin nucleation and the maturation of the autophagosome that can help *Shigella* to avoid recognition by autophagy (Baxt and Goldberg, 2014). Toca-1 enables N-WASP actin-polymerising activity, which is required by *Shigella* to produce actin tails. During the first part of infection (40 min), the interaction between Toca-1 and the *Shigella* effector IcsB prevents the recruitment of LC3 and NDP52 around invasive *Shigella* (Baxt and Goldberg, 2014). The *Shigella* surface protein IcsA/VirG binds N-WASP and polymerizes actin tails. During later stages of *Shigella* infection, the recognition of IcsA by ATG5 and the tecnonin domain-containing protein TECPR1 promotes autophagosome-lysosome maturation (Chen et al., 2012a, Ogawa et al., 2011). However, interactions between Toca-1 and IcsB has been shown to inhibit the binding of ATG5 to IcsA/VirG (Baxt and Goldberg, 2014).

In the case of *Listeria*, the bacterial effector ActA mimics WASP to recruit ARP2/3 and polymerizes actin-comet tails (Van Troys et al., 2008). Differently from *Shigella*, *Listeria* ActA prevents the recruitment of ubiquitin, autophagy receptors, and ATG8-family proteins, inhibiting autophagosome formation (Mostowy et al., 2009b, Dortet et al., 2011, Yoshikawa et al., 2009).

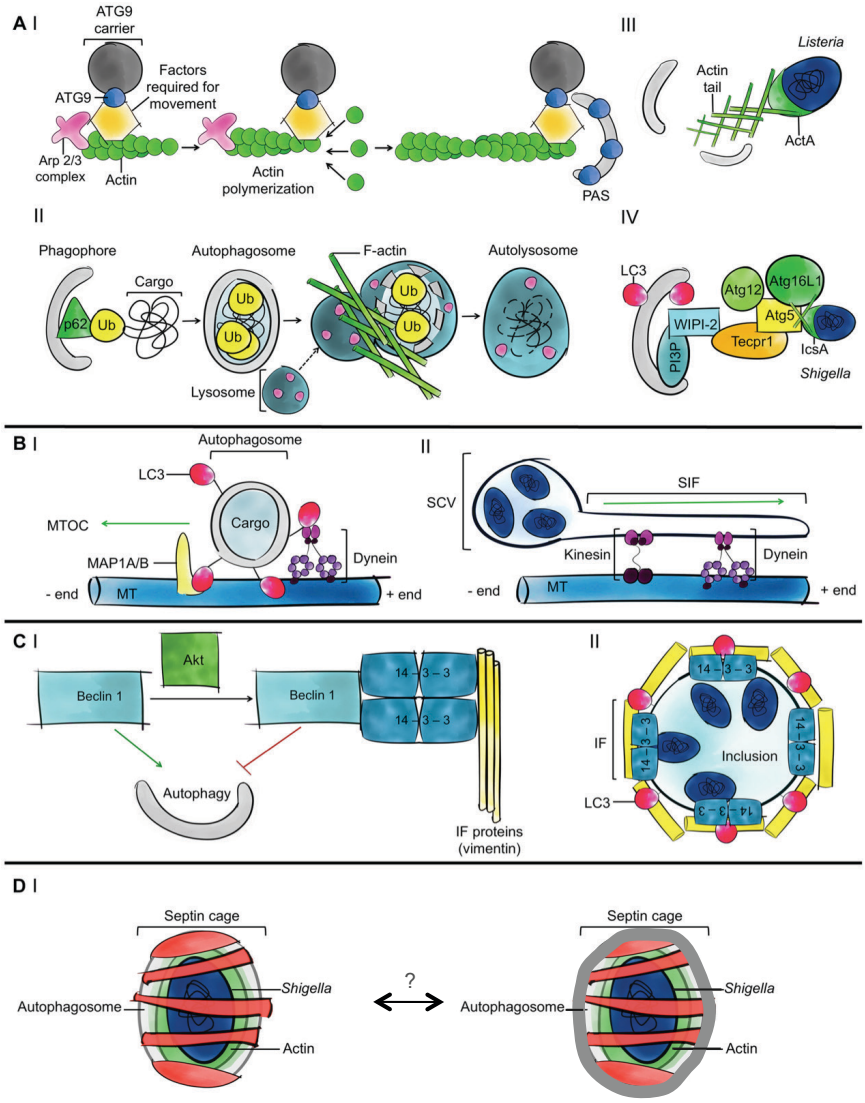

Figure 1.6: The roles of the cytoskeleton in autophagy.
A Actin is an autophagy modulator. (I) Actin polymerization allows ATG9 to deliver membrane to the PAS for autophagosome biogenesis. (II) Fusion between the autophagosome and lysosome is mediated by actin during Ub-mediated autophagy. (III) Recruitment of the Arp2/3 complex to the surface of bacteria leads to actin tail polymerization to escape recognition by autophagy. (IV) *Shigella* IcsA activity promotes polymerization of actin tails. ATG5 recognises the bacterial factor and triggers autophagy.
B Microtubules (MT) regulate autophagosome trafficking. (I) LC3 binds dynein and enables the transport of the autophagosomes. (II) *Salmonella*-induced filaments bind dynein and regulate trafficking of the autophagosomes.
C Intermediate filaments stabilize autophagy. (I) Beclin 1 is phosphorylated by Akt, which promotes a Beclin1/ 14-3-3/vimentin complex to inhibit the activation of autophagy by Beclin1. (II) Model depicting the mechanism used by Chlamydia to establish a replicative niche in a cytoskeleton-dependent manner.
D Septins promote bacterial autophagy. (I) In the process of avoiding autophagy *Shigella* can be entrapped in septin cages and targeted to autophagy. Two models currently available depict the autophagosome inside (left) or outside (right) the septin cage (Image adapted from Mostowy, 2014).

1.4.5.2. Microtubules regulate autophagosome trafficking

Microtubules facilitate the trafficking of vesicles for autophagosome fusion (Geeraert et al., 2010, Moreau et al., 2011, Radhakrishnan and Splitter, 2012). The interaction between the motor protein dynein with LC3 and the microtubule-associated protein 1A and 1B (MAP1A and MAP1B), allows the autophagosomes to travel along microtubules to the lysosomes concentrated near to the MTOC (**Figure 1.6B**)(Korolchuk et al., 2011).

Invasive pathogens can modulate microtubules dynamics during infection (Radhakrishnan and Splitter, 2012). As an example, bacterial T3SS effectors have been shown to modulate the stability of microtubules, and in the case of *Salmonella*, the effector SifA stabilizes the microtubules network to enable trafficking and maturation of the SCV (Brumell et al., 2002). However, more investigation is necessary to understand the full impact of microtubules on autophagy.

1.4.5.3. Intermediate filaments stabilize autophagosomes

Key roles for intermediate filaments in autophagy have been identified. Work has shown that autophagy inhibition using protein phosphatase inhibitors (e.g. okadaic acid) affects the organization of intermediate filaments (Wong et al., 2015, Margiotta and Bucci, 2016). Another study has shown that vimentin interacts with Beclin1, and forms a Beclin1/14-3-3/vimentin complex to inhibit autophagy (**Figure 1.6C)** (Wang et al., 2012).

Pathogens such as *Chlamydia trachomatis* can manipulate intermediate filaments for survival (Kumar and Valdivia, 2008). During infection, *Chlamydia* replicate into a large vacuole known as an inclusion, which interacts with the

eukaryotic protein 14-3-3β, actin, septin and intermediate filaments (Volceanov et al., 2014). Evidence has shown that cytoskeleton-associated inclusions are surrounded by autophagosomes and a non-lipidated form of LC3, indicating that autophagy does not target these bacteria to degradation (Kumar and Valdivia, 2008, Bestebroer et al., 2013).

1.4.5.4. Septins promote bacterial autophagy

Septins have recently been shown to regulate autophagosome biogenesis in yeast during starvation-induced autophagy (Barve et al., 2016). In agreement with this, work using HeLa cells has shown that depletion of septins can decrease autophagy marker recruitment and autophagosome formation, highlighting an interdependent relationship between septins and autophagy (Mostowy et al., 2010).

As mentioned above, septins compartmentalize actin-polymerizing, autophagy-positive *Shigella* into septin cages (Mostowy et al., 2011b, Sirianni et al., 2016). Work using *M. marinum* also showed the recruitment of p62 and LC3B to the septin cage (Mostowy et al., 2011b, Mostowy et al., 2010, Mostowy et al., 2013). Experiments using IcsA-deficient *Shigella* have demonstrated that bacteria not able to polymerize actin are not recognized by septins or autophagy (Mostowy et al., 2011b). Consistent with septin-autophagy interdependence, siRNA specific for p62, NDP52, ATG5, ATG6 or ATG7, showed that septin cages cannot form in autophagy deficient cells (Mostowy et al., 2011b).

1.5. Project Aims

Septin rearrangements and ultrastructures (i.e. the septin cage) have ben shown to function as a mechanism of host defense during *Shigella* infection. How septins assemble into cages and their precise role in bacterial autophagy is yet poorly understood. For this reason, we hypothesised that septins might interact with host factors to assemble into the cages that target bacteria to degradation, in a process triggered by *Shigella*.

The focus of my PhD is to investigate host determinants required for septin cage assembly, and to discover new roles for septins in non-dividing cells. Using *S. flexneri* as a paradigm of infection, my specific aims are:

1. To characterise the *Shigella*-SEPT7 cage and its role in host defence. Previous work has shown that septin cages prevent *Shigella* cell-to-cell spread, and this study shows that SEPT7 is crucial for septin cage assembly and anti-bacterial autophagy.

2. To discover novel determinants required for *Shigella*-septin cage assembly. This study has uncovered new links between septins and mitochondria.

3. To reveal new roles for septins in host cell metabolism. Results have discovered unforeseen links between septins and host cell metabolism.

Aim 1 and 2 are published in EMBO Reports (Sirianni et al., 2016). Aim 3 is a manuscript in preparation.

CHAPTER 2: SEPT7 cages target *Shigella flexneri* to degradation by autophagy

2.1. Introduction

Autophagy was discovered as a non-selective bulk degradation process activated by nutrient starvation (Yang and Klionsky, 2010). Research has shown that autophagy can also selectively target cytosolic material to degradation (Lazarou et al., 2015). Indeed, bacterial autophagy is a selective process important for host immunity against invasive bacteria (Huang and Brumell, 2014, Cemma and Brumell, 2012). The best-characterised mechanism of bacterial autophagy involves the recognition of ubiquitinated substrates associated with bacteria by autophagy receptors like p62 and NDP52 (Zheng et al., Thurston et al., 2009). On the other hand, mounting evidence has shown that several pathogens have evolved mechanisms to exploit or avoid autophagy for intracellular survival (Mostowy and Cossart, 2012a, Huang and Brumell, 2014, Choy and Roy, 2013). The host cytoskeleton has emerged as a key player in the process of autophagy and its ability to restrict or promote bacterial proliferation (Mostowy, 2014). Cytosolic bacteria, such as *Shigella* or *Listeria*, use the host cytoskeleton to polymerise actin for motility (Welch and Way, 2013). Remarkably, the process of actin polymerisation by *Shigella* or *Listeria* has been linked to the activation of autophagy (Mostowy et al., 2011b, Chen et al., 2012a). In the case of *Shigella*, septins have shown to entrap actin-polymerising bacteria in cage-like structures, and target them to autophagy (Mostowy et al., 2011b, Mostowy et

al., 2010). *Shigella*-septin cages colocalise with p62 and NDP52 (Mostowy et al., 2011b), and the depletion of septins by siRNA reduced the recruitment of these autophagy receptors around *Shigella* (Mostowy et al., 2011b). However, the fate of *Shigella* entrapped in septin cages remains to be established.

For this study, we used *Shigella* to investigate septin cage assembly in the human epithelial cell line HeLa. In humans, septins from 4 different subgroups, which assemble to form filaments or ring-like structures (**Table A1**). Septin 7 (SEPT7), which is the only member of its subgroup in humans, is crucial for septin complex assembly and function (Mostowy and Cossart, 2012b, Sellin et al., 2011). In support of this, studies have shown that the depletion of SEPT7 also results in the depletion of other septin at the protein level (Tooley et al., 2009, Estey et al., 2010, Sellin et al., 2011). In addition, cells lacking SEPT7 have defects in cytokinesis and the embryos of SEPT7-deficient mice fail to develop (Spiliotis et al., 2005, Estey et al., 2013, Kinoshita, 2003). Although work has shown that SEPT7 plays a key role in fungal pathogenesis of human endothelial cells (Phan et al., 2013), a role for SEPT7 during bacterial infection had not yet been described. Here, we show that SEPT7 is crucial for septin cage assembly and that *Shigella* entrapped in SEPT7 cages are targeted to degradation by autophagy.

2.2. Characterisation of SEPT7

The first crystal structure of a human septin complex revealed that septins form a non-polar heteromeric complex: SEPT7-SEPT6-SEPT2-SEPT2-SEPT6-SEPT7 (Sirajuddin et al., 2007). SEPT7 is an essential component of any human or mouse septin complex, as it is the sole member of the SEPT7 group (Sellin et al., 2011). Confocal microscopy showed that endogenous SEPT7 and SEPT6-GFP colocalise together on filaments and also cages (**Figure 2.1A**). In agreement with predictions from the crystal structure, these data suggested that SEPT7 assembles together with other septins to form higher order structures inside human tissue culture cells.

To study the function of SEPT7, small interfering RNAs (siRNAs) were used. Cells were treated with control (CTRL) or two different siRNA sequences specific for SEPT7 (SEPT7-1, SEPT7-2). The whole cell extracts of siRNA-treated cells were immunoblotted for endogenous SEPT2, SEPT6, SEPT7, SEPT9 or SEPT11, and the relative amount of proteins quantified by western blot (**Figure 2.1B**). As compared to CTRL cells, cells treated with SEPT7-1 or SEPT7-2 siRNA expressed 86.4 ± 2.6% or 84.8 ± 3.3% less SEPT7 protein, respectively. Consistent with previous observations (Tooley et al., 2009, Estey et al., 2010, Sellin et al., 2011), the depletion of SEPT7 also affected the protein expression levels of SEPT2 (40.6 ± 8.8% or 44.7 ± 7.4%), SEPT6 (32.3 ± 7.4% or 39.6 ± 5.3%), SEPT9 (25.9 ± 6.6% or 15.8 ± 3.3%), and SEPT11 (28.6 ± 5.5% or 42.2 ± 7.4%) (**Figure 2.1B**).

To understand if regulation of septins by SEPT7 occurs at the transcriptional or protein level, the RNA expression of septins was measured by quantitative real time PCR (qRT-PCR, in collaboration with Stephen Buranyi). The relative

transcription of SEPT2, SEPT6, SEPT7 and SEPT9 in SEPT7-siRNA treated cells were compared to a housekeeping gene (GAPDH). These data clearly showed a significant decrease in the RNA expression only of *SEPT7* (19.2 ± 3.5 fold), whereas *SEPT2*, *SEPT6* and *SEPT9* were not affected (**Figure 2.1C**). This suggests that the regulation of septin expression by SEPT7 occurs at the protein level, and septins from other subgroups are being degraded in the absence of SEPT7. Collectively, these results are in agreement with previous studies showing a role for SEPT7 in complex stability (Fung et al., 2014, Tooley et al., 2009, Patzig et al., 2016).

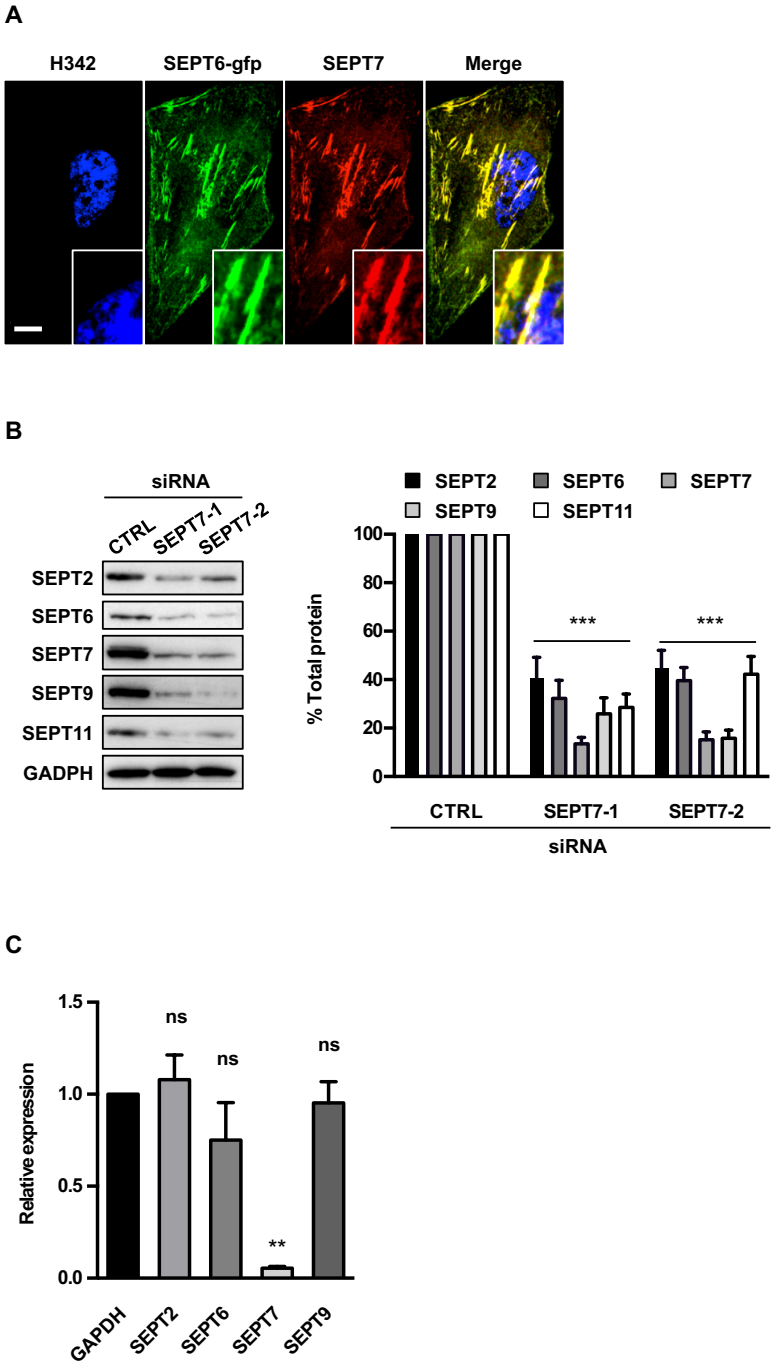

Figure 2.1: SEPT7 is required for septin-complex stability

A. HeLa cells stably expressing SEPT6-GFP were fixed for confocal microscopy and labelled with antibody for endogenous SEPT7. The scale bar represents 5 µm.

B. HeLa cells were treated with control (CTRL) or two SEPT7 (-1 or -2) siRNA for 72 h, and whole cell lysates were immunoblotted for SEPT2 (41 kDa), SEPT6 (50 kDa), SEPT7 (49 kDa), SEPT9 (75 KDa), or SEPT11 (51 kDa). GAPDH (37 kDa) was used as loading control. Graph represents the mean % ± s.e.m. of the relative amount of protein quantified by densitometry. Unpaired Student's t-test, *** = $p<0.001$, n = 8 biological replicates per condition.

C. HeLa cells were treated with control (CTRL) or SEPT7 siRNA for 72 h, and the transcription level of *SEPT2, SEPT6, SEPT7* or *SEPT9* was quantified by qRT-PCR. GAPDH was used as control. Graph represents the mean ± s.e.m. of the relative expression of *GAPDH, SEPT2, SEPT6, SEPT7* and *SEPT9* mRNA from 2 independent experiments per treatment. Unpaired Student's t-test, ns = non significant; ** = $p<0.01$, n = 2 biological replicates, n = 3 technical replicate per condition.

2.3. SEPT7 is crucial for *Shigella*-septin cage formation

Previous studies on *Shigella*-infected HeLa cells have shown that septins from different subgroups (SEPT2, SEPT3, SEPT6, SEPT7) assemble into cages to prevent actin-based motility (Mostowy et al., 2010, Mostowy et al., 2009a). In addition, SEPT7-cages have been observed in zebrafish cells *in vitro* and larvae *in vivo* (Mostowy et al., 2013). The recruitment of SEPT7 to *Shigella*-septin cages was investigated using confocal microscopy. SEPT6-GFP was used as a positive marker for septin cage assembly, and SEPT6 and SEPT7 have been already shown to directly interact (Mostowy et al., 2009b, Sirajuddin et al., 2007). Consistent with this, SEPT7 was recruited to SEPT6 cages (**Figure 2.2A**).

Next, the recruitment of SEPT7 cages to *Shigella* during the course of infection was quantified (**Figure 2.2B**). As a result, 9.2 ± 1.4%, 10.1 ± 0.7%, and 15.7 ± 2.1% of bacteria recruited SEPT7 cage-like structures at 2 h 40 minutes post infection (minpi), 3 h 40 minpi, and 4 h 40 minpi, respectively. The number of SEPT7-cages recruited to intracellular bacteria is consistent with previous observation made for SEPT2 and SEPT9 (Mostowy et al., 2010).

To understand the architecture of SEPT7 cages, structured illumination microscopy (SIM, in collaboration with Sina Krokowski) was used. Results showed high-resolution images of SEPT7 cages which assembled into 3.2 ± 0.7 μm (length) × 1.2 ± 0.1 μm (width) cages around *S. flexneri* (**Figure 2.2C**). These values are consistent with values previously obtained for SEPT2 cages using stochastic optical reconstruction microscopy (STORM) (Mostowy et al., 2010), and suggest that SEPT7 cages are significantly bigger then entrapped bacterium.

Studies have shown that the recruitment of septins to *Shigella* is dependent upon actin polymerisation (Mostowy et al., 2010, Mostowy and Cossart, 2011b). Consistent with this, SEPT7-cages colocalise actin-polymerising *Shigella* (**Figure 2.2D**). To test if the recruitment of SEPT7 to *Shigella*-septin cages is dependent on actin polymerisation, actin polymerisation was inhibited using cytochalasin D. At 4h 40minpi, cells treated with DMSO were observed to compartmentalise 14.8 ± 0.4 % *Shigella* inside SEPT7 cages. The inhibition of actin dynamics with cytochalasin D significantly reduced (2.9 ± 0.8 fold) the recruitment of SEPT7 cages around *Shigella* at 4 h 40 minpi (**Figure 2.2E**).

To understand the role of SEPT7 in septin cage formation, cells were treated with SEPT7 siRNA and infected with *Shigella* for 4 h 40 min for quantitative microscopy. Samples were labelled for SEPT2, SEPT7 or SEPT9. A significant reduction of SEPT2 (5.0 ± 1.6 fold), SEPT7 (5.7 ± 0.6 fold), and SEPT9 (5.0 ± 1.0 fold) cages was observed in SEPT7-depleted cells, highlighting an essential role for SEPT7 in *Shigella*-septin cage formation (**Figure 2.2F**).

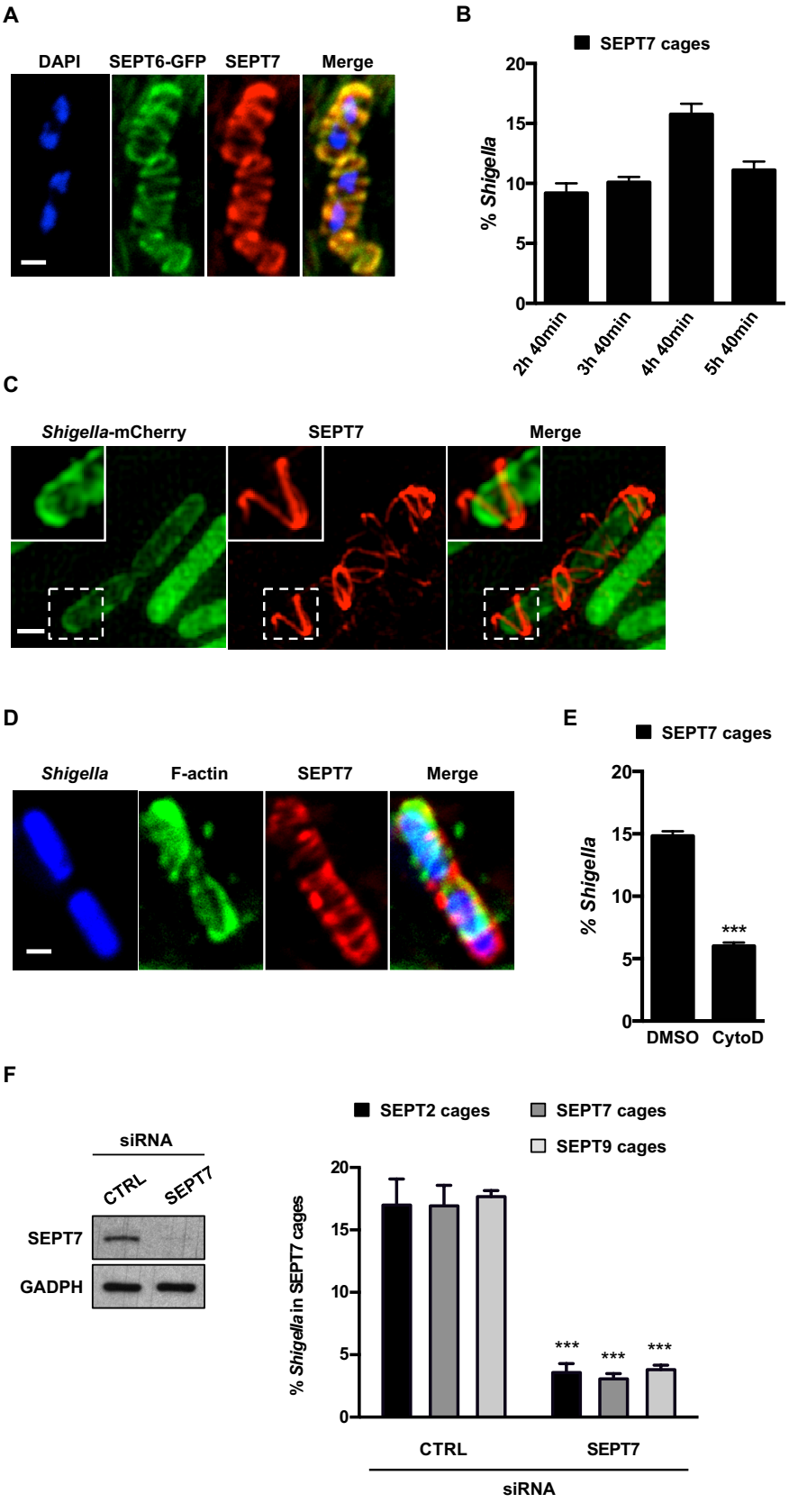
A
DAPI
SEPT6-GFP
SEPT7
Merge
B
SEPT7 cages
% Shigella
20
15
10
5
0
2h 40min
3h 40min
4h 40min
5h 40min
C
Shigella-mCherry
SEPT7
Merge
D
Shigella
F-actin
SEPT7
Merge
E
SEPT7 cages
% Shigella
20
15
10
5
0
***
DMSO
CytoD
F
siRNA
CTRL
SEPT7
SEPT7
GADPH
SEPT2 cages
SEPT7 cages
SEPT9 cages
% Shigella in SEPT7 cages
20
15
10
5
0
***
***
***
CTRL
SEPT7
siRNA

Figure 2.2: SEPT7 is crucial for *Shigella*-septin cage formation
A. HeLa cells stably expressing SEPT6-GFP were infected with *S. flexneri* for 4 h 40 min, fixed for confocal microscopy, and labelled with antibody for endogenous SEPT7. The scale bar represents 1 µm.
B. HeLa cells were infected with *S. flexneri* for 2 h 40 min, 3 h 40 min, 4 h 40 min, and 5 h 40 min, then fixed and labelled with antibodies endogenous SEPT7 for quantitative microscopy. Graphs represent the mean % ± s.e.m. of *Shigella* inside SEPT7 cages. n = 3 biological replicates.
C. HeLa cells were infected with *S. flexneri*-mCherry for 4 h 40 min, fixed for 3D-SIM, and labelled with antibodies to endogenous SEPT7. Inset images show SEPT7 assembly into helix-like structure around *S. flexneri*. The scale bar represents 1 µm.
D. HeLa cells were infected with *S.flexneri* for 4 h 40 min, fixed for confocal microscopy, and labelled with phalloidin for actin and antibody for endogenous SEPT7. The scale bar represents 1 µm.
E. HeLa cells were infected with *S.flexneri* for 4 h 40 min, treated with DMSO or cytochalasin D (CytD) for 30 minutes prior fixation. Graph represents the mean % ± s.e.m. of *Shigella* inside SEPT7 cages. Unpaired Student's t-test, *** = $p<0.001$, n = 3.
F. HeLa cells were treated with control (CTRL) or SEPT7 siRNA for 72 h. Whole cell lysate of siRNA-treated cells were immunoblotted for GAPDH (37 kDa) or SEPT7 (49 kDa) to show the efficiency of SEPT7 depletion. GAPDH was used as loading control. siRNA-treated cells were infected with *S. flexneri* for 4 h 40 min then fixed and labelled with antibodies to SEPT2, SEPT7, or SEPT9 for quantitative microscopy. Graphs represent the mean % ± s.e.m. of *Shigella* inside SEPT2, SEPT7, or SEPT9 cages. Unpaired Student's t-test, *** = $p<0.001$, n = 3 biological replicates per condition.

2.4. The autophagy receptor p62 interacts with septins during *Shigella* infection

The autophagy receptors p62 and NDP52 target *Shigella* to an autophagy pathway dependent upon septin and actin (Mostowy et al., 2011b). Here we investigated the interplay between p62 and SEPT7. HeLa cells were infected with *Shigella*, then fixed and labelled endogenous p62 or SEPT7 for quantitative microscopy. In agreement with previous observations made for SEPT2 and SEPT9 (Mostowy et al., 2010), we observed that 69.1 ± 2.6% of *Shigella* entrapped in SEPT7 cages also colocalise with p62 (**Figure 2.3A**). The interaction between p62 and septins was investigated by co-immunoprecipitation in HeLa cells stably expressing SEPT6-GFP. This cell line was chosen instead of stably expressing SEPT7-GFP HeLa cells, as the overexpression of SEPT6 is better tolerated by the cells and does not inhibit *Shigella* invasion (Serge Mostowy, personal communication). Previous work has shown that SEPT6-GFP colocalises with p62 and NDP52 at the *Shigella*-septin cage, but immunoprecipitation experiments on infected cells using antibodies for SEPT2 or SEPT9 failed to capture any physical interaction (Mostowy and Cossart, 2011b). Here, to maximise the number of cells infected by *Shigella*, HeLa cells were infected with *S. flexneri* M90T AfaI, a hyper-invasive strain that expresses an adhesin from *Escherichia coli* (Mazon Moya et al., 2014). Pulldowns of SEPT6-GFP in uninfected or infected cells were performed using GFP-Trap magnetic agarose beads, and the interactions analysed by western blot (**Figure 2.3B**). Results from co-immunoprecipitation experiments confirmed that SEPT6-GFP interacts with SEPT2, SEPT6, SEPT7, SEPT9 and SEPT11 (i.e. septins expressed in HeLa cells) in both uninfected and infected cells. The autophagy receptor p62 pulled down with

septins only in *Shigella*-infected cells, highlighting a specific interaction during infection. Using the same conditions, several co-IP attempts failed to show an interaction between SEPT6-GFP and NDP52, suggesting a close association between septins and p62 (Mostowy, 2014).

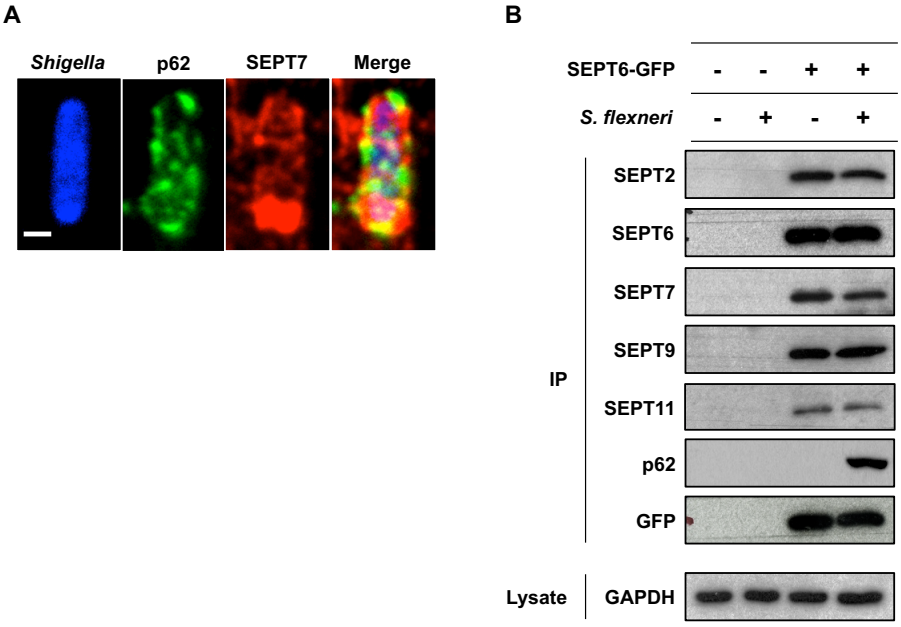

Figure 2.3: The autophagy receptor p62 interacts with septins during *Shigella* infection

A. HeLa cells were infected with *S. flexneri* for 4 h 40 min, fixed for confocal microscopy, and labelled with antibody for endogenous p62 and SEPT7. The scale bar represents 1 μm.

B. HeLa cells stably expressing SEPT6-GFP were infected with *S. flexneri* AfaI for 4 h, harvested, and then tested with Co-IP. Empty vector and/or uninfected HeLa cells were used in parallel as control. GFP-trap magnetic agarose beads were used to isolate SEPT6-GFP from cells, and extracts were immunoblotted for SEPT2 (41 kDa), SEPT6 (50 kDa), SEPT7 (49 kDa), SEPT9 (75 KDa), SEPT11 (51 kDa), GFP (27 kDa) or p62 (62 kDa). The lysates were immunoblotted for GAPDH (37 kDa) as control for cellular protein levels.

2.5. Use of inducible fluorescent *Shigella* strains for single bacterial analysis

To test the role of septin cages in the restriction or promotion of bacterial replication, individual bacteria entrapped by septin cages were analysed. To allow single bacterial analysis, inducible fluorescent (x-light) *Shigella* strains were generated based on isopropyl β-D-1-thiogalactopyranoside (IPTG) inducible plasmids (gift from Prof. Ilan Rosenshine, The Hebrew University of Jerusalem). Reporter genes encoding GFP or mCherry were cloned downstream of a *tac* promoter under the control of the LacI repressor (**Figure 2.4A**). Binding of IPTG to LacI induces conformational change of the repressor and loss of contact with *tac*; in living (or metabolically active) x-light *Shigella* this induces expression of the reporter gene *gfp* or *mcherry* and enables subsequent fluorescence. To analyse GFP/mCherry expression, x-light *Shigella* were grown in TCS medium to an absorbance (600 nm) of 0.6 to allow analysis at exponential growing phase. To test the ability of *Shigella* to respond to IPTG the culture was split so that half of the culture was treated with 70% isopropanol for 30 min and the other half remained untreated. The two halves were then treated with 0.1 mM IPTG and stained for SYTOX orange®, a marker for compromised cellular membrane characteristic of dead cells (**Figure 2.4B**). Bacteria that failed to respond to IPTG (98.7 ± 0.4%, **Figure 2.4B and 2.4C**) were also positive for SYTOX, suggesting that bacteria were metabolically inactive or dead. These data confirmed that x-light *Shigella* is a reliable tool for quantitative microscopy. We next tested the ability of x-light *Shigella* to respond to IPTG during infection of HeLa cells. Cells were infected with x-light *Shigella* for 30 min, treated with IPTG for 30 min, and then fixed for microscopy. In agreement with the fact that *Shigella* are professional

intracellular pathogens (Sansonetti, 2006), 99 ± 0.1% of x-light *Shigella* responded to IPTG after 1 hpi, suggesting that metabolically active bacteria can respond to the treatment inside cells.

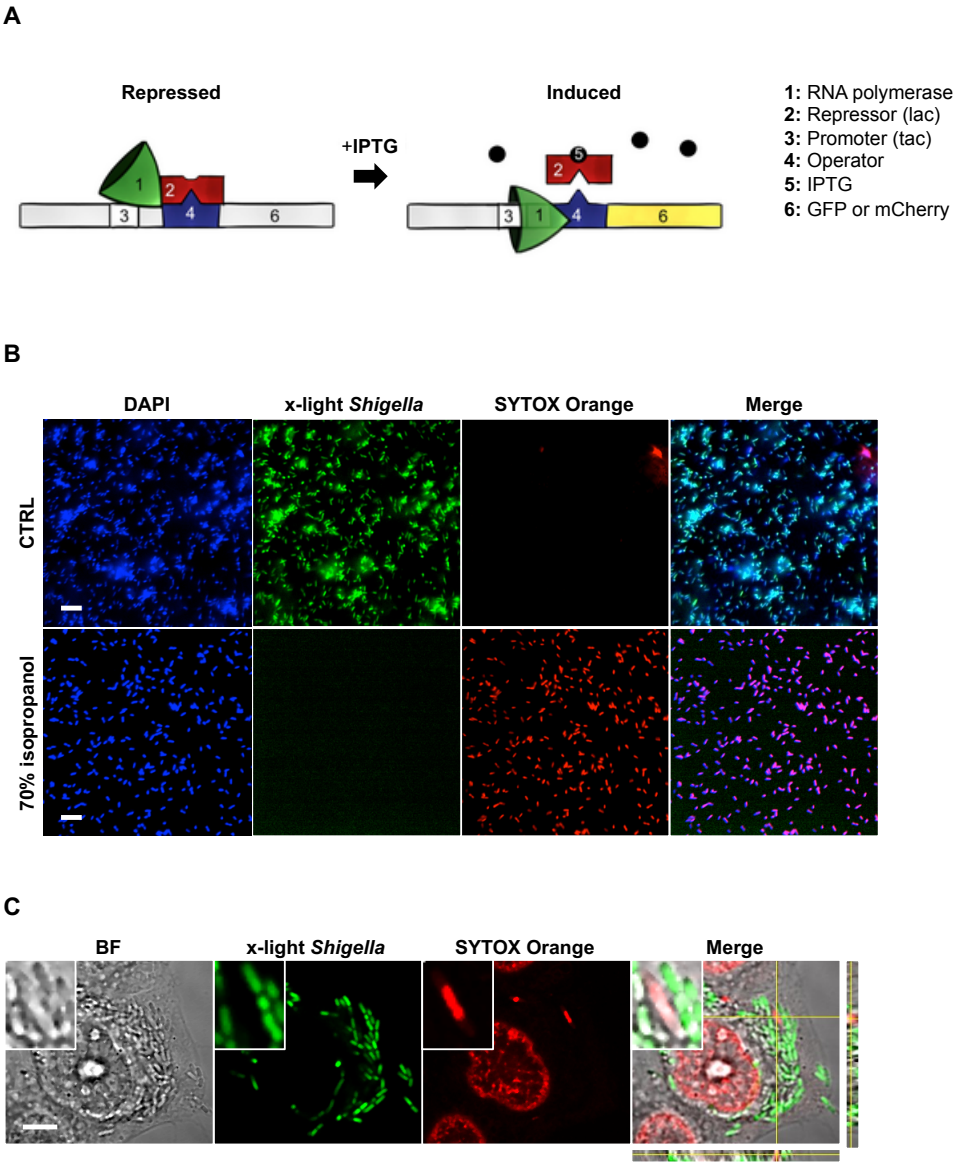

Figure 2.4: Use of inducible fluorescent *Shigella* strains for single bacterial analysis
A. Model depicting the x-light system used for single bacterial analysis. *S. flexneri* M90T carry an inducible plasmid (x-light *Shigella*) engineered with the LacI repressor system from *Escherichia coli*, and a GFP or mCherry gene downstream of the operator. In the presence of IPTG, LacI binds the molecule, and stops its repression on the operator. As a consequence the fluorescent protein is synthesised when bacteria are metabolically active (cartoon from Sirianni *et al.*, 2016).

B. Control (CTRL) or isopropanol-treated x-light *Shigella* GFP were induced with IPTG for 30 min, and then labelled with SYTOX Orange for 10 min. The scale bar represents 5 μm.
C. HeLa cells were infected with x-light *Shigella* GFP for 3 h, induced with IPTG for 30 min, and then treated with 0.03% saponin + SYTOX Orange for 15 min. Representative image shown here. Orthogonal view from image z-stack shows intracytosolic x-light negative, SYTOX-positive *Shigella.* The scale bar represents 5 μm.

2.6. *Shigella* entrapped by septin cages are targeted to degradation

To test if septin cages restrict or promote bacterial replication, HeLa cells were infected with x-light *Shigella* for 4 h, then IPTG was added for 30 min prior to fixation, and the percentage of intracellular bacteria that respond to IPTG was quantified (**Figure 2.5A**). We found that 45.5 ± 1.7% of bacteria entrapped in SEPT7 cages were metabolically active (**Figure 2.5B**). In contrast, 91.4 ± 0.8% of intracellular bacteria not entrapped in septin cages were metabolically active (**Figure 2.5B**). Consistent with the fact that bacteria in cages are also targeted to autophagy (Mostowy et al., 2010, Mostowy et al., 2011b), similar values were obtained for bacteria recruiting p62 (46.7 ± 2.5%) compared to p62-negative bacteria (88.3 ± 1.1%) (**Figure 2.5C, 2.5D**). To investigate whether septins can be recruited to already dead bacteria, infected cells were treated with the antibiotic erythromycin (in collaboration with Sina Krokowski). In the presence of erythromycin, there is a significant reduction of SEPT7 cages suggesting that septins recognise living bacteria (**Figure 2.5E**).

When quantified over time, the % of IPTG-inducible *Shigella* entrapped in SEPT7 cages decreased from 58.9 ± 3% at 3 h 40 minpi to 45.5 ± 1.7% at 4 h 40 minpi, (**Figure 2.5F**). Although no statistical difference was observed for values obtained at different time points, it is tempting to speculate bacterial metabolic activity is decreased in septin cages over time (**Figure 2.2B**) (**Figure 2.5F**). Together, our observations support the view that bacterial autophagy can be an important mechanism of host defence in the case of *Shigella* (Ogawa et al., 2005, Mostowy and Cossart, 2012a, Mostowy et al., 2013). Although these results suggest that septin cages recognise live bacteria to restrict their proliferation, the increased ability of septin cages to

restrict the metabolic activity of bacteria during the course of an infection awaits investigation.

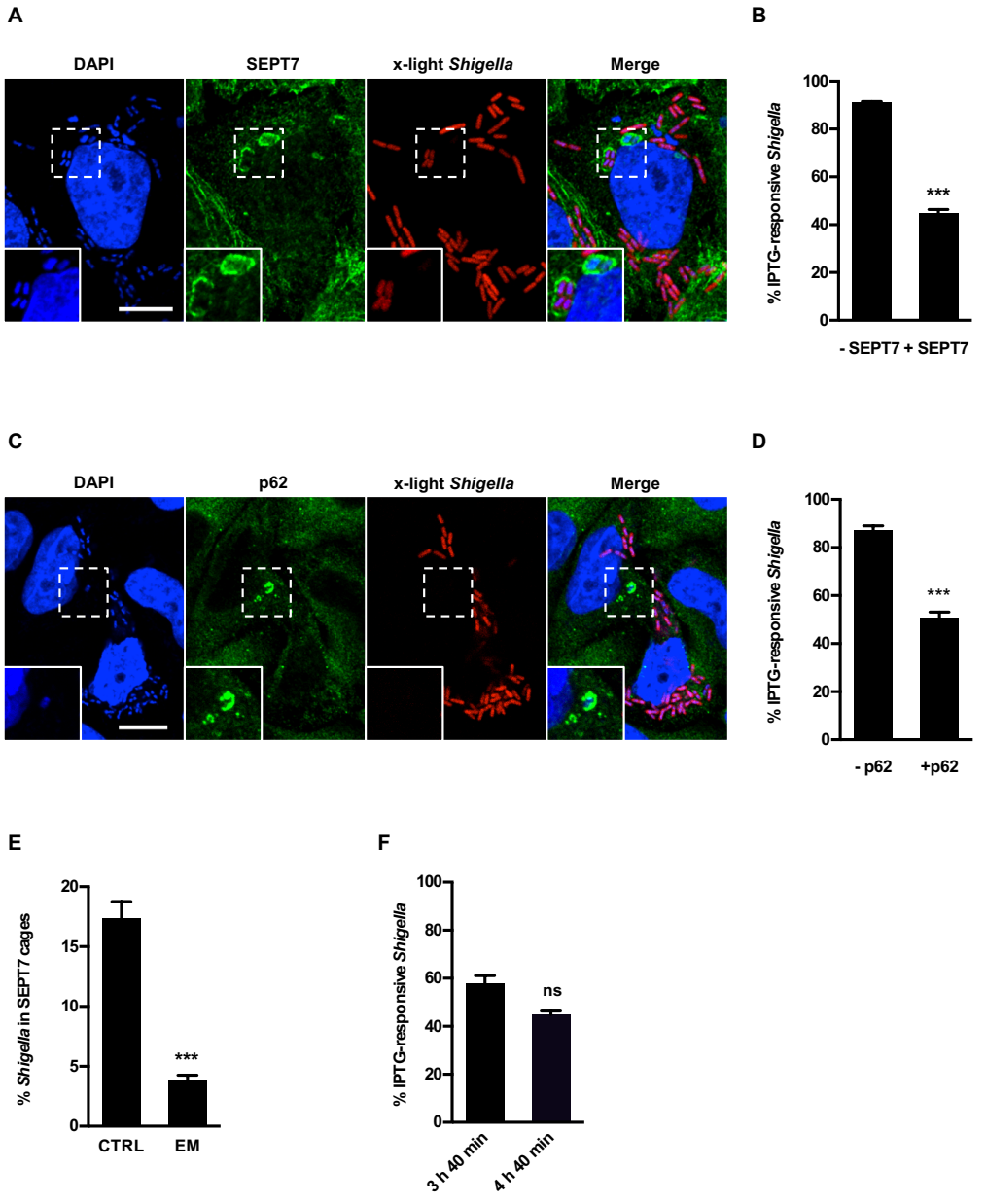

Figure 2.5:*Shigella* entrapped by septin cages are targeted to degradation
A. HeLa cells were infected with x-light *Shigella* mCherry for 4 h 40 min for confocal microscopy. IPTG was added 30 min prior to fixation, and then samples were labelled with antibody for SEPT7. The scale bar represents 5 µm.
B. HeLa cells were infected with x-light *Shigella* mCherry for 4 h 40 min for quantitative confocal microscopy. IPTG was added 30 min prior to fixation, and then samples were labelled with antibody for SEPT7. Graph represents mean % ± s.e.m. of

Shigella responding to IPTG outside (-) or inside (+) SEPT7 cages. Unpaired Student's t-test, *** = p<0.001, n=4 biological replicates.
C HeLa cells were infected with x-light *Shigella* mCherry for 4 h 40 min for confocal microscopy. IPTG was added 30 min prior to fixation, and then samples were labelled with antibody for p62. The scale bar represents 5 µm.
D. HeLa cells were infected with x-light *Shigella* mCherry for 4 h 40 min for quantitative confocal microscopy. IPTG was added 30 min prior to fixation, and then samples were labelled with antibody for p62. Graph represents mean % ± s.e.m. of *Shigella* responding to IPTG without (-) or with (+) p62. Unpaired Student's t-test, *** = p<0.001, n=4 biological replicates.
E. HeLa cells were infected for 1 h 30 min, treated with ethanol (CTRL) or erythromycin (EM) for 2 h prior to fixation, and then labelled with antibody for SEPT7. Graph represents mean % ± s.e.m. of *Shigella* in SEPT7 cages. Unpaired Student's t-test, *** = p<0.001, n =3 biological replicates.
F. HeLa cells were infected with x-light *Shigella* for 3 h 40 min or 4 h 40 min for quantitative confocal microscopy. IPTG was added 30 min prior to fixation, and then samples were labelled with antibody for SEPT7. Graph represents mean % ± s.e.m. of *Shigella* responding to IPTG inside SEPT7 cages. Unpaired Student's t-test, ns = non significant, n = 3 biological replicates.

2.7. Identification of proteins enriched at the *Shigella*-septin cage

To identify novel determinants for septin cage assembly, tandem affinity purification (TAP) combined with proteomics analysis was employed. This work was done in collaboration with Stephen Buranyi, who engineered a FLAG-2xStrep SEPT6 vector for expression in HeLa cells, and carried out the TAP experiments (see material and methods section). FLAG-2xStrep tags are translated in a short AA sequence (WSHPQFEKGGWSHPQFEKGGDYKDDD DN) that does not cause steric interference to the interaction within SEPT6-tagged complexes. In addition, FLAG sequence combined with 2xStrep tags would increase specificity and quality of protein pulldowns. Protocols were optimized to obtain >80% of cells infected. To maximize the number of cells infected with *Shigella*, FLAG-2xStrep-SEPT6-transfected HeLa cells were infected with the hyperinvasive strain *S. flexneri* AfaI (**Figure 2.6A**). Subsequently, sequential FLAG and Strep affinity purification steps were performed on the infected cell lysates, and bound proteins identified using mass spectrometry (MS). In parallel, control pulldown experiments and MS was also performed on proteins isolated from cells that were non-transfected and non-infected, non-transfected and infected, transfected and non-infected and transfected and cytochalasin D treated. The data sets were additionally filtered through the CRAPome repository (Mellacheruvu et al., 2013) to remove contaminant proteins from the list. Using this approach, we identified 99 proteins putatively associated to SEPT6 in uninfected cells (**Table 2.1**), and 56 proteins associated with SEPT6 in *Shigella* infected cells (**Table 2.2**). Among the proteins, 31 were identified to associate with SEPT6 in both *Shigella* infected and non-infected control cells; these include SEPT2, SEPT6, SEPT7, SEPT9, and SEPT11. The autophagy markers p62 and LC3B were

observed only in infected cells (**Table 2.1**). The interaction between FLAG-2xStrep-SEPT6 and p62 was confirmed using co-immunoprecipitation experiments (**Figure 2.6B**), consistent with results already observed using SEPT6-GFP HeLa cells (described in **Figure 2.3**).

Based on analysis from the Gene ontology (GO) database (analysis done by Dr. Vanessa Sancho Shimizu), the list of proteins associated with SEPT6 were categorised into 6 groups (**Figure 2.6C**). We observed that 11.0% of proteins associated to SEPT6-tagged complexes in non-infected cells bound to septins in *Shigella*-infected cells are classified as exclusively mitochondrial. By contrast, 21.4% of mitochondrial proteins associated to SEPT6-tagged complexes in *Shigella*-infected cells. A higher percentage of mitochondrial proteins might be the result of reduced recovery of septin-associated proteins, due to a less efficient pull down (Table 2.2). Nevertheless, these data suggested interplay between septins and mitochondria during infection. For this reason, we carried out investigation of septin-mitochondria interactions, described in the next chapter.

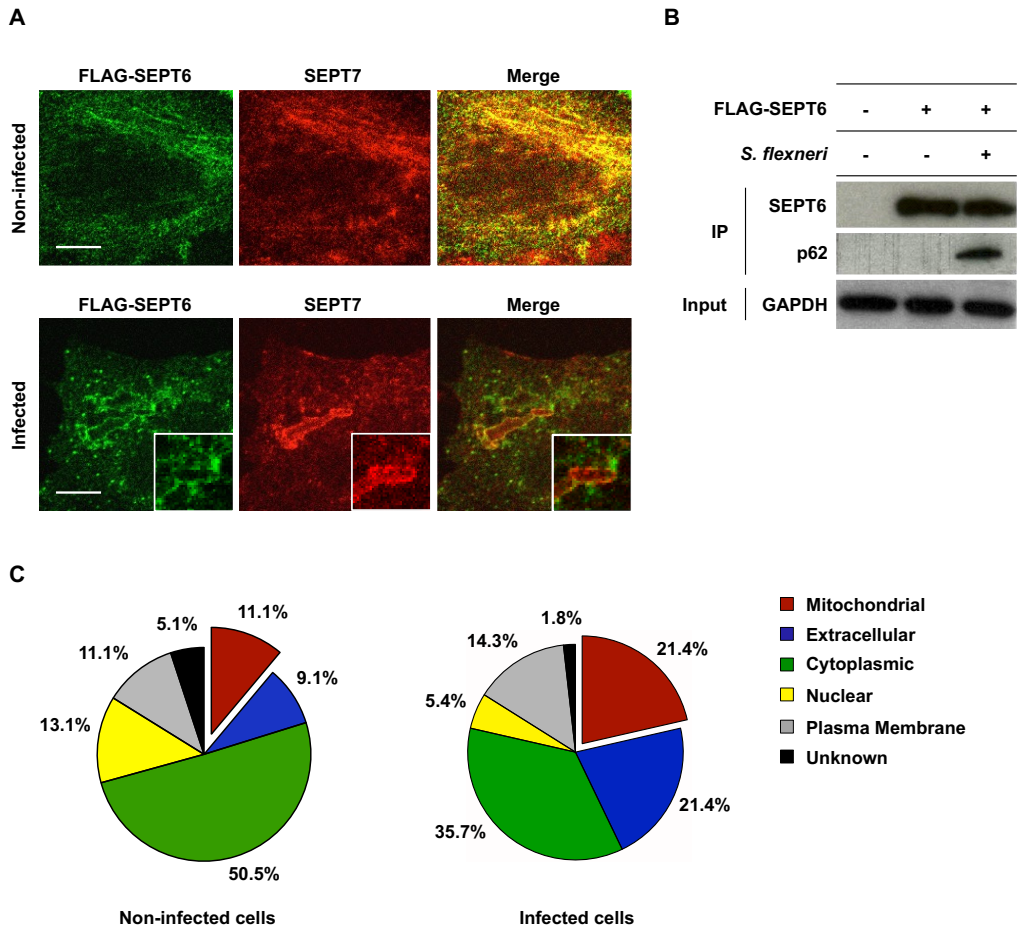

Figure 2.6: Proteomic analysis of proteins enriched at the septin cytoskeleton
A. HeLa cells were transfected with STREP-FLAG SEPT6 for 24 h, then fixed for confocal microscopy and labelled for endogenous SEPT7. Where mentioned, cells were infected with *S. flexneri* AfaI for 4 h. Representative images of non-infected and infected cells. The scale bar represents 5 µm.
B. HeLa cells were transfected with STREP-FLAG SEPT6 for 24 h, infected with *S. flexneri* AfaI for 4 h, harvested, and then tested with Co-IP. Empty vector and/or uninfected HeLa cells were used in parallel as control. Anti-FLAG M2 magnetic beads, 3xFLAG eluent peptides and Strep-Tactin magnetic beads were used to isolate STREP-FLAG SEPT6 from cells. Extracts were than immunoblotted for SEPT6 (50 kDa), GFP (27 kDa) or p62 (62 kDa). The lysates were immunoblotted for GAPDH (37 KDa) as control for cellular protein levels.
C. The protein pulldown experiments identified 99 proteins putatively associated to the septin cytoskeleton in uninfected cells, and 56 proteins putatively associated to the *Shigella*-septin cage. Proteins are categorised into 6 groups based on analysis from the Gene ontology database. See also **Table A2** and **Table A3.**

2.8. Summary

In this chapter we provide evidence that human SEPT7 regulates other septins at the protein level, and propose that its depletion impairs septin complex stability. In line with what described for other septin groups, the inhibition of actin polymerisation limited the recruitment of SEPT7 on septin cages. Possible explanations may lie in interdependence between the assembly of septin ultrastructures and the actin turnover. Mechanistically, we were not able to provide further evidence. However, we show that SEPT7 is essential for septin cage assembly during *Shigella* infection. Quantitative confocal microscopy showed that SEPT7 cages colocalise with the autophagy marker p62, and co-immunoprecipitation showed the interaction of SEPT6 with p62 during *Shigella* infection. To investigate the fate of *Shigella* entrapped in septin cages, we analysed the metabolic activity of bacteria at the level of the single cell. Analysis using IPTG-inducible *Shigella* strains showed that bacteria compartmentalised by SEPT7 cages are less responsive to IPTG compared to *Shigella* not entrapped in cages. Similar results were obtained for *Shigella* colocalising with p62 or not, supporting the fact that septin cages target bacteria to degradation by autophagy. Our quantitative analysis showed that only ~15% of intracellular *Shigella* are entrapped in septin cages. As a result, only a small amount of *Shigella* is effectively targeted to degradation, which justifies the low impact of septins against infection of *Shigella* in a clinic framework. However, the relevance of our results gives reason to further investigate the mechanism of septin assembly in order increase the host ability to restrict bacterial dissemination. Proteomics was then employed to identify novel host determinants that underpin septin cage assembly. Interestingly, MS analysis showed that 24.4% of proteins associated to septins

during *Shigella* infection are classified as exclusively mitochondrial. This suggests an unexpected interplay between septins and mitochondria during *Shigella* infection. The interplay between septins and mitochondria is investigated in the next chapter.

CHAPTER 3: Mitochondria promote septin cage assembly for antibacterial autophagy

3.1. Part I: mitochondria and septin cage assembly

3.1.1. Introduction

The process of septin cage assembly is not fully understood. Septins recognise cellular membrane characterised by micron-scale curvature, including the cleavage furrow, the annulus of spermatozoa, and the phagocytic cup surrounding invasive bacterial pathogens (**Figure 3.1A**) (Lobato-Marquez and Mostowy, 2016, Bridges et al., 2016, Tanaka-Takiguchi et al., 2009). However, a source of membrane for cytosolic septin assembly has not yet been identified. Interestingly, proteomics revealed that 21.4% of proteins associated with septins during infection of *Shigella* are classified as exclusively mitochondrial (Chapter 2). These results suggest that mitochondria may play a role in septin cage assembly.

Mitochondria are highly dynamic organelles that form a network regulated by fission and fusion. Dynamin-related protein 1 (Drp1) is a cytosolic GTPase essential to mediate mitochondrial fission (Bleazard et al., 1999, Smirnova et al., 2001). In the absence of Drp1, mitochondria form elongated tubular networks, with potential effects on cellular development (Hailey et al., 2010, Rambold et al., 2011). By contrast, mitofusin 1 (Mfn1) is a protein required for mitochondrial fusion (Ishihara et al., 2004). In the absence of Mfn1, mitochondria are fragmented and can be targeted to autophagy (Praefcke and

McMahon, 2004). Interestingly, mitochondria have been suggested to provide membrane for the autophagosome biogenesis during starvation (Hailey et al., 2010). In this context, we investigate in this section the role of mitochondria in *Shigella*-septin cage assembly.

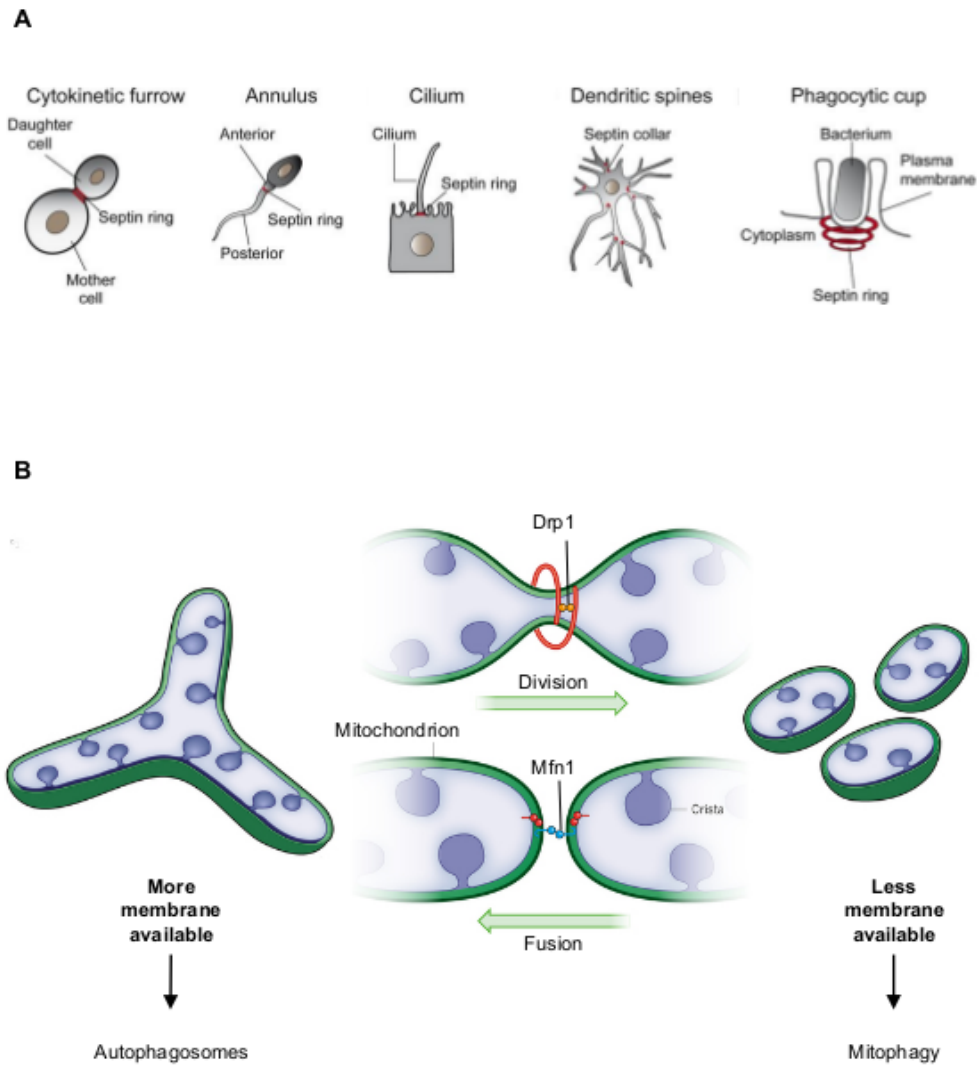

Figure 3.1:
A Morphological hallmarks of eukaryotic cells characterised by micron-scale membrane curvature and septin assembly (From Lobato-Marquez, 2016).
B Schematic for a proposed means by which starvation-induced autophagosomes utilise mitochondrial membrane during biogenesis (Adapted from Friedman, 2014).

3.1.2. Mitochondria closely associate with the *Shigella*-septin cage

Studies have shown a close relationship between septin assembly and phospholipid membranes (Bridges et al., 2016, Tanaka-Takiguchi et al., 2009). Mixing septin complexes with phospholipid-based liposomes *in vitro*, work has shown that septins (i) assemble more efficiently in the presence of phospholipid membrane, and (ii) contribute shape to the phospholipid membranes (Bridges et al., 2016, Tanaka-Takiguchi et al., 2009). More recently, it has been proposed septins recognise micron-scale membrane curvature in eukaryotic cells [1]. Our proteomic analysis has revealed that mitochondrial proteins are associated with septins during *Shigella* infection (Chapter 2). We therefore investigated the relationship between mitochondria and septin assembly.

Use of cytochalasin D is well known to induce septin assembly into rings of ~0.6 μm in diameter (Kinoshita et al., 2002). Uninfected cells were treated with cytochalasin D, and the association of mitochondria to cytosolic septin rings was quantified. Mitochondria localised with septin rings (**Figure 3.2A**), suggesting a link between septin ring assembly and mitochondria. By using confocal microscopy and MitoTracker CMXRos to label mitochondrial membrane, we also observed that mitochondria also closely associate with *Shigella*-septin cages. After 4 h 40 min of *Shigella* infection, quantitative analysis revealed that 80 ± 1.4% of septin cages associated with mitochondria (**Figure 3.2B**).

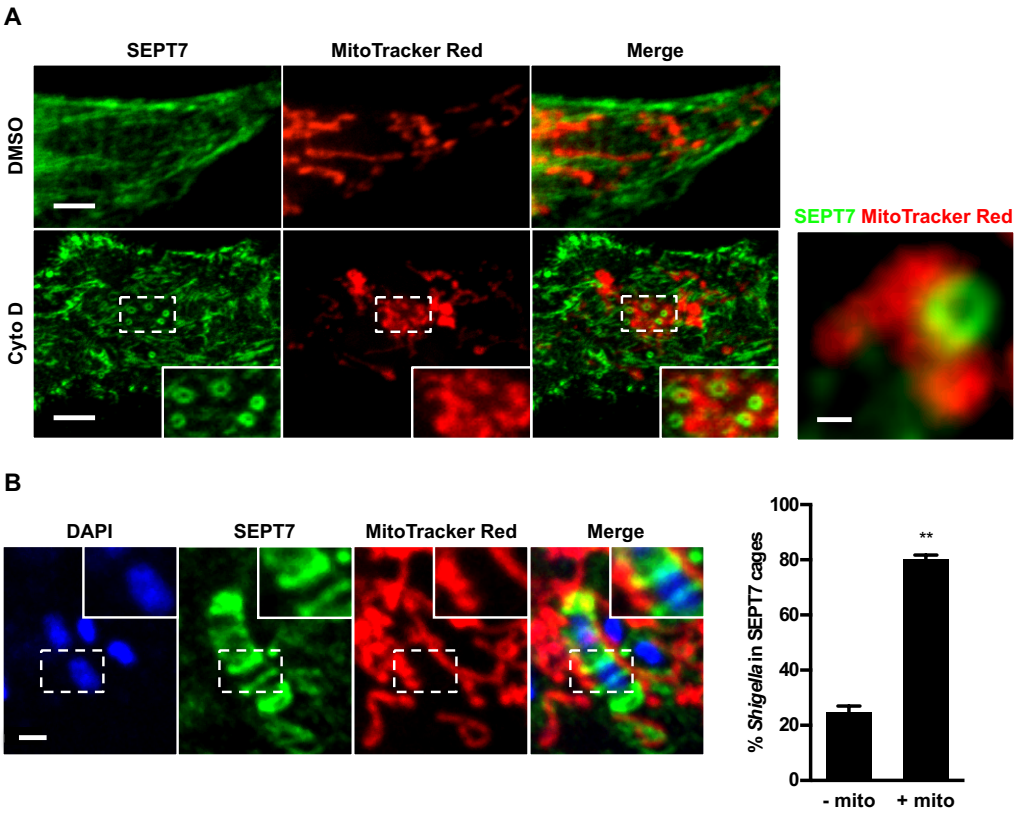

Figure 3.2: Mitochondria associate with septin rings and cages

A HeLa cells were stained with MitoTracker Red CMXRos, treated with DMSO or cytochalasin D for 30 min, then fixed and labelled for endogenous SEPT7 for confocal microscopy. Inset images highlight mitochondria closely associated with septin rings. The scale bar represents 5 µm. The right-most image represents a detail of SEPT7 ring associated to mitochondrial membrane. The scale bar represents 0.5 µm.

B. HeLa cells were infected with *S. flexneri* for 4 h 40 min, labelled with MitoTracker Red CMXRos, fixed and labelled with antibody for endogenous SEPT7 for quantitative confocal microscopy. The scale bar represents 1 µm. Graph represents the mean % ± s.e.m. of SEPT7 cages associated to mitochondria. Unpaired Student's t-test, ** = $p<0.01$, n = 3 biological replicates.

3.1.3. Mitochondria support *Shigella*-septin cage assembly

To investigate the association of mitochondria and septin cages entrapping bacterium we used correlative light-electron microscopy (CLEM). This technique allowed us to locate specific *Shigella*-septin cages by confocal microscopy, and the same region of interest was subsequently observed by transmission electron microscopy (TEM, in collaboration with Mike Hollinshead, University of Cambridge). SEPT6-GFP HeLa cells were seeded on gridded, glass-bottom dishes to specifically localise septin cages during *Shigella* infection (**Figure 3.3A**). Remarkably CLEM showed mitochondria closely associated with *Shigella*-septin cages and distinct from the double-membraned autophagosome surrounding bacterium (**Figure 3.3B**).

Previous work has suggested that mitochondria contribute membrane to the growing autophagosome during starvation (Hailey et al., 2010). In this study, Hailey *et al.* showed that the outer mitochondrial membrane marker YFP-Mito^{cb5}TM, a transmembrane (TM) targeting sequence of an isoform of cytochrome b5 (cb5), colocalised with ATG5 and LC3 during starvation (Hailey et al., 2010). By testing Mito^{cb5}TM in *Shigella* infected HeLa cells, we were not able to show that mitochondria supply membranes to septin cages (**Figure 3.3C**). Instead, live cell imaging using cells expressing mito-BFP revealed that septin rings assemble around *Shigella* at the sites of contact with mitochondria (**Figure 3.3D**). Taken together, these results suggest that mitochondria support septin assembly into the cages that entrap *Shigella*.

A

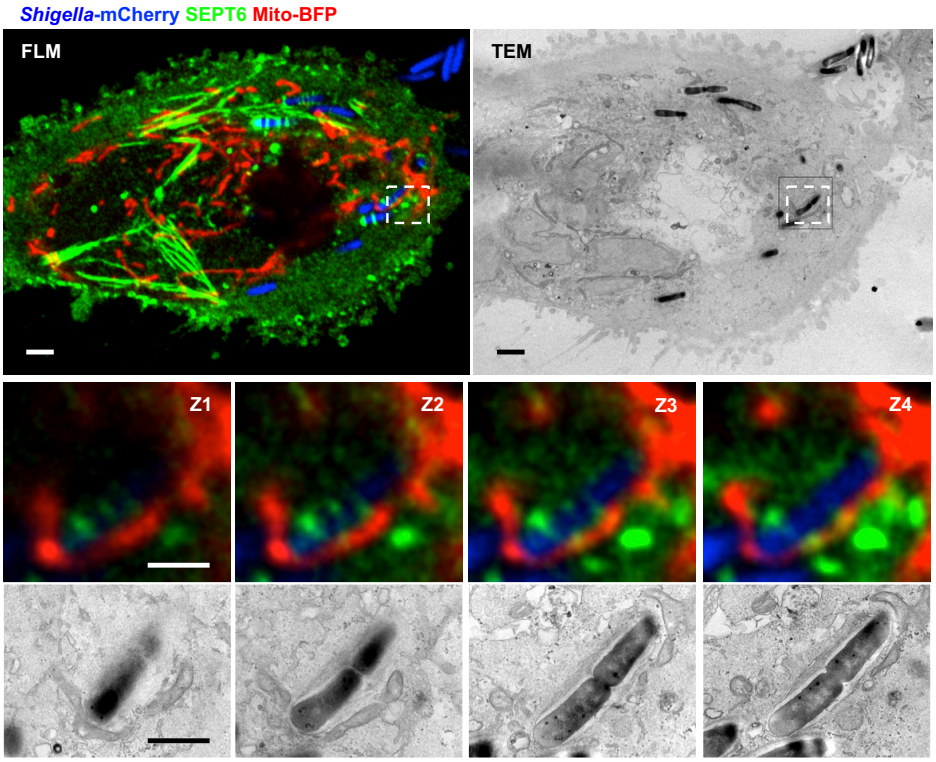
Shigella-mCherry SEPT6 Mito-BFP
FLM
TEM
Z1
Z2
Z3
Z4

B

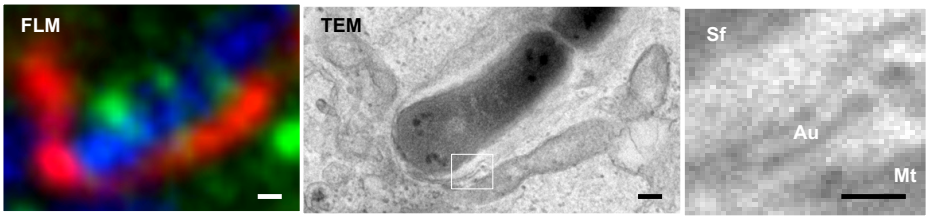
Shigella-mCherry SEPT6-GFP Mito-BFP
FLM
TEM
Sf
Au
Mt

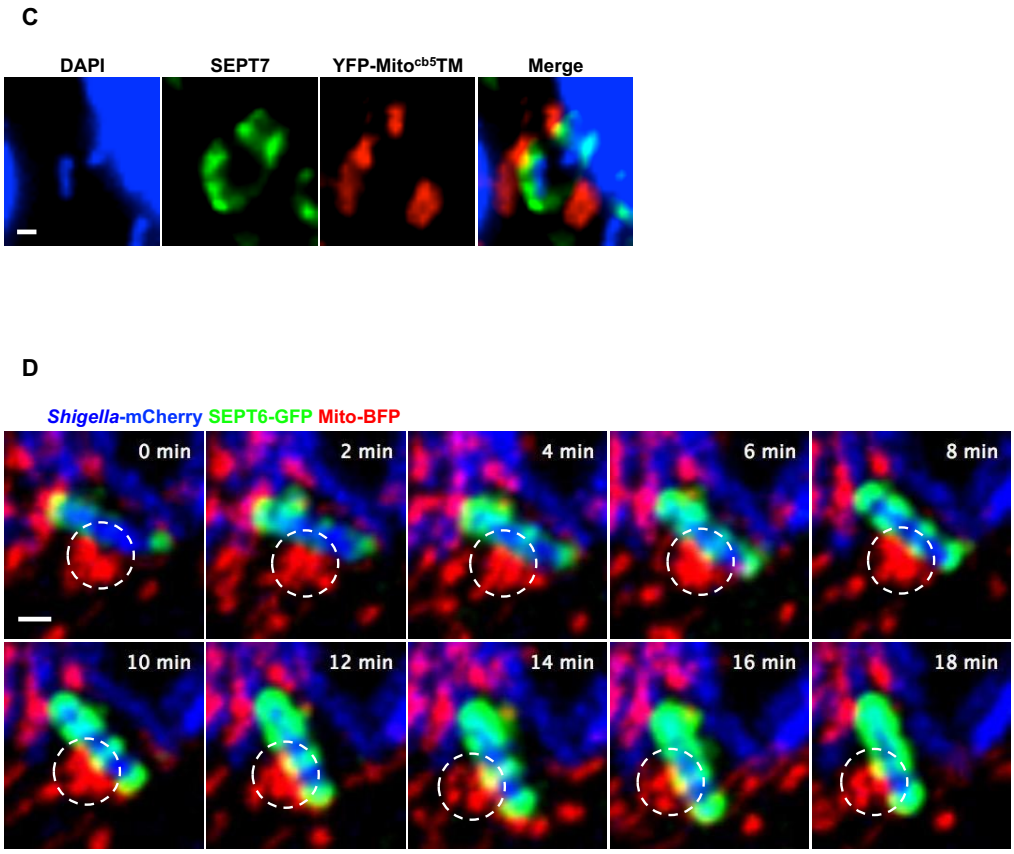

Figure 3.3: Mitochondria support *Shigella*-septin cage assembly

A. HeLa cells stably expressing SEPT6-GFP were transfected with mito-BFP for 24 h, infected with *Shigella*-mCherry for 4 h 40 min, and processed for CLEM. Z-stack (Z1-Z4) series of septin cages were acquired by fluorescent light microscopy (FLM), and then samples were processed for TEM. SEPT6 is shown in green, mitochondria in red, and *Shigella* in blue. The scale bar represents 5 µm. The scale bar in Z-stack (Z1-Z4) series represents 1 µm.

B. HeLa cells stably expressing SEPT6-GFP were transfected with Mito-BFP for 24 h, infected with *Shigella*-mCherry for 4 h 40 min, and processed for CLEM. SEPT6 is shown in green, mitochondria in red, and *Shigella*-mCherry in blue. Septin cages identified by fluorescent light microscopy (FLM) were processed for TEM. In the right-most image is enlarged from the boxed region in the TEM images, bacterium (Sf), double membrane of autophagy (Au) and the mitochondrial membrane (Mt). The scale bar represents 100 nm.

C. HeLa cells were transfected with YFP-Mito^{cb5}TM for 24 h, infected with *S. flexneri* M90T for 4 h 40 min, then fixed and labelled for endogenous SEPT7 for Widefield microscopy. Representative images shown here. The scale bar represents 1 µm.

D. HeLa cells stably expressing SEPT6-GFP were transfected with Mito-BFP for 24 h, then infected with *Shigella*-mCherry for 2 h for live confocal microscopy. Time frame sequence shows a septin cage assembling around *Shigella*. Mitochondria (dashed circle). Each frame was acquired every 2 min. The scale bar represents 1 µm.

3.1.4. What is the role of mitochondrial fission / fusion in septin cage assembly?

To test if septin-mitochondria interactions promote septin cage assembly, siRNA experiments were performed. Given that Drp1 is critical for mitochondrial fission, we depleted Drp1 to generate elongated, tubular mitochondrial networks so that mitochondrial membrane will be more available for septin cage assembly (Hailey et al., 2010, Rambold et al., 2011). Drp1 siRNA treated cells were then infected with *Shigella* for 4 h 40 min. In this case we observed a significant increase in *Shigella*-septin cages (1.4 ± 0.1 fold) (**Figure 3.4**). Drp1 is therefore the first host factor identified that can counteract septin cage assembly during *Shigella* infection. Given that Mfn1 is critical for mitochondrial fusion, we depleted Mfn1 to generate fragmented mitochondria so that mitochondrial membrane will be less available for septin cage assembly (Hailey et al., 2010, Rambold et al., 2011, de Brito and Scorrano, 2008). When Mfn1-depleted cells were infected with *Shigella* for 4 h 40 min, we observed that the number of septin cages is significantly reduced (2.6 ± 0.1 fold; **Figure 3.4**). Together, these findings demonstrate that mitochondria promote septin assembly into the cages that entrap *Shigella* for antibacterial autophagy.

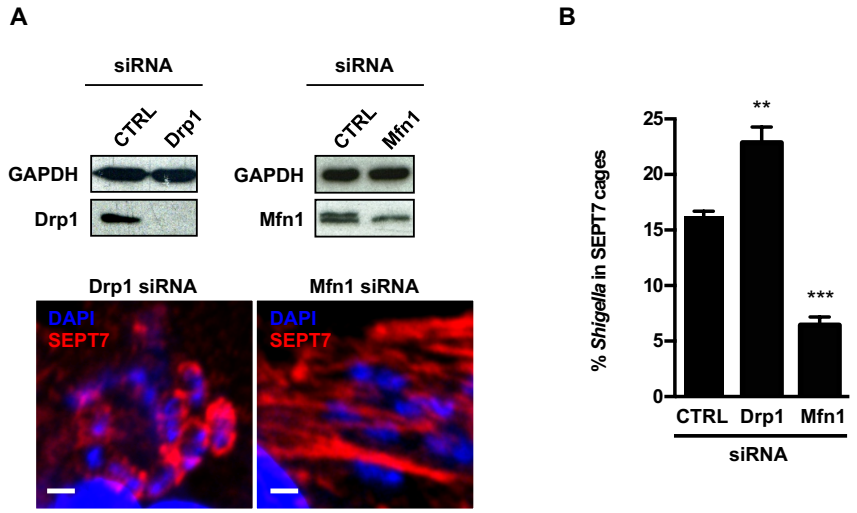

Figure 3.4: Septin-mitochondria interactions are linked to septin cage assembly
HeLa cells were treated with control (CTRL), Drp1, or Mfn1 siRNA for 72 h. (**A**) Whole cell lysates were immunoblotted for Drp1 (81 kDa) or Mfn1 (84 kDa) to show the efficiency of depletion. The anti-Mfn1 antibody generated and extra band of 75 kDa that could be identified as a non-specific binding. GAPDH (37 kDa) was used as loading control. (**B**) siRNA-treated cells were infected with *S. flexneri* for 4 h 40 min, then fixed for microscopy and stained for endogenous SEPT7 for quantitative confocal microscopy. Graph represents the mean % ± s.e.m. of *Shigella* inside SEPT7. Unpaired Student's t-test, ** = p <0.01; *** = p<0.001, n = 4 biological replicates per condition.

3.2. Part II: A new role for septins in mitochondrial fission

3.2.1. Introduction

Mitokinesis is a recently described event in which actin and non-muscle myosin II form an actomyosin ring around the mitochondria to generate a constriction site that facilitates Drp1-mediated fragmentation (Hatch et al., 2014, Korobova et al., 2013, Manor et al., 2015). Septins are well known to regulate the formation and action of the actomyosin ring during cytokinesis at the cleavage furrow (Bridges and Gladfelter, 2015, Renshaw et al., 2014, Glotzer, 2005). Here, septins scaffold the recruitment of proteins necessary to create the driving force for constriction of the plasma membrane that leads to cell division (Proctor et al., 2012, Lee et al., 2012, Pollard, 2010). Moreover, mitochondrial fission defects have been observed *in vivo* in mice knocked out for Sept4 (Kissel et al., 2005). Considering this, we investigated a relationship between septins and mitochondrial dynamics.

Shigella invasion induces mitochondrial fragmentation (Carneiro et al., 2009, Suzuki et al., 2007, Willingham et al., 2007). *Shigella* IcsA is a bacterial transmembrane protein used to polymerise actin for intracellular motility (Goldberg and Theriot, 1995). In addition, actin and non-muscle myosin II are important for *Shigella*-septin cage assembly. Given the role for actomyosin in Drp1-mediated mitochondrial fission (Korobova et al., 2013, Mostowy et al., 2010, Mostowy and Cossart, 2011a, De Vos et al., 2005), we investigated the hypothesis that *Shigella* use mitochondrial fragmentation to escape from septin cage formation.

3.2.2. A role for septins in mitochondrial fission

Experiments using confocal microscopy and SEPT6-GFP HeLa cells revealed that septins localise to sites of mitochondrial fission (**Figure 3.5A**). We then employed electron microscopy (EM) to see high resolution of septins-mitochondria interaction (in collaboration with Michael Hollinshead). To visualise septin filament by EM, a novel protocol was developed using diaminobenzidinetetrahydrochloride (DAB)- haptoglobin related protein (HPR) immunolabelling for SEPT7, and this provided further evidence for the recruitment of septins to sites of mitochondrial fission (**Figure 3.5B**). To investigate the interplay between septins and mitochondria, live-cell imaging experiments and super resolution microscopy was performed (in collaboration with Sina Krokowski, who acquired the images, and Dr. Ricardo Henriques, who helped developing imaging algorithm). HeLa cells stably expressing SEPT6-GFP and labelled with MitoTracker Red CMXRos were visualised using a super-resolution optical fluctuating imaging (SOFI)- based method (**Figure 3.5C**). Time lapse imaging of one super resolution frame every 30 seconds was performed, and then super resolution reconstructions were generated using a SOFI-based algorithm on Fiji (Gustafsson et al., 2016). Using this, septins were observed to induce constriction and fission of mitochondria. Together, fixed and live cell microscopies suggest that septins coordinate timing and position of mitochondrial fission.

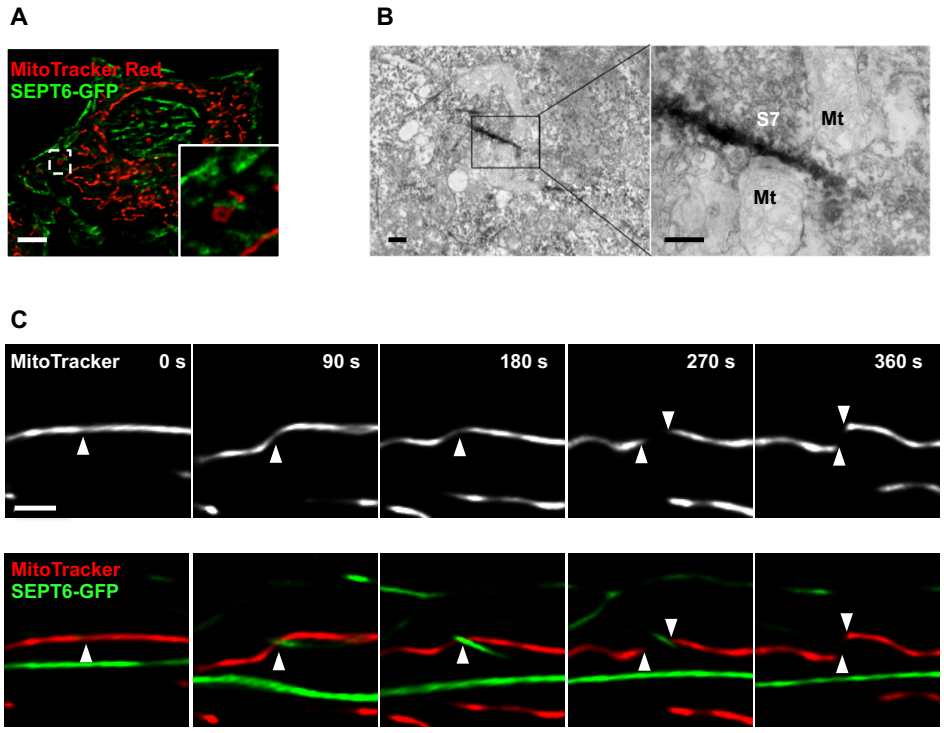

Figure 3.5: A role for septins in mitochondrial fission

A. HeLa cells expressing SEPT6-GFP were stained with MitoTracker Red CMXRos, and fixed for confocal microscopy. Inset image highlights location of septins at sites of mitochondrial fission. The scale bar represents 5 μm.

B. HeLa cells were fixed and labelled with antibody against SEPT7 and secondary antibody coupled to HRP, and processed for TEM. The right image is enlarged from the boxed region in the TEM image, SEPT7 (S7) filament (labelled in black), and mitochondrial (Mt) fission site. The scale bar represents 100 nm.

C. HeLa cells expressing SEPT6-GFP were stained with MitoTracker Red CMXRos for live SOFI-based super resolution microscopy. Each image was reconstructed from 100 raw TIRF frames using a custom made SOFI-based algorithm. Arrows highlight SEPT6 association with location of mitochondrial fission. The scale bar represents 1 μm.

3.2.3. SEPT7 colocalises with Drp1 at sites of mitochondrial fission

Drp1 assembles into higher-order oligomers for mitochondrial fission. Using confocal microscopy we observed that Drp1 localises with SEPT7 at sites of mitochondrial fission (**Figure 3.6A**). To investigate the relationship between septins and Drp1-mediated fission, SEPT7 was targeted to mitochondria using an ActA-SEPT7-mRFP fluorescent construct (gift from Dr Elias Spiliotis). In brief, ActA-SEPT7-mRFP expresses a fusion protein of SEPT7 tagged to the mitochondrial targeting sequence from *Listeria* effector ActA, which displays characteristic motifs of mitochondrial import targeting signals (Pistor et al., 1994). Observations made by using fluorescent mean-intensity profiling showed that ActA-SEPT7-mRFP colocalised with both Drp1 and SEPT7 (**Figure 3.6B**), and also mitochondria fragments (**Figure 3.6C**). When quantified, Pearson's correlation coefficient analysis revealed that mitochondria colocalising with ActA-SEPT7-mRFP associated more with Drp1 compared to mitochondria in cells not expressing the ActA-SEPT7-mRFP construct (**Figure 3.6D**). Together, these results support a role for septins in Drp1-mediated mitochondrial fission.

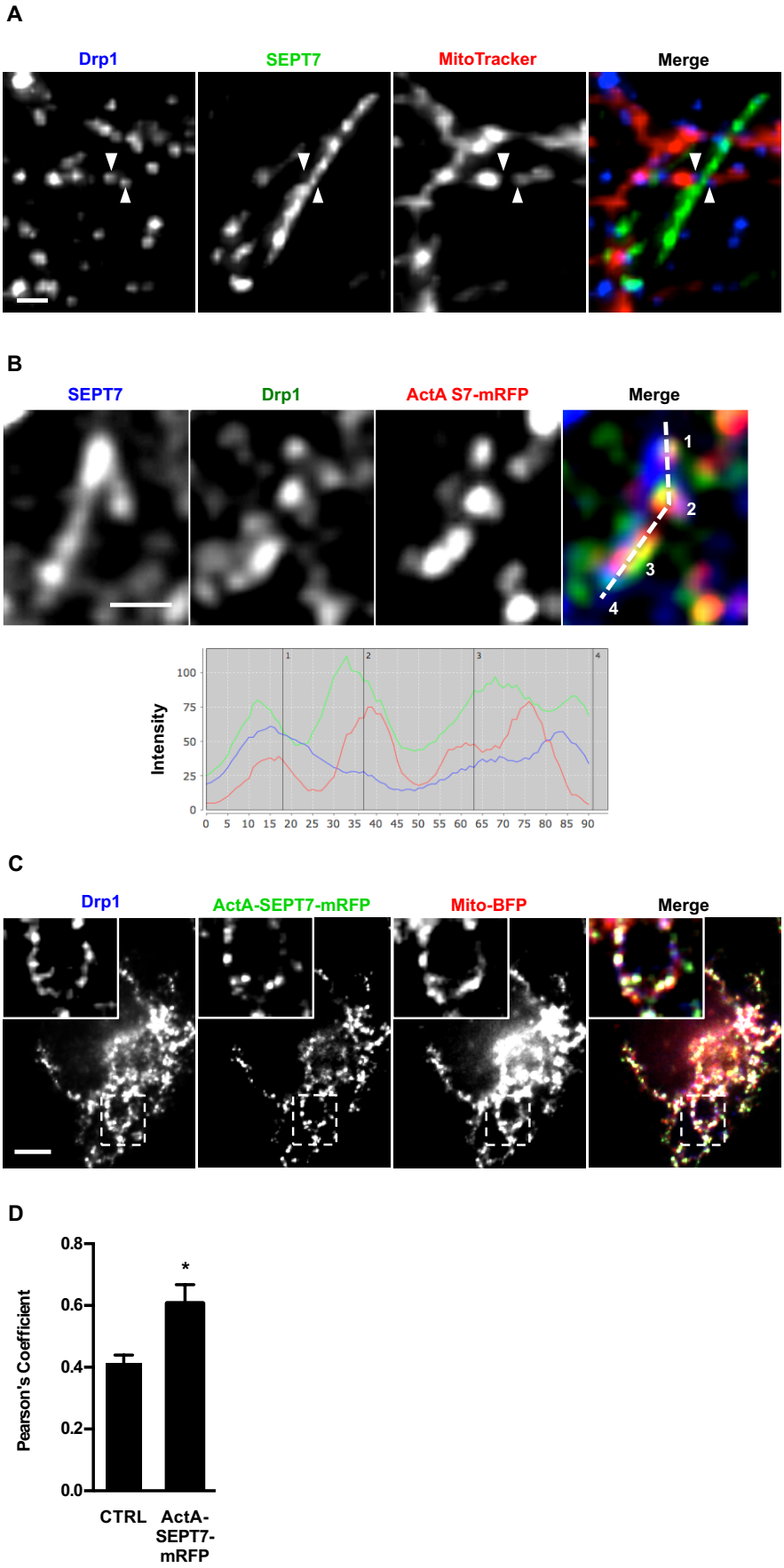
A
Drp1
SEPT7
MitoTracker
Merge
B
SEPT7
Drp1
ActA S7-mRFP
Merge
1
2
3
4
Intensity
100
75
50
25
0
0 5 10 15 20 25 30 35 40 45 50 55 60 65 70 75 80 85 90
C
Drp1
ActA-SEPT7-mRFP
Mito-BFP
Merge
D
Pearson's Coefficient
0.8
0.6
0.4
0.2
0.0
*
CTRL
ActA-SEPT7-mRFP

Figure 3.6: SEPT7 colocalises with Drp1 at sites of mitochondrial fission
A. HeLa cells were labelled with MitoTracker Red CMXRos, fixed for microscopy, and labelled with antibodies to SEPT7 and Drp1. Arrows highlight one example of Drp1 and SEPT7 closely associated with a site of mitochondrial fission. The scale bar represents 1 μm.
B. HeLa cells were transfected with Mito-BFP and ActA-SEPT7-mRFP, fixed and labelled with antibody to Drp1 for confocal microscopy. The scale bar represents 1 μm. Representative graph of fluorescent mean-intensity profile shown here.
C. HeLa cells were transfected with Mito-BFP and ActA-SEPT7-mRFP, fixed and labelled with antibody to Drp1 for microscopy. The scale bar represents 5 μm. Inset images highlight Drp1 and SEPT7 associated with sites of mitochondrial fission.
D. HeLa cells were transfected with Mito-BFP and ActA-SEPT7-mRFP, fixed and labelled with antibody to Drp1 for quantitative microscopy. Unpaired Student's t-test, * = $p<0.05$, n = 3 biological replicates.

3.2.4. Drp1 interacts with septins to enhance mitochondrial fission

The role of septins in mitochondrial fission was investigated by measuring the length of mitochondria in septin-depleted cells. HeLa cells were treated with siRNA sequence specific for septins (SEPT2, SEPT7, or SEPT9), Drp1, or SEPT7 + Drp1. The depletion of protein expression was assessed by western blot (**Figure 3.7A**). siRNA treated cells were then stained for MitoTracker Red (CMXRos**)**, and mitochondria length was measured (**Figure 3.7B, 3.7C**)**.** In the absence of SEPT7, mitochondria were significantly longer than in control cells (6.4 ± 0.6 μm versus 3.5 ± 0.2 μm). A similar increase was observed in the absence of SEPT2 (5.1 ± 0.1 μm) or SEPT9 (5.9 ± 0.1 μm). In agreement with expectations from the literature (Korobova et al., 2013, Korobova et al., 2014), similar values were quantified in cells without Drp1 versus control cells (6.2 ± 0.3 μm) (**Figure 3.7C)**. The simultaneous depletion of SEPT7 and Drp1 did not lead to further increase in mitochondria length as compared to single depletion experiments, suggesting that SEPT7 and Drp1 are acting in the same mitochondrial fission pathway (**Figure 3.7C**). To test for septin-Drp1 interactions, co-immunoprecipitation experiments were performed on HeLa cells expressing SEPT6-GFP (in collaboration with Julia Pfanzelter, Francis Crick Institute). Co-immunoprecipitation experiments showed that SEPT6-GFP interacts with other septins (SEPT2, SEPT7) and Drp1 (**Figure 3.7D**).

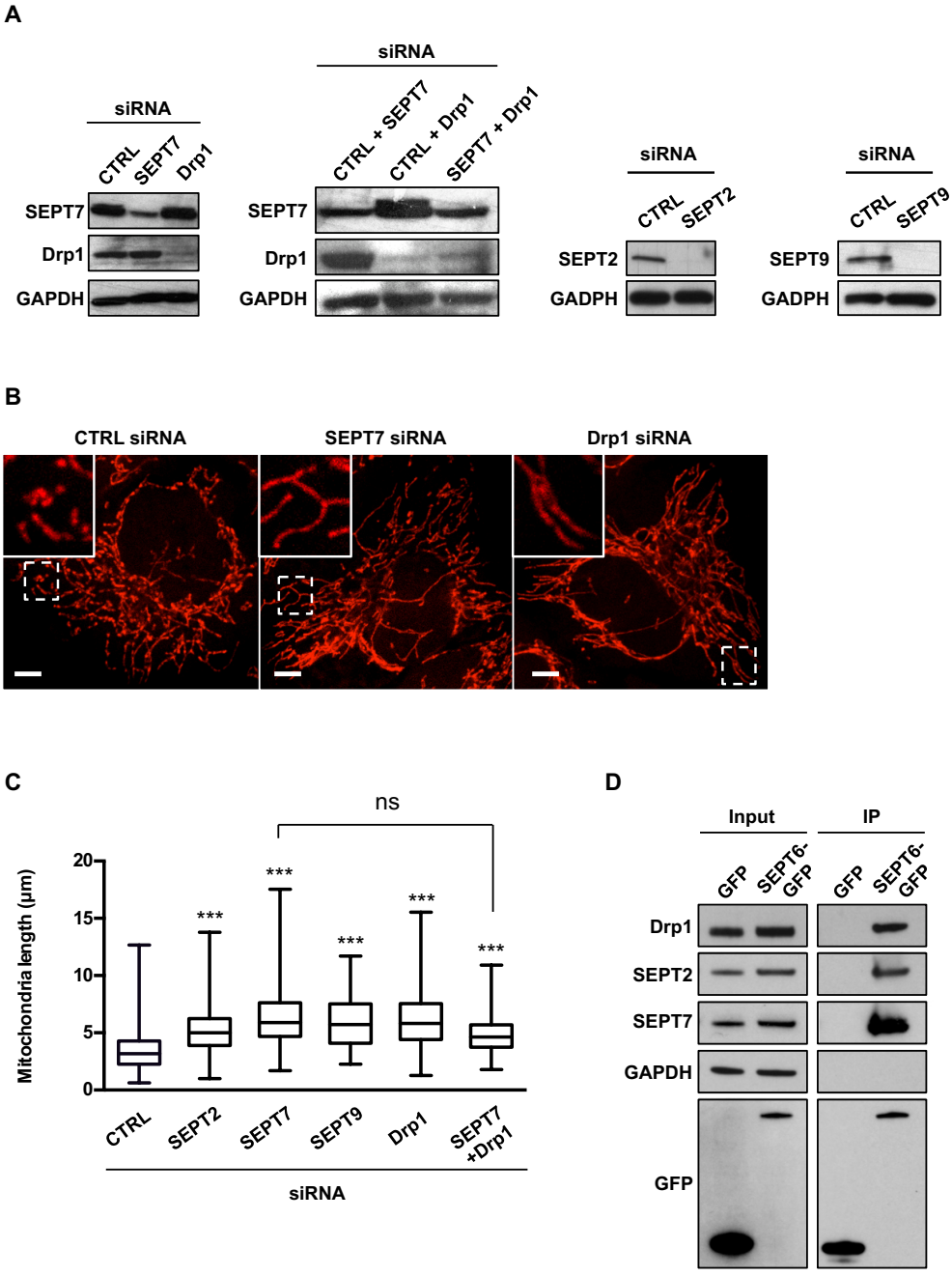

Figure 3.7: Drp1 interacts with septins to enhance mitochondrial fission

A. HeLa cells were treated with control (CTRL), SEPT2, SEPT7, SEPT9, Drp1, or SEPT7+Drp1 siRNA for 72 h. Whole cell lysate of siRNA-treated cells were immunoblotted for indicated antibodies to show the efficiency of siRNA depletion. GAPDH was used as a loading control.

B. HeLa cells were treated with control (CTRL), SEPT7, or Drp1 siRNA for 72 h, labelled with MitoTracker Red CMXRos, and fixed for confocal microscopy. The scale bar represents 5 µm.

C. HeLa cells were treated with control (CTRL), SEPT2, SEPT7, SEPT9, Drp1, or SEPT7+Drp1 siRNA for 72 h, labelled with MitoTracker Red CMXRos, and fixed for

quantitative confocal microscopy. Graph represents the distribution in length (µm) ± s.e.m. of mitochondria in siRNA-treated cells (analysis of at least 349 measurements per biological replicate). Two-way ANOVA, *** = $p<0.001$, ns = non significant, n = 3 biological replicates per condition.

D. HeLa cells stably expressing SEPT6-GFP were harvested, and then tested with Co-IP. HeLa cells expressing GFP were used in parallel as control. GFP-trap magnetic agarose beads were used to isolate SEPT6-GFP from cells, and extracts were immunoblotted for Drp1 (81 kDa), SEPT2 (41 KDa), SEPT7 (49 kDa), or GFP (27 kDa). The lysates were immunoblotted for GAPDH (37 kDa) as control for cellular protein levels.

3.2.5. Septins stabilise phosphorylated Drp1 to mitochondria

The activity of Drp1 is regulated by the phosphorylation of specific serine residues. In particular, phosphorylation of serine 616 of Drp1 (P-Drp1) is required for mitochondrial fission (Chang and Blackstone, 2010, Rambold et al., 2011). Our data has shown that septins influence the recruitment of Drp1 to the sites of mitochondrial fission. The depletion of SEPT7 does not significantly affect levels of Drp1 or Drp1 S616 phosphorylation (**Figure 3.8A**). However, levels of Mfn1 are significantly increased in the absence of SEPT7 (1.7 ± 0.1 fold; **Figure 3.8A**). These results are in agreement with elongated mitochondria induced by the depletion of SEPT7.

Pearson's coefficient analysis revealed that the co-localisation of P-Drp1 to mitochondria is significantly decreased in SEPT7-depleted cells as compared to control cells (**Figure 3.8B**). By contrast, the intensity of Mfn1 labelling along mitochondria is significantly increased in SEPT7-depleted cells as compared to control cells (**Figure 3.8C**). Together, these data suggest that septins stabilise the active form of Drp1 (i.e. P-Drp1) to the mitochondria and enable fission.

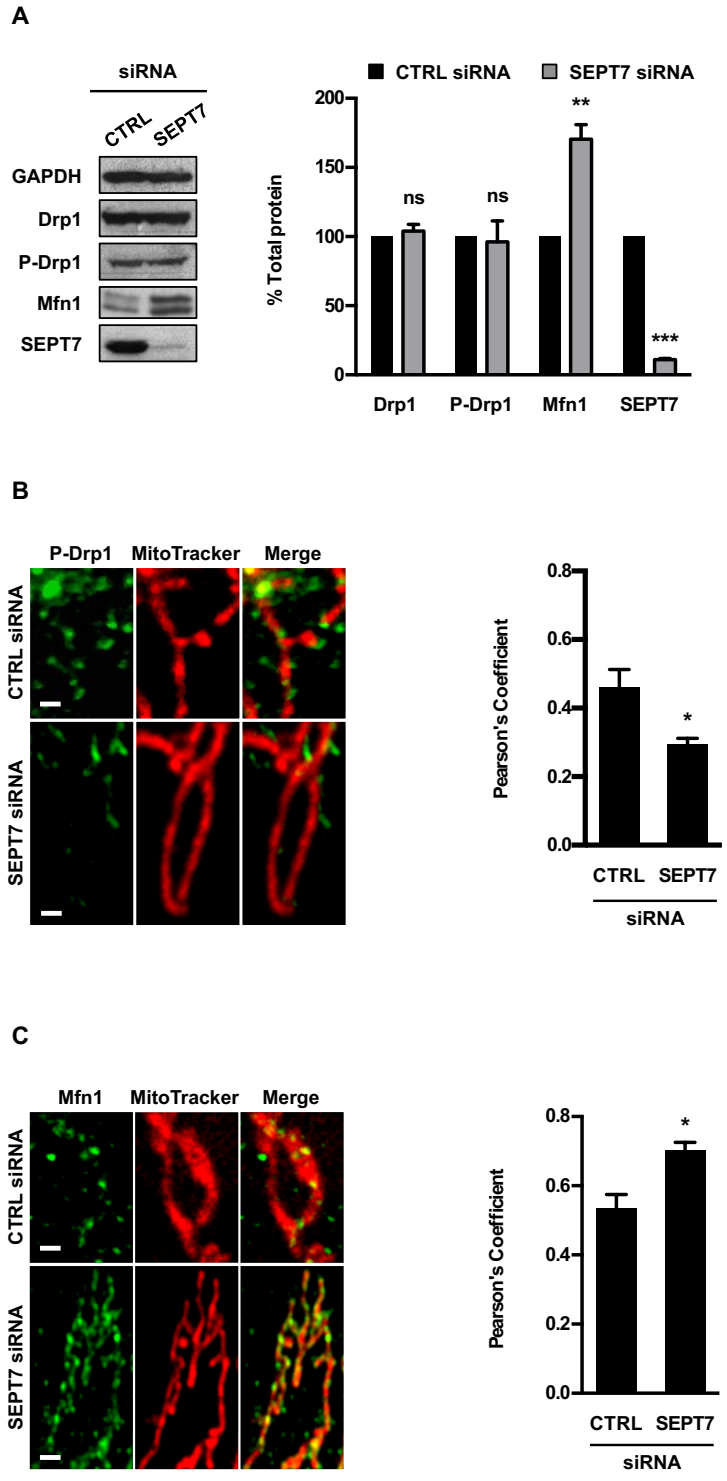

Figure 3.8: Septins facilitate the recruitment of the phosphorylated form of Drp1 to the mitochondria

A. HeLa cells were treated with control (CTRL) or SEPT7 siRNA for 72 h, and whole cell lysates were immunoblotted for SEPT7 (49 kDa), Drp1 (81 kDa), phosphorylated Drp1 (P-Drp1, 82 kDa), or Mfn1 (84 kDa). GAPDH (37 kDa) was used as loading control. Graph represents the mean % ± s.e.m. of the relative amount of Drp1, P-Drp1,

Mfn1, or SEPT7 proteins quantified by densitometry. Unpaired Student's t-test, ns = non-significant; ** = $p<0.01$, *** = $p<0.001$, n = 3 biological replicates per condition.
B. HeLa cells were treated with control (CTRL) or SEPT7 siRNA for 72 h, labelled with MitoTracker Red CMXRos, then fixed and labelled for endogenous P-Drp1 for quantitative confocal microscopy. Representative images shown here. The scale bar represents 1 μm. The co-localisation of P-Drp1 to mitochondria was significantly decreased as compared to control cells as measured by Pearson's correlation coefficient ± s.e.m. (analysis of at least 250 cells per biological replicate). Unpaired Student's t-test, * = $p<0.05$, n = 5 biological replicates.
C. HeLa cells were treated with control (CTRL) or SEPT7 siRNA for 72 h, labelled with MitoTracker Red CMXRos, then fixed and labelled for endogenous Mfn1 for quantitative confocal microscopy. Representative images shown here. The scale bar represents 1 μm. The co-localisation of Mfn1 to mitochondria was significantly increased as compared to control cells as measured by Pearson's correlation coefficient ± s.e.m. (analysis of at least 250 cells per biological replicate). Unpaired Student's t-test, * = $p<0.05$, n = 5 biological replicates.

3.2.6. *Shigella* fragment mitochondria to counteract septin cage entrapment

The role of mitochondrial fission was then investigated in the septin caging against *Shigella.* Live cell imaging was performed in Mfn1-depleted cells, which are characterised by a hyper-fissed mitochondrial network. In this case we did not observe septin cage formation. In agreement with septin cage formation dependent upon fused mitochondria, we did not observe *Shigella*-septin cages when targeting SEPT7 to mitochondria using the ActA-SEPT7-mRFP construct. By contrast, we showed using Drp1-depleted cells that non-fragmented, tubular mitochondria support septin cage assembly (**Figure 3.9A**). Next, we analysed the metabolic activity of *Shigella* entrapped by septin cages in Drp1-depleted cells. In agreement with a role for septin cages in the restriction of bacterial replication (Chapter 2), these results showed that 33.4 ± 1.7 % of *Shigella* entrapped in SEPT7 cages are metabolically active (**Figure 3.9B**). Together, these findings indicate that the assembly and lethal action of septin cage assembly are promoted by non-fragmented mitochondria.

Work using *Shigella* has played a key role in the discovery that pathogens can modulate mitochondria to promote survival or death of the host cell (Carneiro et al., 2009, Suzuki et al., 2007, Willingham et al., 2007). *Shigella* infection of non-myeloid cells activates a pathway dependent on Binip3 and cyclophilin D, two regulators of mitochondrial permeability during oxidative stress. As a result, mitochondria lose inner membrane potential, leading to mitochondrial damage and necrotic cell death (Carneiro et al., 2009). In addition, *Shigella* can induce mitochondrial fragmentation to survive and spread from cell-to-cell (Lum and Morona, 2014). We hypothesised that *Shigella* might promote

mitochondrial fragmentation as a mechanism to avoid septin cage entrapment. Consistent with this hypothesis, quantitative microscopy revealed that *Shigella* compartmentalised by septin cages associated with mitochondria, that is 2.2 ± 0.1 fold longer than mitochondria surrounding cytosolic *Shigella* lacking septin cages **(Figure 3.9C**). Cytosolic *Shigella* express the effector IcsA to polymerise actin for intracellular motility (Goldberg and Theriot, 1995). Experiments using *Shigella* ΔIcsA showed that mitochondria surrounding these bacteria are no different than mitochondria from non-infected cells, and are not as fragmented as in cells infected with wild type *Shigella* (**Figure 3.9D**). These data strongly suggest that *Shigella*-mediated actin polymerization induces mitochondrial fragmentation as a mechanism to counteract septin cage assembly. The role of Drp1 in this process awaits investigation.

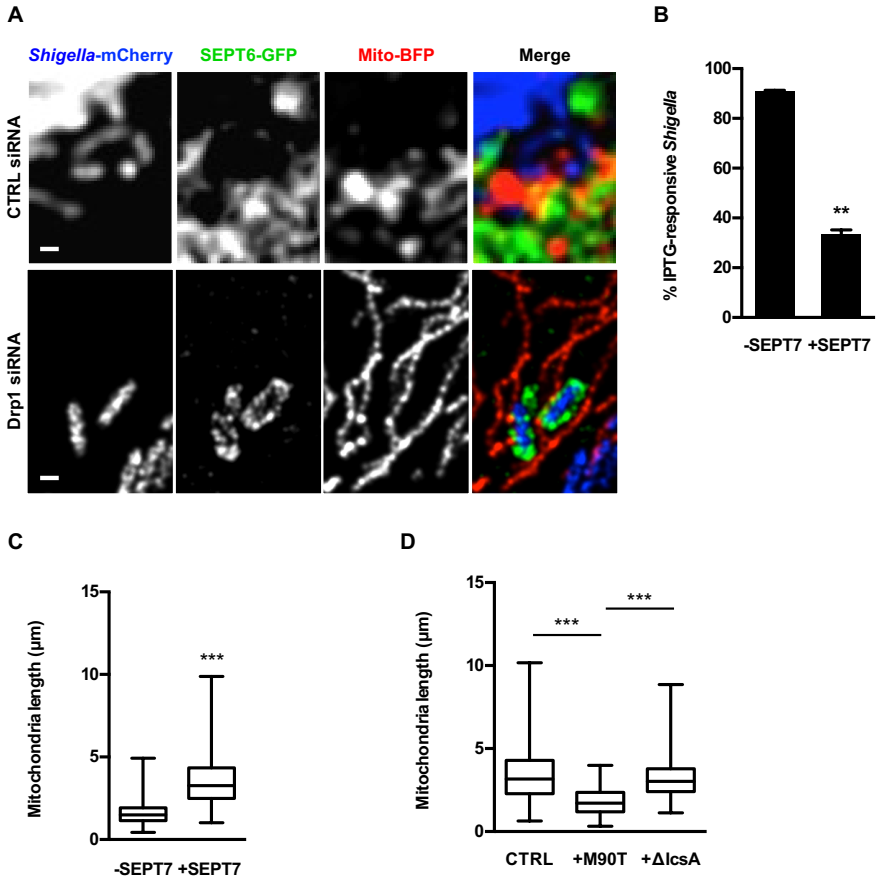

Figure 3.9: *Shigella* fragment mitochondria to counteract septin cage entrapment

A. HeLa cells stably expressing SEPT6-GFP were treated with CTRL or Drp1 siRNA for 72 h, transfected with mito-BFP 24 h, and then infected with *S. flexneri*-mCherry for 2 h for live-cell confocal microscopy. Representative image shows interplay between two *Shigella*-septin cages and fused mitochondria. The scale bar represents 1 µm.

B. HeLa cells were treated with Drp1 siRNA for 72 h, and then infected with x-light *Shigella* mCherry for 4 h 40 min for quantitative confocal microscopy. IPTG was added 30 min prior to fixation, and then samples were labelled with antibody for SEPT7. Graph represents mean % ± s.e.m. of *Shigella* responding to IPTG outside (-) or inside (+) SEPT7 cages. Student's t-test, ** = $p<0.01$, n = 3 biological replicates.

C. HeLa cells were infected with *S. flexneri* M90T for 4 h 40 min, labelled with MitoTracker Red CMXRos, and fixed for quantitative confocal microscopy. Boxplots show the length of mitochondrial (µm) ± s.e.m. surrounding *Shigella* outside (-) or inside (+) SEPT7 cages (analysis of at least 395 measurements per biological replicate). Unpaired Student's t-test; *** = $p<0.001$, n = 3 biological replicates.

D. HeLa cells were either kept uninfected as a control or were infected with *S. flexneri* M90T or *S. flexneri* ΔIcsA for 4 h 40 min. Samples were labelled with MitoTracker Red CMXRos, and fixed for quantitative confocal microscopy. Boxplots show length of mitochondria (µm) ± s.e.m. in uninfected cells (CTRL), surrounding *S. flexneri* M90T (+M90T) or *S. flexneri* ΔIcsA (+ΔIcsA) (analysis of at least 750 measurements per biological replicate). Unpaired Student's t-test; *** = $p<0.001$, n = 3 biological replicates per condition.

3.3. Summary

Proteomic analysis revealed a list of mitochondrial proteins associated to the *Shigella*-septin cage, and suggested a role for septin-mitochondria interactions during bacterial infection. Septin assemblies recognise micron scale membrane curvature, and septin assembly is membrane facilitated (Bridges et al., 2016, Tanaka K, 1991). Results from section I of this chapter showed that mitochondria support septin cage formation for anti-*Shigella* autophagy, and identified Drp1 as a novel determinant that limits septin cage assembly.

Use of siRNA and a variety of cutting edge microscopy techniques identified a new role for septins in Drp1-mediated mitochondrial fission. In section II we showed that Drp1 and septins can interact with each other, and that the targeting of SEPT7 to mitochondria increased Drp1-mediated mitochondrial fragmentation. In agreement with septins having a role in the recruitment of Drp1 to mitochondria for fission, SEPT7 depletion reduced the recruitment of P-Drp1 around mitochondria. Although Pearson's analysis from co-localisation experiments are in line with other observations, a dispute may be raised by the use of anti-phospho antibodies for quantitative microscopy. Epitope on phosphorylated proteins may not be always accessible to the antibody against phosphorylated amino acids. Finally, results showed that actin-polymerizing *Shigella* fragment mitochondria in order to counteract septin cage assembly. Collectively, these results show that mitochondria promote septin cage assembly for antibacterial autophagy, and *Shigella* employ mitochondrial fragmentation to avoid entrapment by septin cages.

CHAPTER 4: The exploitation of host cell metabolism by intracellular *Shigella* is mediated by septins

4.1. Introduction

Previous work has established a close relationship between septins and autophagy, showing that septin cages are dependent upon the recruitment of autophagy markers, including p62 and NDP52 (Mostowy et al., 2011b). Septin-autophagy interactions were confirmed in Chapter 2, where results showed that septin cages serve as mechanism of host defence that targets *Shigella* to degradation by autophagy. However, work so far has strictly focused on bacteria entrapped by septin cages which represents ~15% of intracellular *Shigella*. On the other hand, the impact of septins or autophagy on the fate of intracellular bacteria not entrapped septin cages, which represents ~85% of intracellular *Shigella*, remains to be established.

Cytosolic bacteria have been shown to trigger autophagy through host cell starvation (Tattoli et al., 2012, Steele et al., 2015). However, the role of host cell starvation on bacterial survival remains unclear (Popp et al., 2015, Prentice et al., 2007, McConville, 2014, Steeb et al., 2013). Recent studies have described the ability of some bacterial pathogens, including *F. tularensis* and *Salmonella*, to harvest autophagy-derived nutrients for intracellular growth (Tattoli et al., 2012, Steele et al., 2013). In the case of *F. tularensis*, these bacteria induce non-canonical autophagy and harvest amino acids as carbon source for intracellular replication (Steele et al., 2013, Chong et al., 2012). In the case of *Salmonella*, these bacteria regulate starvation-induced autophagy

and escape autophagy-mediated degradation by recruiting mammalian target of rapamycin (mTOR) to the SCV (Sancak et al., 2008, Sancak et al., 2010). Interestingly, starvation-induced autophagy triggered during *Salmonella* infection is caused by membrane damage and similarly to *Salmonella*, cytosolic *Shigella* triggers starvation induced autophagy after rupturing membrane of the phagocytic vacuole (Tattoli et al., 2012). Although *Salmonella* has been shown to transiently induce AA starvation, *Shigella* can induce long lasting AA starvation (Tattoli et al., 2012). The role of starvation induced autophagy in the restriction or promotion of bacterial replication remains to be fully defined, and is likely to be bacterial dependent.

A recent study performed metabolomics and revealed that intracellular *Shigella* is able to obtain nutrients by redirecting host metabolites derived from glycolytic pathways (Kentner et al., 2014). Although infected cells maintained normal glycolytic activity, the output of this metabolic pathway was mostly acetate instead of pyruvate and lactate. As pyruvate is a high-energy carbon source, *Shigella* uptake pyruvate to produce acetate and ATP to enable intracellular replication (**Figure 4.1**) (Kentner et al., 2014). These metabolomics data show that *Shigella* can hijack host cell metabolism to replicate within the host cell.

During my PhD, a link between septins and the metabolic activity of *Shigella* entrapped in septin cages has been established (Chapter 2). In particular, we showed that higher proportion of bacteria outside the septin cage are metabolically active then bacteria inside the septin cage, demonstrating that septins have a role in the restriction of bacterial replication (Chapter 2). In this chapter, we investigated the role of septins and autophagy on the fate of

intracellular bacteria not compartimentalised by septin cages. We studied the relationship between septins, starvation-induced autophagy, and host cell metabolism to investigate their impact on the survival of intracellular *Shigella*.

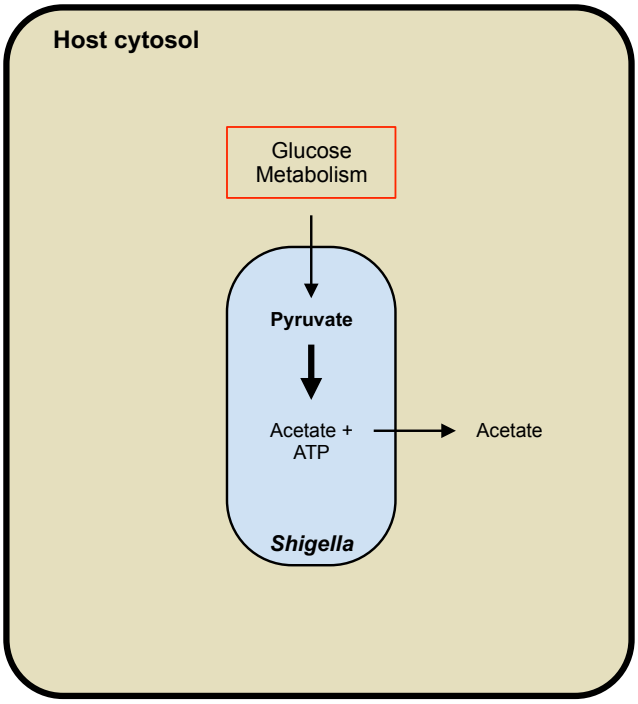

Figure 4.1: Metabolic overview of *Shigella*-infected cells.
During infection of HeLa cells, *Shigella* takes up glucose-derived pyruvate from the host cell cytoplasm and converts it to acetate. By hijacking host cell metabolism, *Shigella* gathers high-energy nutrients to benefit intracellular replication.

4.2. Septins and autophagy are required for the proliferation of cytosolic *Shigella* not entrapped in septin cages

To test the role of septins and autophagy on *Shigella* intracellular replication at the population level, gentamycin survival assays with siRNA-treated cells were employed. HeLa cells were transfected with siRNA sequences specific for SEPT2, SEPT7, SEPT9, p62 or NDP52 for 72h, and the level of protein depletion was assessed by western blot (**Figure 4.2A**). To address bacterial intracellular replication over time, siRNA-treated cells were infected with *Shigella* M90T for 1 h 40 min, 2 h 40 min or 5 h 40 min at 100:1 MOI. Cells were lysed, plated, and counted the next day. To investigate intracellular replication (and not host cell invasion), bacterial counts at 2 h 40min or 5 h 40 min results were normalized to bacterial counts at the earliest time point tested (i.e.1 h 40 min which represents bacterial entry, **Figure 4.2B, 4.2C**). Two different siRNA sequences for SEPT7 (SEPT7 siRNA-1 and SEPT7 siRNA-2) were used. Surprisingly, SEPT7 depletion resulted in 4.4 ± 1.2 or 2.1 ± 0.3 fold, respectively, less *Shigella* intracellular replication after 5 h 40 min (**Figure 4.2B**). Similar results were obtained in cells depleted for SEPT2 (1.8 ± 0.4 fold) or SEPT9 (1.7 ± 1.1 fold), supporting the hypothesis that septins can regulate the intracellular replication of *Shigella*.

Autophagy can promote or restrict bacterial replication (Yu et al., 2014, Mostowy, 2013, Sirianni and Mostowy, 2014). Works using *F. tularensis, Salmonella, S. aureus,* or *Listeria* have shown that non-canonical autophagy can benefit the replication of some intracellular pathogens (Birmingham et al., 2008, Cemma and Brumell, 2012, Mestre et al., 2010, Yu et al., 2014, Steele et al., 2013). In the case of *Salmonella*, cytosolic bacteria replicate when associated with p62 and/or LC3B, and bacterial replication significantly

decreased when autophagy components were depleted (Yu et al., 2014). In the case of *Shigella*, cytosolic bacteria also replicate less after 5 h 40 min when cells are depleted of p62 (3.7 ± 1.1 fold-change) or NDP52 (2.6 ± 0.4 fold-change) (**Figure 4.2C**). These data suggest that replication of intracellular *Shigella* may be linked to autophagy.

We thus hypothesized that septins and autophagy have a role in the replication of intracellular *Shigella* not entrapped in septin cages. To test this, we performed quantitative microscopy to count metabolically active *Shigella* in cells depleted for septins or autophagy. HeLa cells were treated with CTRL, SEPT7 or p62 siRNA and infected with x-light *Shigella* (our IPTG-inducible fluorescent strain) at MOI of 100 for 4 h 40 min. After fixation, cells were labelled with endogenous SEPT7 to exclude septin-caged bacteria from analysis. Metabolically active x-light *Shigella* express mCherry fluorescent protein upon induction with IPTG (**Figure 4.2D**), and consistent with our previous observations (Chapter 2), 92.1 ± 0.5 % of *Shigella* are metabolically active outside SEPT7 cages in CTRL cells. By contrast, 69.9 ± 2.3% or 68.1 ± 2.4% of *Shigella* were responsive to IPTG in SEPT7- or p62- depleted cells, respectively (**Figure 4.2D**). These results show that in the absence of SEPT7 or p62, a significantly lower percentage of intracellular *Shigella* are metabolically active. Collectively, analysis at the level of population (survival assays) and single cell (quantitative microscopy) indicate that septin / autophagy depletion does not affect *Shigella* survival per se. Instead, these data suggest that septin / autophagy is required for the replication of intracellular bacteria.

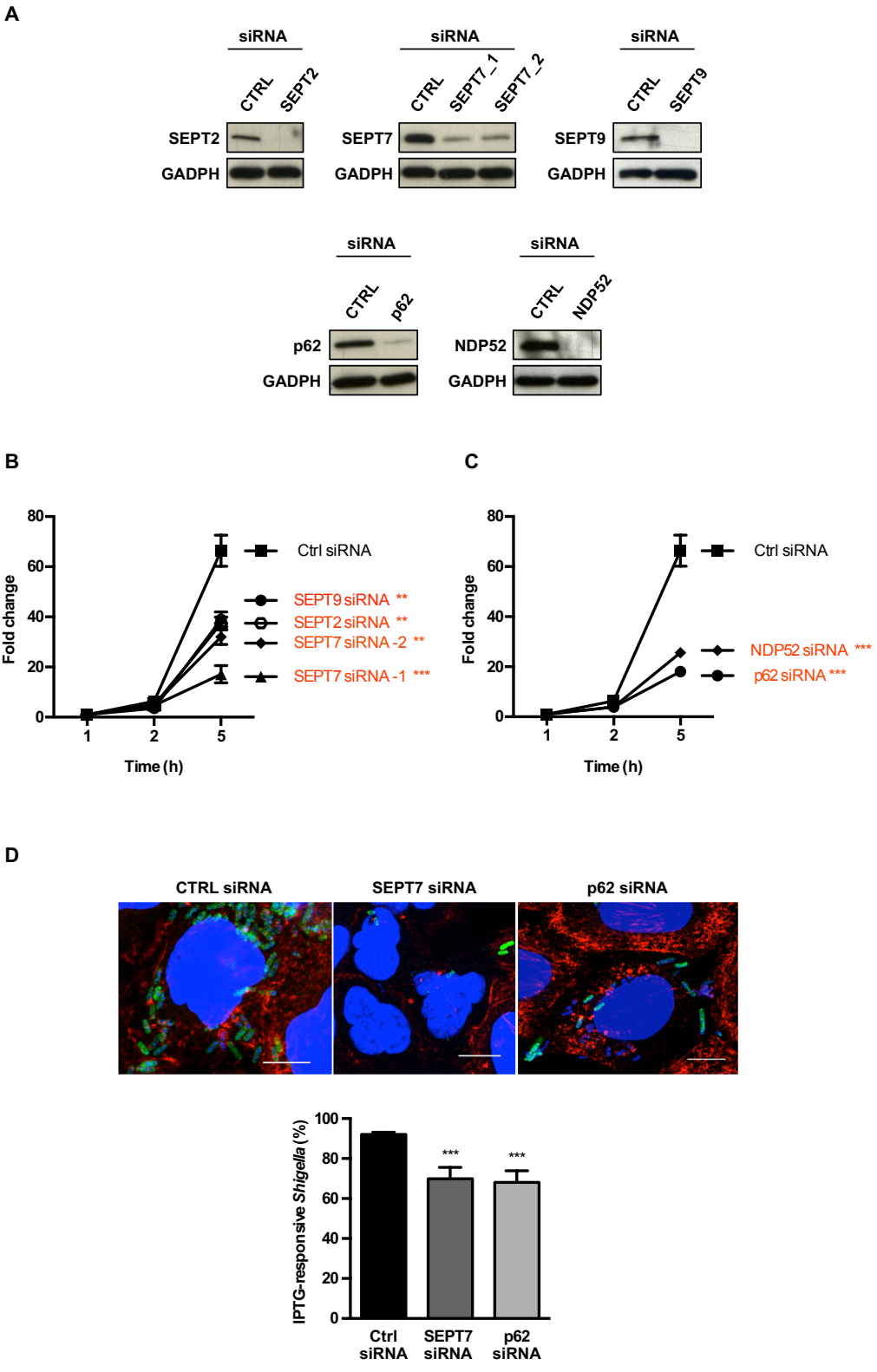
A
siRNA
CTRL
SEPT2
SEPT2
GADPH
siRNA
CTRL
SEPT7_1
SEPT7_2
SEPT7
GADPH
siRNA
CTRL
SEPT9
SEPT9
GADPH
siRNA
CTRL
p62
p62
GADPH
siRNA
CTRL
NDP52
NDP52
GADPH
B
Fold change
Time (h)
Ctrl siRNA
SEPT9 siRNA **
SEPT2 siRNA **
SEPT7 siRNA -2 **
SEPT7 siRNA -1 ***
C
Fold change
Time (h)
Ctrl siRNA
NDP52 siRNA ***
p62 siRNA ***
D
CTRL siRNA
SEPT7 siRNA
p62 siRNA
IPTG-responsive Shigella (%)
***
***
Ctrl siRNA
SEPT7 siRNA
p62 siRNA

Figure 4.2: Septins and autophagy are required for the proliferation of cytosolic *Shigella*

Cells were transfected with indicated siRNAs for 72 h. **(A)** Lysates of HeLa cells treated with siRNA for GAPDH, CTRL, SEPT2, SEPT7-1, SEPT7-2, SEPT9, p62 or NDP52 were blotted with indicated antibodies to assess the efficiency of protein depletion. GAPDH was used as a loading control.

(B & C) siRNA-treated HeLa cells were infected with *Shigella* M90T for 1h40min, 2h40min and 5h40min at 100:1 MOI. At each time-point cells were permeabilised with 0.1% Triton X-100, then serial dilutions (1, 1:10. 1:100, 1:1000) were plated on LB agar plates for CFU count the next day. Graphs represent mean % ± s.e.m. of *Shigella* intracellular fold-change normalized by 1h40min post infection. P-values were obtained using unpaired Student's t-test ** = $p<0.01$, *** = $p<0.001$, n = 5 biological replicates per condition.

(D) HeLa cells treated with CTRL, SEPT7-1 or p62-siRNA were infected with x-light *Shigella* mCherry for 4 h 40 min for quantitative confocal microscopy. IPTG was added 30min prior to fixation, and then samples were labelled with antibody for SEPT7 and Hoechst 342 (H342) for *Shigella.* Metabolically active x-light *Shigella* would express mCherry fluorescent protein when responding to IPTG. The scale bar represents 5 µm. Graph represents mean % ± s.e.m. of *Shigella* responding to IPTG outside SEPT7 cages. P-values were obtained using unpaired Student's t-test; *** = $p<0.001$; n=6 biological replicates per condition.

4.3. Amino acid starvation induces autophagy flux in SEPT7-depleted HeLa cells

Some cytosolic pathogens are able to harvest autophagy-derived nutrients from the host cell environment by inducing AA starvation. AA starvation is known to activate autophagy, and can be used as a tool to investigate the turnover (or flux) of autophagy markers, including p62, NDP52 or LC3-II. Autophagy flux assays have been previously performed in SEPT2 or SEPT9-depleted cells, where less autophagy activity was observed (Mostowy et al., 2010). These results are in line with new data showing that septins are required for autophagosome formation during starvation (Barve et al., 2016). However, the precise role of SEPT7 in starvation-induced autophagy has yet to be established. For these reasons, we investigated the effect of starvation and autophagy flux in SEPT7 depleted cells.

To test if starvation could be induced in SEPT7-depleted cells, cells were treated with Earle's Balanced Salt Solution (EBSS) to induce starvation and activate autophagy (Mizushima et al., 2010), and autophagy flux was analysed (**Figure 4.3A**). Accordingly, the difference in fold change of autophagy markers represents the amount of protein delivered to lysosomal degradation. After 6 h of EBSS treatment in CTRL cells, the levels of p62, NDP52 or LC3-II significantly decreased by 1.9 ± 0.2, 2.4 ± 0.2, or 1.9 ± 0.3 fold, respectively (**Figure 4.3B, C, D,** CTRL: lane 2). These results highlight the well known role for AA starvation in the activation of autophagy to recycle cytosolic material, and replenish nutrients needed for cellular functions. To block autophagy flux, bafilomycin A1 was employed to inhibit the acidification of autophagosomes (Klionsky et al., 2016, Dooley et al., 2014). In line with expectations, the use of

bafilomycin A1 led to an accumulation of p62, NDP52 and LC3-II (**Figure 4.3B, C, D,** CTRL: lane 3).

The effects of starvation on autophagy flux were next quantified in SEPT7-depleted cells. After treatment with EBSS, the expression of p62, NDP52 or LC3-II significantly decreased by 1.5 ± 0.2, 3.1 ± 0.7, or 1.8 ± 0.2 fold, respectively (**Figure 4.3B, C, D,** SEPT7: lane 2). These results suggest that SEPT7-depletion does not affect the ability of cells to be starved. Moreover, treatment of SEPT7-depleted cells with bafilomycin A1 led to a significant accumulation in the levels of p62, NDP52 or LC3-II (**Figure 4.3B, C, D,** SEPT7: lane 3), suggesting that autophagy flux is not significantly affected by the depletion of SEPT7. Together these results show that SEPT7 does not play an obvious role in autophagy of HeLa cells.

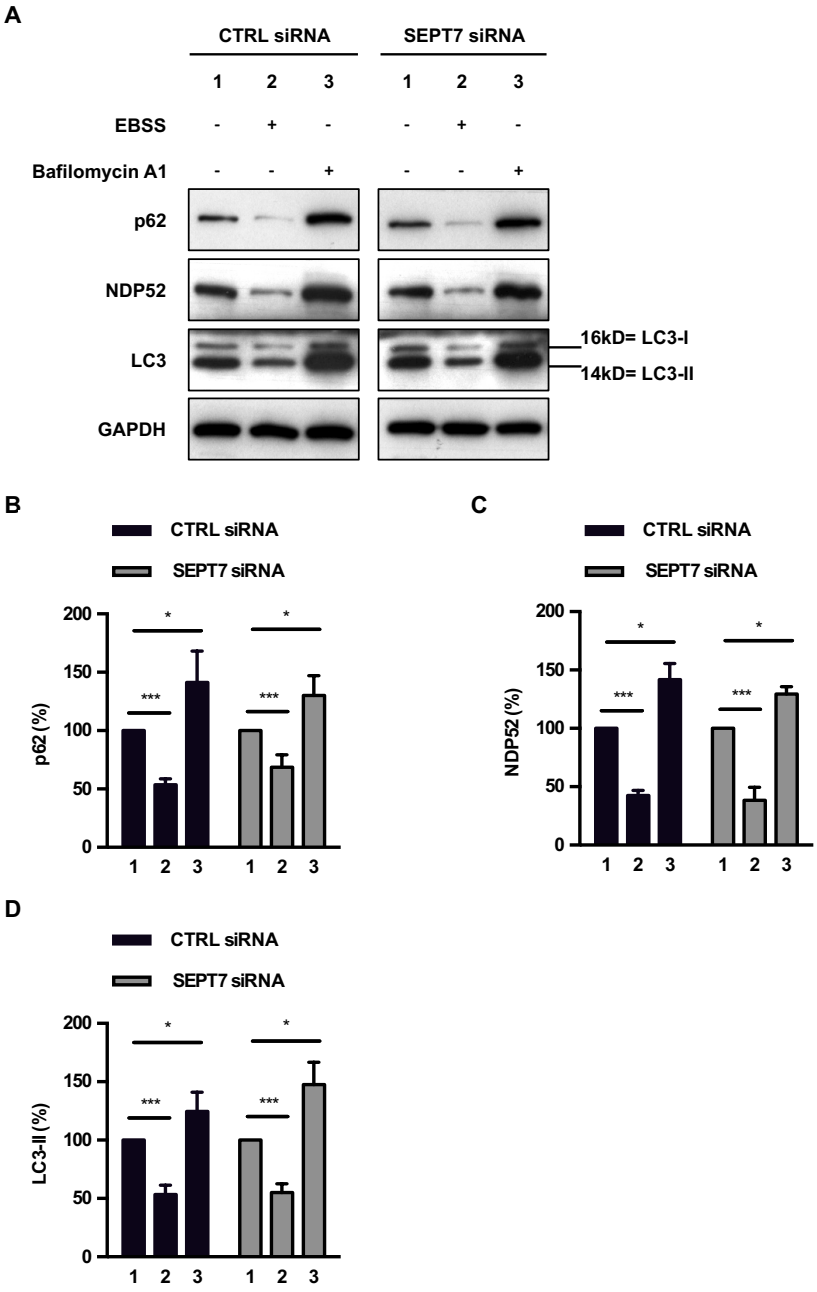

Figure 4.3: Autophagy flux assays in siRNA treated HeLa cells

HeLa cells were treated with control CTRL or SEPT7 siRNA for 72hr. Amino acid starvation was induced with EBSS for 6 hr. Bafilomycin A1 treatment was used for 6 hr to inhibit acidification of autophagosomes. Whole cell lysates were immunoblotted for endogenous GAPDH, p62, NDP52 or LC3. GAPDH was used as a loading control.
(**A**) Representative western blot of 4 independent experiments per siRNA treatment shows the protein levels of p62 (62 kDa), NDP52 (52 kDa) or LC3 in HeLa cells. Each siRNA treatment was tested with (+) or without (-) EBSS or Bafilomycin A1.
(B,C, & D) Graphs represent the mean % ± s.e.m. of the relative amount of p62 (**B**), NDP52 (**C**), or LC3-II (**D**) quantified by densitometry from 4 independent experiments from each experimental condition, in CTRL- or SEPT7- treated HeLa cells. P-values were obtained using 2way ANOVA; * = $p < 0.05$, *** = $p < 0.001$; n=4 biological replicates per siRNA treatment.

4.4. Shigella is unable to trigger amino acid starvation in SEPT7-depleted cells

Previous work has established a close relationship between starvation and autophagy during *Shigella* infection (Tattoli et al., 2012). We thus investigated the role of SEPT7 in the ability of *Shigella* to induce AA starvation using autophagy flux assays. Cells were treated with CTRL or SEPT7 siRNA, and infected with hyper invasive *Shigella* M90T AfaI for 4 h 40 min (**Figure 4.4A)**. In CTRL cells, levels of p62 and NDP52 between non-infected and infected cells were first analysed (**Figure 4.4B,C)**. In agreement with *Shigella*'s ability to trigger starvation-induced autophagy, levels of p62 and NDP52 decreased by 1.5 ± 0.1 and 1.6 ± 0.1 fold, respectively, in cells infected with *Shigella* (**Figure 4.4B,C,** CTRL: lane 2) as compared to non-infected cells (**Figure 4.4B,C,** CTRL: lane 1).

Next, to study autophagy flux during *Shigella* infection, cells were treated with EBSS or bafilomycin A1. Starvation with EBSS during *Shigella* infection led to a significant decrease in levels of p62 (2.3 ± 0.2 fold) or NDP52 (5.2 ± 1.5 fold) (**Figure 4.4B,C,** CTRL: lane 4). These results are similar to what observed in non-infected cells (**Figure 4.4B,C,** CTRL: lane 3), suggesting that starvation-induced autophagy can be further activated in *Shigella*-infected cells. Treatment with bafilomycin A1 then resulted in the accumulation of autophagy markers in both infected and non-infected cells (**Figure 4.4B,C,** CTRL: lane 5 and 6).

Next we analysed the ability of *Shigella* to trigger starvation-induced autophagy in SEPT7 depleted cells. Interestingly, the levels of p62 or NDP52

did not significantly decrease during infection of SEPT7-deleted cells (**Figure 4.4B,C,** SEPT7: lane 2). This suggests that *Shigella* is not able to induce the turnover of autophagy markers in the absence of SEPT7. By contrast, EBSS-mediated starvation during *Shigella* infection led to a significant decrease in levels of p62 (4.7 ± 1.5 fold) or NDP52 (3.1 ± 0.5 fold) (**Figure 4.4B,C,** SEPT7: lane 4), and treatment with bafilomycin A1 blocked the degradation of autophagy markers (**Figure 4.4B,C,** SEPT7: lane 6). These results are in agreement with autophagy flux assays performed in non-infected SEPT7-depleted cells (**Figure 4.3)**, and show that SEPT7 does not play an obvious role during EBSS-mediated starvation. Taken together, these results suggest that *Shigella* triggers cellular starvation in a process dependent upon SEPT7, and highlights a newfound role for septins in starvation-induced autophagy during *Shigella* infection.

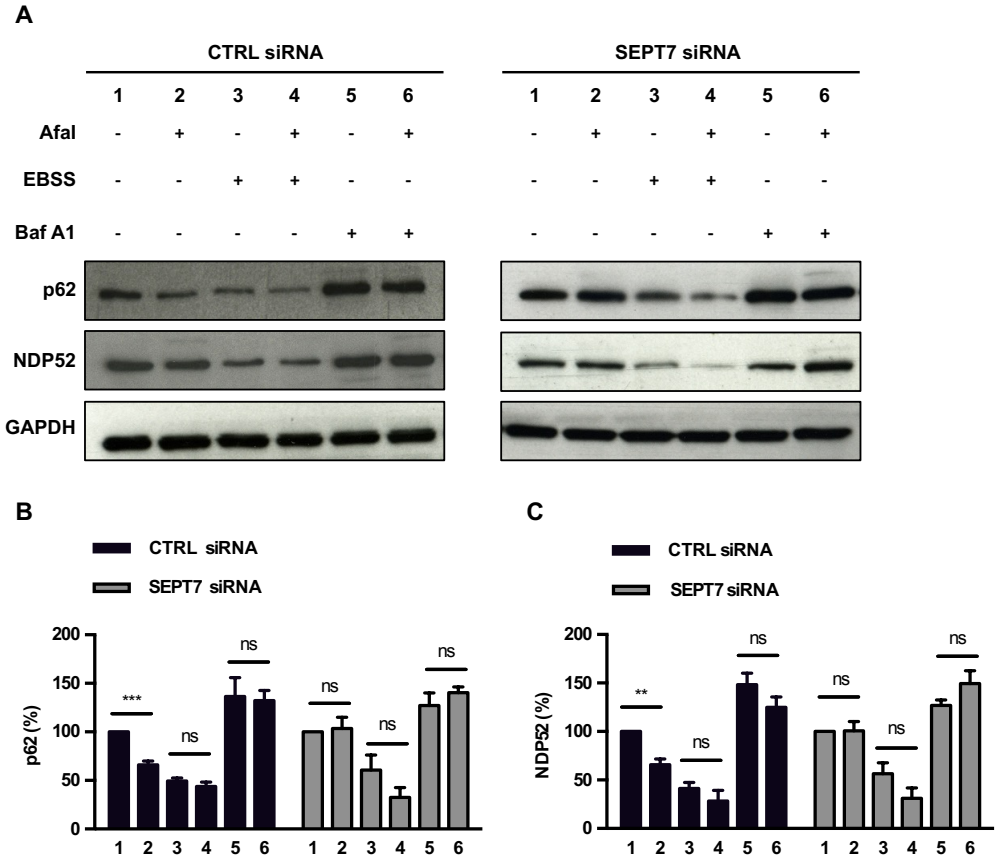

Figure 4.4: *Shigella* is unable to trigger the starvation-induced autophagy in SEPT7-depleted cells

Autophagy flux assay of HeLa cells treated with control CTRL or SEPT7 siRNA for 72hr. Cells were infected with *Shigella* AfaI for 4 h 40 min. Amino acid starvation was induced with EBSS for 6hr.

(A) Representative western blot of 4 independent experiments per siRNA treatment shows the protein levels of p62 (62 kDa) and NDP52 (52 kDa) in HeLa cells. Each siRNA treatment was tested with (+) or without (-) EBSS, Bafilomycin A1, or *Shigella* infection. Experimental conditions are depicted in lane 1 to 6.

(B & C) Graphs represent the mean % ± s.e.m. of the relative amount of p62 (**B**) or NDP52 (**C**) quantified by densitometry from 4 independent experiments from each experimental condition, in CTRL- or SEPT7- treated HeLa cells. P-values were obtained using two-way ANOVA; ns= non significant, ** = $p < 0.01$, *** = $p < 0.001$; n=4 biological replicates per siRNA treatment.

4.5. SEPT7-depletion affects *Shigella*-induced phosphorylation of host stress factor eIF2α

Previous work has shown that activation of autophagy during *Shigella* infection relies on the phosphorylation of eIF2α (P- eIF2α) (Tattoli et al., 2012). eIF2α controls mRNA translation and AA homeostasis during cellular stress, and its phosphorylation results in acute AA starvation (Wek et al., 2006). Phosphorylation eIF2α peaks after 2 h of *Shigella* infection in HeLa cells (Tattoli et al., 2012). We thus tested if eIF2α can be phosphorylated during *Shigella* infection in SEPT7 depleted cells. To maximize the number of cells infected with *Shigella*, siRNA-treated cells were infected with the hyper invasive strain *Shigella* AfaI at MOI of 10 for 1, 2, 3, and 4 h, and the expression level of P-eIF2α was quantified by western blot (**Figure 4.5A**). The amount of protein was normalised to the earliest time point tested (i.e. 0 h which represents non-infected cells). As expected (Tattoli et al., 2012), levels of P-eIF2α increased by 1.7 ± 0.1 fold after 2 h of *Shigella* infection in CTRL (**Figure 4.5B**). These results show that *Shigella* AfaI is able to induce host stress response during infection of HeLa cells. We then quantified levels of P-eIF2α in SEPT7-depleted cells. Remarkably, we did not observe an increase in P-eIF2α levels during infection by *Shigella* in the absence of SEPT7 (**Figure 4.5C**). These observations suggest that septins are involved in the host stress response and AA homeostasis, and that *Shigella* is unable to trigger autophagy in cells without SEPT7.

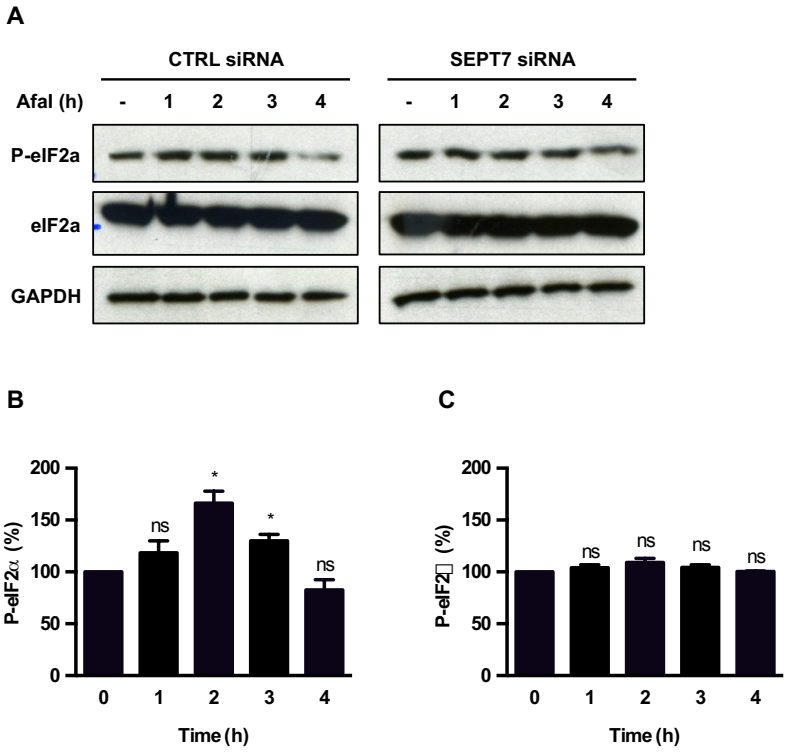

Figure 4.5: SEPT7 mediates the host cell stress response induced by *Shigella*
(**A)** HeLa cells were treated with control CTRL and SEPT7 siRNA for 72hr, then infected with *Shigella* AfaI for 1 h 40 min, 2 h 40 min, 3 h 40 min, and 4 h 40 min. Whole cell lysates were immunoblotted for endogenous GAPDH (37 kDa), eIF2α (38 kDa) and P-eIF2α (38 kDa). GAPDH was used as a loading control.
(B) Graph represents the mean % ± s.e.m. of the relative amount of P-eIF2α quantified by densitometry in CTRL-treated cells from 3 independent experiments per treatment. Data were normalized by uninfected HeLa cells (0 h). P-values were obtained using Student's t-test, ns = non significant; * = $p<0.05$; n=3 biological replicates per condition.
(C) Graph represents the mean % ± s.e.m. of the relative amount of P-eIF2α quantified by densitometry in SEPT7-treated cells from 3 independent experiments per treatment. Data were normalized by non-infected HeLa cells (0 h). P-values were obtained using unpaired Student's t-test, ns = non significant. n=3 biological replicates per condition.

4.6. Host cell metabolism is not significantly regulated by starvation or SEPT7

Metabolomic analysis of *Shigella*-infected cells has revealed that *Shigella* diverts nutrients from the host cell to benefit its intracellular growth (Kentner et al., 2014, Wei and Murphy, 2016, Pieper et al., 2013). In particular, *Shigella* obtains high-energy nutrients from the host cell by redirecting pyruvate from glucose metabolism (Kentner et al., 2014). Although *Shigella*-infected cells maintain a 'normal' metabolism that allows host cells to survive and produce energy, *Shigella* is able to retain pyruvate and digest it further into acetate and ATP for its own benefit. Therefore, pyruvate is a carbon source used by *Shigella* to increase its intracellular growth (Kentner et al., 2014).

The activation of AA starvation is linked to the ability of *Shigella* to harvest nutrients from the host cell. To investigate a role for SEPT7 in this process, we used liquid chromatography mass-spectrometry accurate mass retention time (LC-MS AMRT) in collaboration with Dr. Gerald Larrouy Maumus who performed the LC-MS AMRT (Larrouy-Maumus et al., 2013). LC-MS AMRT is a novel technique used to quantify metabolites in tissue culture cells (Hird et al., 2014). As a result, metabolomics can identify difference in metabolite levels between two or more population of cells (Zhu et al., 2013). To test the role of SEPT7 and / or starvation in host cell metabolism, we prepared extracts from CTRL- or SEPT7-depleted HeLa cells and advanced these samples for LC-MS AMRT.

To ensure optimal conditions, experimental settings (i.e. siRNA treatment and starvation in HeLa cells) were validated by western blot prior to metabolome

analysis (**Figure 4.6A**). p62 and LC3 were used as markers of starvation-induced autophagy. In line with observations from our autophagy flux assays (**Figure 4.3**), treatment with EBSS led to a decrease in the level of p62 and LC3-II in both CTRL and SEPT7-depleted cells (**Figure 4.6A**).

A difference in abundance from the total pool of metabolites between CTRL or SEPT7-depleted cells was first assessed (**Figure 4.6B and C**). siRNA-treated cells were lysed into a buffer containing acetonitrile/methanol/water at −40°, and collected for analysis by LC-MS AMRT. During the mass spectrometry process, samples are fragmented into small ion particles characterized by a negative or positive charge. The electron mass of compounds is detected by electrospray tandem mass spectrum as hundreds or thousands of peaks, with a unique mass/charge (m/z) and retention time (Larrouy-Maumus et al., 2013). Prior to statistical analysis, results are normalised to the amount of residual proteins in the metabolome extracts, in order to avoid false positives from proteins derived from the serum in the culturing medium. Finally, the positive and negative ion counts of each metabolite were plotted into a Log2 scale scattered cloud-plot, which represents the distribution in abundance of metabolites between CTRL (Y axis)- and SEPT7 (X axis)-treated cells. In non-starved conditions (**Figure 4.6B**), most values of our data defined a cloud plot distributed uniformly along a slope of 45°, suggesting no significant difference between CTRL (Y axis)- and SEPT7 (X axis)-treated cells. Interestingly, cells depleted of SEPT7 mostly showed a normal central metabolism, though a few metabolites showed significant alteration (described below). In the case of starvation (**Figure 4.6C)**, data were also uniformly distributed along a slope of 45° between CTRL (Y axis)- and SEPT7 (X axis)-treated cells, suggesting no significant difference between siRNA-treated cells. Together, these results

suggest that the depletion of SEPT7 or starvation do not significantly alter the levels of metabolites in HeLa cells.

A

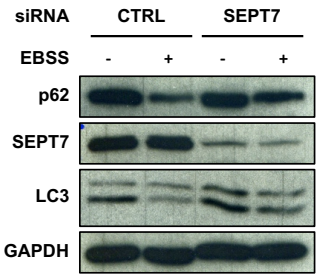

B

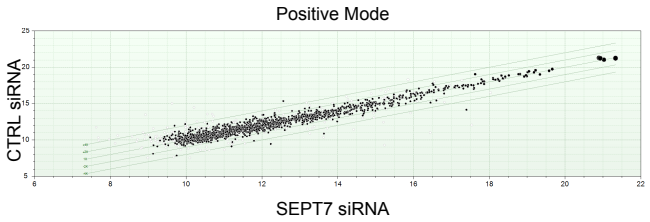

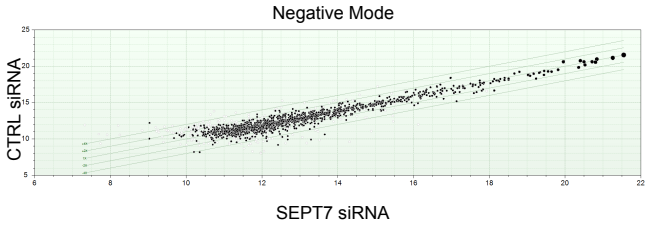

C

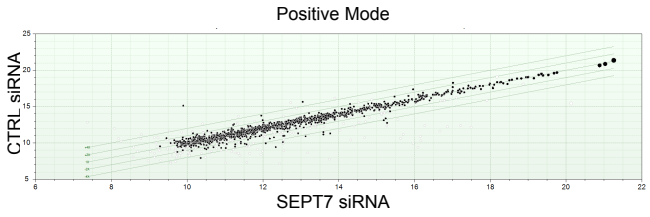

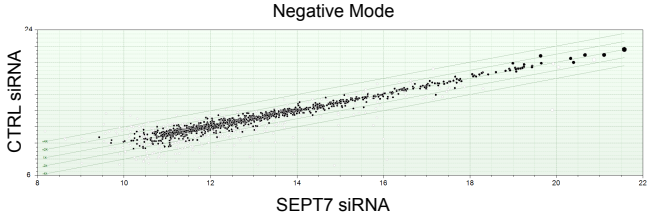

Figure 4.6: Central host metabolism is not impaired by SEPT7 depletion and starvation

HeLa cells treated with control CTRL or SEPT7 siRNA for 72hr. Amino acid starvation was induced with EBSS for 6hr.

(A) Whole cell lysates were immunoblotted for endogenous GAPDH (37 kDa), p62 (62 kDa), NDP52 (52 kDa) or LC3 (14-16 kDa). GAPDH was used as a loading control. Representative blot showing the protein expression of cells with (+) or without (-) EBSS treatment; n=3 biological replicates per condition.

(B) Representative scattered cloud-plot showing the ion counts of each metabolite normalised to the amount of residual proteins in the metabolome extract from CTRL- (Y-axis) and SEPT7 (X-axis) siRNA- treated HeLa cells in DMEM+10%FBS. Positive mode = $(M + H)^{+}$; Negative mode = $(M - H)^{=}$; n=3 biological replicates per condition.

(C) Representative scattered cloud-plot showing the ion counts of each metabolite normalised to the amount of residual proteins in the metabolome extract from CTRL- (Y-axis) and SEPT7 (X-axis) siRNA- treated HeLa cells in EBSS. Positive mode = $(M + H)^{+}$; Negative mode = $(M - H)^{=}$; n=3 biological replicates per condition.

4.7. SEPT7 mediates host cell metabolic pathways critical for *Shigella* proliferation

To understand the role of SEPT7 in metabolic pathways hijacked by *Shigella* for its intracellular proliferation, we selectively analysed metabolites involved in energy and carbon metabolism. We focused on (i) phosphoenolpyruvate (PEP), (ii) hexose phosphate, (iii) aspartic acid and (iv) lactate for the following reasons. (i) PEP is involved in the glycolytic pathway as a precursor for pyruvate and is preferentially used by *Shigella* (Kentner et al., 2014). (ii) Hexose phosphate is part of the pentose-phosphate pathway, an alternative glycolytic pathway used by *Shigella* to produce pyruvate from glucose; hexose phosphate is a secondary host source of energy for *Shigella* (Kentner et al., 2014, Saier et al., 1975). (iii) Aspartic acid is an essential amino acid used as precursor for amino acid biosynthesis (Birsoy et al., 2015). (iv) Lactate is a fermented product that host cells can use, instead of PEP, to generate pyruvate (Kentner et al., 2014).

Our results using LC-MS AMRT showed that the depletion of SEPT7 led to a significant reduction in PEP (4.5 ± 0.1-fold, $p<0.01$ **Figure 4.7A,** DMEM + 10% FBS), hexose phosphate (2.3 ± 0.1, $p<0.05$, **Figure 4.7B,** DMEM + 10% FBS) and aspartic acid (2.3 ± 0.2 fold change, $p<0.01$, **Figure 4.7C,** DMEM + 10% FBS). On the other hand, lactate significantly increased (2.7 ± 0.5, $p<0.01$, **Figure 4.7D,** DMEM + 10% FBS). As PEP, hexose phosphate, and aspartic acid are important carbon sources of energy derived by host glycolytic pathways hijacked by *Shigella* (Kentner et al., 2014), these results suggest that SEPT7 depletion affects host metabolic pathways critical for *Shigella* proliferation. Although lactate is a final product of fermentation from glucose, it

is not a critical source of pyruvate for *Shigella* (Kentner et al., 2014). These results suggest that SEPT7-depleted cells use fermentation as an alternative pathway to produce pyruvate for normal cellular functions.

Given that SEPT7 depleted cells do not undergo AA starvation during infection of *Shigella* (**Figure 4.4**), we hypothesized that without SEPT7 *Shigella* cannot access nutrients for proliferation. We tested the effect of starvation on carbon metabolism in non-infected, siRNA-treated cells. The treatment with EBSS restored levels of PEP, hexose phosphate, aspartic acid and lactate in SEPT7-depleted cells to the levels observed for CTRL cells (**Figure 4.7,** EBSS**)**. Importantly, these results suggest that defects in the carbon metabolism induced by SEPT7-depletion can be rescued during starvation. Together, metabolomic analysis has uncovered a novel link between SEPT7, autophagy, and the availability of nutrients to intracellular *Shigella*.

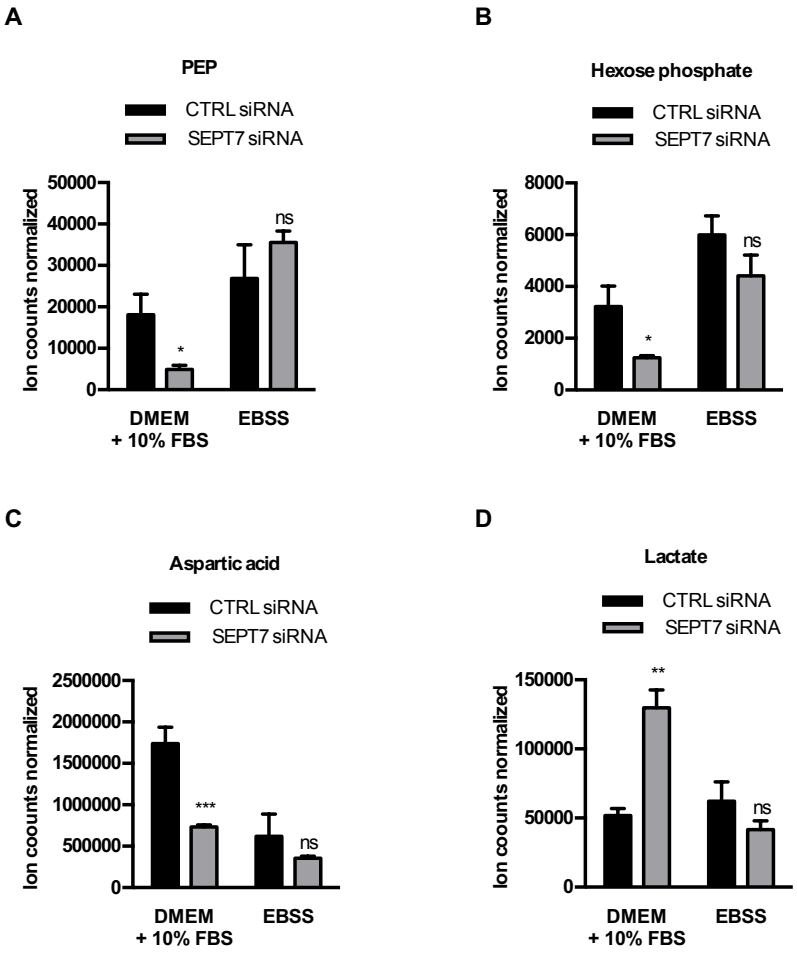

Figure 4.7: SEPT7 depletion affects host metabolic pathways critical for *Shigella* proliferation.

Graph represents the ion counts normalised to the amount of residual proteins in the metabolome extract ± s.e.m. of PEP (**A**), hexose phosphate (**B**), aspartic acid (**C**) and lactate (**D**) between siRNA-treated HeLa cells in DMEM+10%FBS or EBSS. P-values were obtained using unpaired Student's t-test, ns = non significant; * = $p<0.05$; ** = $p<0.01$; *** = $p<0.0001$; n=3 biological replicates per condition.

4.8. Starvation rescues *Shigella* proliferation in SEPT7-depleted cells

Using metabolomics we have shown that AA starvation restores metabolites essential for *Shigella* to replicate inside the host cell cytosol. Next, we investigated the effect of AA starvation on *Shigella* proliferation, in cells depleted of SEPT7. Similar to survival assays performed in section 4.1, cells treated with CTRL or SEPT7 siRNA were starved and infected with *Shigella* M90T for 1 h 40 min, 2 h 40 min or 5 h 40 min. CFU counts were performed the next day, and the results were all normalized according to counts reflecting bacterial entry (i.e. the earliest time point tested 1 h 40 min, **Figure 4.8A**). Consistent with data in section 4.1, the intracellular replication of *Shigella* in SEPT7-depleted cells decreased by 2.6 ± 0.5 fold after 5 h 40 min in non-starved conditions (**Figure 4.8A,** DMEM +10% FBS). Strikingly, AA starvation rescued the intracellular replication of *Shigella* in SEPT7-depleted cells **(Figure 4.8A,** EBSS). These results indicate that AA starvation can rescue the intracellular replication defects observed for *Shigella* in the absence of SEPT7.

Shigella can trigger autophagy (Tattoli et al., 2012)(see section 4.3). We thus investigated the intracellular replication of *Shigella* in p62-depleted cells +/- starvation. After treatment with CTRL or p62 siRNA, cells were starved and infected with *Shigella* M90T for 1 h 40 min, 2 h 40 min or 5 h 40 min. In section 4.1 we showed that *Shigella* replicates significantly less inside p62-depleted cells; this was also observed here where *Shigella* intracellular replication was decreased 2.6 ± 0.3 fold after 5 h 40 min in non-starved conditions (**Figure 4.8B,** DMEM +10% FBS). In agreement with results obtained in SEPT7-depleted cells, treating cells with EBSS restored *Shigella*

replication in p62-depleted cells to levels observed for control cells (**Figure 4.8B,** EBSS). These results demonstrate that starvation-induced autophagy has an important role for *Shigella* and its intracellular proliferation.

Results from Chapter 4 have shown that cytosolic *Shigella* not entrapped in septin cages sense the global effect on host metabolism and autophagy triggered by the subset of bacteria linked to septin cage assembly. To investigate a link between AA starvation and the metabolic activity of intracellular *Shigella* at the single bacterium level, siRNA-treated HeLa cells were starved and infected with x-light *Shigella* for 4 h 40 min. After fixation, cells were labelled with endogenous SEPT7 to exclude septin-caged *Shigella* from analysis, and also to confirm SEPT7 depletion by microscopy (**Figure 4.8C**). In agreement with results from survival assays showing similar intracellular replication of *Shigella* with or without EBSS-mediated starvation (**Figure 4.8A**), the percentage of metabolically active bacteria is the same in CTRL cells with or without starvation. These results are also consistent with previous work showing that EBSS-mediated starvation has no additional effect on the proliferation of intracellular *Shigella* (Tattoli et al., 2012).

The metabolic activity of *Shigella* was next quantified in SEPT7-depleted cells (**Figure 4.8C**). In this case, the percentage of metabolically active bacteria is significantly higher in starved cells (94.7 ± 0.3%) compared to non-starved cells (65.3 ± 2.4%). In line with survival assays showing more intracellular replication of *Shigella* in SEPT7-depleted cells upon starvation, these results indicate that EBSS-mediated AA starvation in SEPT7-depleted cells restores the percentage of metabolically active bacteria to the level of CTRL cells (93.8 ± 0.6%, **Figure 4.8C)**. Similar results were obtained when metabolic activity of *Shigella* was assessed in p62-depleted cells. In this case, the % of

metabolically active *Shigella* was significantly higher in starved cells (94.4 ± 1.2%) compared to non-starved cells (63.7 ± 1.8%). Collectively, these results suggest that AA starvation mediates the metabolic activity of intracellular *Shigella* outside of septin cages, and EBSS-mediated starvation can increase the proliferation of bacteria in SEPT7- or p62 -depleted cells. These results highlight a close relationship between AA starvation, septins, autophagy and the intracellular proliferation of *Shigella*.

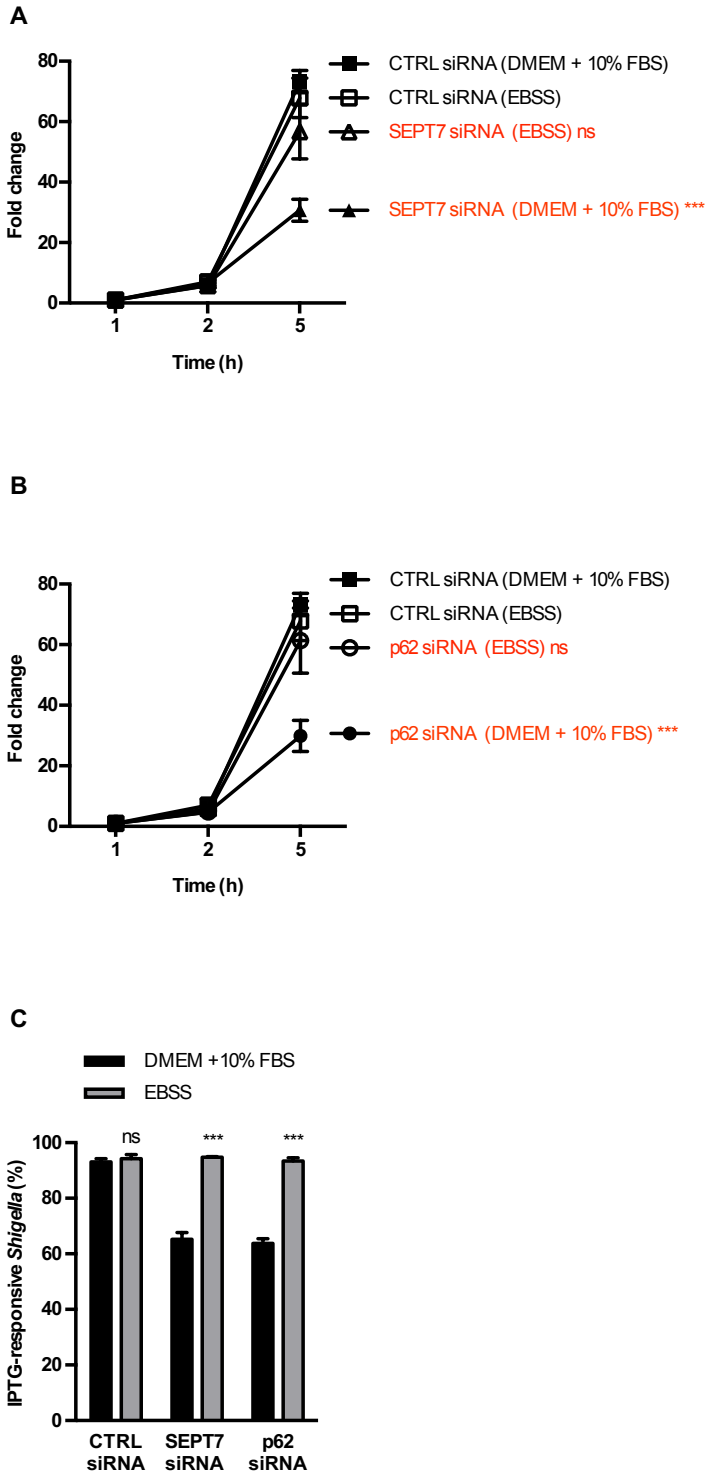

Figure 4.8: Starvation restores *Shigella* proliferation in SEPT7- or p62-depleted cells
Cells were transfected with CTRL, SEPT7 or p62 siRNAs for 72 h. Amino acid starvation was induced with EBSS for 6hr.
(A & B) siRNA-treated HeLa cells were infected with *Shigella* M90T for 1h40min, 2h40min and 5h40min at 100:1 MOI. At each time-point cells were lysed with 0.1% Triton X-100, then serial dilutions (1, 1:10. 1:100, 1:1000) were plated on LB agar

plates for CFU count the next day. Graphs represents mean % ± S.E.M. of *Shigella* intracellular fold-change normalized by 1h40min post infection in **(A)** DMEM + 10% FBS or **(B)** EBSS. P-values were obtained using Student's t-test; ns =non significant; ** = $p<0.001$; n = 3 biological replicates per condition.

C) HeLa cells treated with CTRL, SEPT7 or p62-siRNA were infected with x-light *Shigella* mCherry for 4 h 40 min for quantitative confocal microscopy. IPTG was added 30min prior to fixation, and then samples were labelled with antibody for SEPT7 and Hoechst 342 (H342) for *Shigella.* Metabolically active x-light *Shigella* would express mCherry fluorescent protein when responding to IPTG. Graph represents mean % ± S.E.M. of *Shigella* responding to IPTG outside SEPT7 cages in DMEM + 10% FBS or EBSS. P-values were obtained using Student's t-test; *** = $p<0.001$; n=3 biological replicates per condition.

4.9. Summary

In this chapter we show that AA starvation and septins are crucial for intracellular proliferation of *Shigella* not entrapped in septin cages. Remarkably, SEPT7 mediates the ability of *Shigella* to induce AA starvation for its intracellular proliferation.

We have shown that, in the absence of SEPT7, *Shigella* is not able to induce the degradation of autophagy markers, nor phosphorylate eIF2α to trigger the AA starvation process. Survival assays showed that in the absence of SEPT7 intracellular *Shigella* failed to replicate. Consistent with this, single cell analysis by microscopy showed that depletion of SEPT7 reduces the percentage of intracellular bacteria that are metabolically active. In agreement with a close relationship between septins and autophagy, similar results were observed in p62-depleted cells.

Intracellular pathogens have evolved strategies to survive inside the host cell where access to nutrients is limited and under control of the host (Killackey et al., 2016). A variety of bacterial pathogens can harvest autophagy-derived nutrients for intracellular growth (Wang et al., 2009, Niu et al., 2012, Steele et al., 2013). Indeed, *Shigella* diverts host metabolic pathways for intracellular growth yet the underlying mechanisms remain to be established (Kentner et al., 2014, Wei and Murphy, 2016, Pieper et al., 2013). Here, we investigated the relationship between septins, starvation-induced autophagy, and host cell metabolism to identify their impact on the survival of intracellular *Shigella*. A previous study revealed that *Shigella* increases its intracellular growth by redirecting pyruvate, an essential carbon source for *Shigella,* from the host

glycolytic pathway (Kentner et al., 2014). In our study, metabolomics revealed that SEPT7-depeted cells have impaired carbon metabolism. This was identified by decreased levels of PEP, hexose phosphate and aspartic acid, all of which act as precursors of pyruvate in the glycolytic pathway exploited by *Shigella* (Kentner et al., 2014). Our work has identified, for the first time, that nutrients required by *Shigella* are less available in the absence of SEPT7. Induction of AA starvation by EBSS restored the absence of PEP, hexose phosphate and aspartic acid observed in SEPT7-depleted cells. The precise link between SEPT7 and the metabolic activity of host cells during *Shigella* infection awaits investigation.

CHAPTER 5: DISCUSSION

5.1. Highlight

Studies on host-pathogen interactions have helped to discover key roles for the cytoskeleton in infection biology. The cytoskeleton is recognised as a crucial determinant in innate immunity to intracellular bacterial pathogens (Mostowy and Shenoy, 2015, Mostowy et al., 2010). In the case of autophagy, cytoskeletal rearrangements have been shown to restrict or promote bacterial proliferation (Mostowy, 2013, Sirianni and Mostowy, 2014). *Shigella flexneri* is paradigm of infection for the study of bacterial autophagy. *S. flexneri* is well known to subvert host cell actin to polymerise tails and avoid cytosolic immune responses. However, septins form cage-like structures around actin polymerising *Shigella*, to restrict bacterial dissemination and promote host defence.

Shigella-septin caging has been shown to restrict actin tail polymerisation, and promote recognition by autophagy. However, many issues remain. For example, what is the precise fate of *Shigella* entrapped in septin cages? Host factors underlying septin assembly also remains to be fully established. Moreover, the role of septins / autophagy on cellular metabolism during bacterial infection is mostly unknown.

In this thesis I have (i) studied how the host cell employs septins to restrict *Shigella* replication, (ii) characterised novel host factors to promote septin

cage assembly, and (iii) highlighted new roles for septins in host cell metabolism. My main findings are:

- Septin cages restrict the proliferation of cytosolic *Shigella* (Chapter 2).
- Mitochondria promote septin cage assembly and the lethal action of septin cages (Chapter 2 and 3).
- Dynamin-like protein 1 (Drp1) interacts with septins to enhance mitochondrial fission (Chapter 3).
- *Shigella* fragment mitochondria to counteract septin cage assembly and bacterial autophagy (Chapter 3).
- Septins are linked to amino acid starvation and the cytosolic replication of *Shigella* (Chapter 4).

5.2. Septin cages target *Shigella* to degradation by autophagy

Autophagy is a component of cell-autonomous immunity viewed to restrict the proliferation of intracellular bacteria. Ubiquitination is the best-characterised mechanism of bacterial recognition by autophagy, in which ubiquitin-binding adaptor proteins (such as p62, NDP52) target ubiquitinated substrates around bacteria to the autophagosome. However, some bacteria evolved strategies to avoid autophagy, and in some cases autophagy has been described to promote bacterial replication. *Shigella flexneri* is a well-characterised model organism used to study host-pathogen interactions and bacterial autophagy, and in particular has been instrumental in the discovery of septin caging.

By using a fluorescent IPTG inducible *Shigella* strain (x-light) we could show that ~50% of *Shigella* entrapped by septin cages responded to IPTG and were thus metabolically active. Our experiments indicate that septin cages recognise live bacteria and target them to degradation by autophagy (Sirianni

et al., 2016). In the future, generating bacterial strains, which express pH-sensitive fluorescent proteins, could help to investigate the lethal action of septin caging in real time. Material enclosed within autophagosomes can be degraded following acidification of the double membrane vacuole (i.e. after lysosomal fusion). Given this, the light emitted by a pH-sensitive fluorescent *Shigella* targeted to autophagy would shift to a different wavelength in the last step of autophagy.

5.3. What are the host determinants that underlie *Shigella*-septin cage assembly?

Proteomics suggested interactions between septins and mitochondria during *Shigella* infection (Sirianni et al., 2016). Mitochondria have been described as a source of membrane for autophagosome biogenesis during starvation (Hailey et al., 2010), and we hypothesised that mitochondria could support septin cage assembly during *Shigella* infection. Using a variety of high-resolution microscopy techniques, septin rings were shown to assemble at the sites of contact with mitochondria (**Figure 3.3**). The use of YFP-Mito^{cb5}TM (a marker for outer mitochondrial membrane) has previously been used to show colocalisation of autophagy markers (ATG5 and LC3) with mitochondria, and to suggest that mitochondria can supply membrane for the growing phagophore (Hailey et al., 2010). However, in our infection scenario, the use of YFP-Mito^{cb5}TM did not show that mitochondria supply membrane to septin cages. Moreover, CLEM analysis clearly showed that mitochondrial membrane is distinct from the autophagosomes surrounding the bacterium (**Figure 3.3B**). The precise role of mitochondria in septin cage assembly and autophagosome formation awaits investigation.

5.4. Septins interact with Drp1 to enhance mitochondrial fission.

We have identified a novel link between mitochondria and septin cage assembly during *Shigella* infection. Dynamin-related protein 1 (Drp1) and mitofusin 1 (Mfn1) are key mediators of mitochondrial fission and fusion, respectively (Rambold et al., 2011). Depending on the levels of Drp1 or Mfn1, mitochondria form a tubular (i.e. in Drp1-depleted cells) or fragmented (i.e. in Mfn1-depleted cells) network that can provide more or less membrane available for septin cage assembly (Hailey et al., 2010). These experiments identified Drp1 as the first discovered host factor that restricts the process of septin caging (Sirianni et al., 2016).

An important question that emerged from this discovery is whether septins are involved in the process of mitochondrial dynamics. During cytokinesis, septins are recruited to the cleavage furrow and enable constriction of the actomyosin ring for cell division (Glotzer, 2005). Similarly, actomyosin has been observed to form a pre-constriction complex at the site of contact between ER and mitochondria to facilitate the recruitment of Drp1 around mitochondria and mediate fission (Hatch et al., 2014). However, a role for septins during mitochondrial division had not been tested. We use super resolution and confocal microscopy, along with immunoprecipitation experiments, and show that septins co-localise with Drp1 at sites of mitochondrial fission (**Figure 3.6A**) (Sirianni et al., 2016). This discovery strongly supports the hypothesis that septins facilitate the localisation of Drp1 to the mitochondrial membrane and enable fission. The precise role of septins in mitochondrial division will be an exciting future avenue of investigation.

How does mitochondrial fission influence septin cage assembly during *Shigella* infection? Pathogens can modulate the mitochondria to promote death or survival of the host (Carneiro et al., 2009). Actin polymerising *Shigella* induces mitochondrial fragmentation (Lum and Morona, 2014). Using siRNA and infection assays with *Shigella* ΔIcsA (i.e. a bacterial strain unable to polymerise actin in the cytosol), we determined that *Shigella*-mediated actin polymerisation is responsible for mitochondrial fragmentation and escape from septin caging. These results highlight mitochondrial fragmentation as key for bacterial escape from cell-autonomous immunity.

In conclusion, this study has shown that mitochondria support septin assembly into the cages that entrap *Shigella* for autophagy. Moreover, actin polymerisation triggered by *Shigella* IcsA fragments mitochondria and promotes escape from septin caging and bacterial autophagy (**Figure 5.1)**.

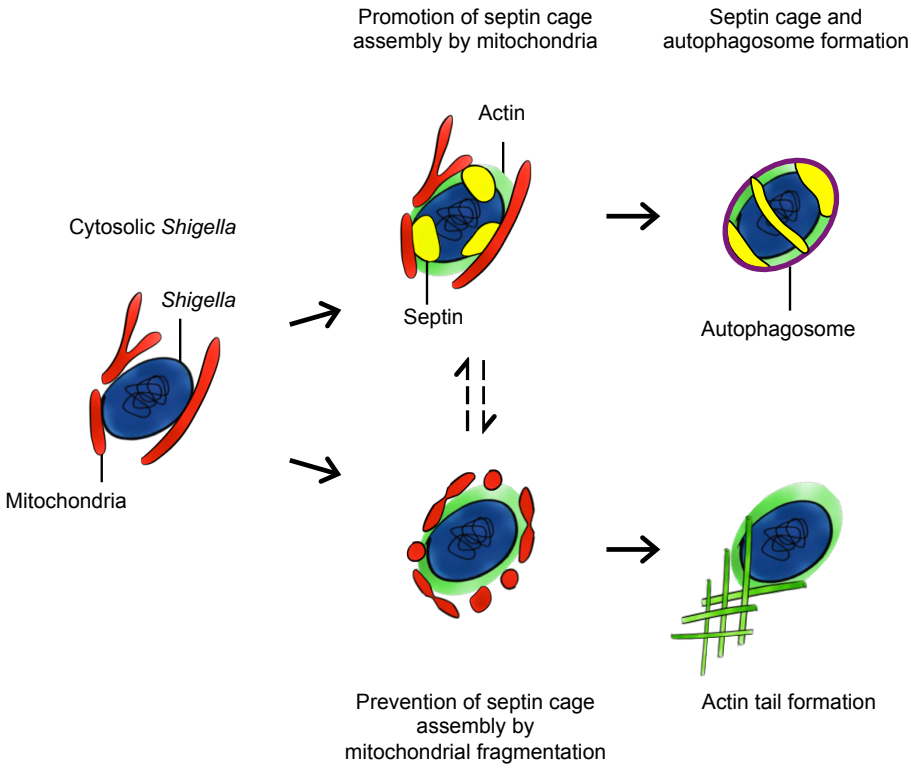

Figure 5.1: Proposed circumstances of mitochondria promoting *Shigella*-septin caging versus actin tail formation.
(i) Mitochondria support septin cage assembly for antibacterial autophagy, and (ii) *Shigella* fragment mitochondria to counteract septin cage assembly. Depending on the fragmentation of mitochondria by IcsA, *Shigella* will be compartmentalised in septin cages or spread cell-to-cell via actin-based motility (Image adapted from Sirianni *et al*, 2016).

5.5. A new role for septins in host cell metabolism

Chapter 4 of my thesis set out to investigate the interplay between septins and host cell metabolism during infection by *Shigella*. This uncovered a new role for septins in contributing to bacterial replication inside the host cell cytosol.

Recent evidence has shown that invasive pathogens harvest autophagy-derived nutrients for intercellular replication. However, the role of host cell nutritional status on pathogen survival remains to be fully established (Popp et al., 2015, McConville, 2014, Steeb et al., 2013).

Is *Shigella* able to induce autophagy and harvest nutrients to benefit its own intracellular replication? Previous work has shown that the invasion of *Shigella* triggers amino acid starvation and activates autophagy (Tattoli et al., 2012). In this thesis, we have discovered a role for septins in amino acid starvation during *Shigella* infection. In addition, we have shown that septins and autophagy can be important for the replication of intracellular *Shigella* not entrapped in septin cages (**Figure 4.2B,C**). It will next be interesting to investigate how septins can affect host cell metabolism, and why this is specific for starvation pathways or high-energy carbon sources.

Why do *Shigella* require septins for access autophagy-derived nutrients? Work has shown that *Shigella* hijacks carbon metabolism to survive inside the host cell (Kentner et al., 2014). In my thesis, we used metabolomics to investigate the role of septins in host cell metabolism, and how this could influence *Shigella* infection. By using siRNA-treated cells and amino acid starvation experiments, we found that SEPT7 depletion modulates the levels of phosphoenolpyruvate (PEP), hexose phosphate, aspartic acid and lactate. Interestingly, starvation of SEPT7-deficient cells rescued the levels of PEP,

hexose phosphate, aspartic acid and lactate. Remarkably, survival assays in septin-depleted cells confirmed that starvation rescued *Shigella* metabolic activity and intracellular replication. For the first time, these results uncovered a link between septins and autophagy in relation to host metabolism and the nutrients required by *Shigella* for intracellular replication.

The relationship between septins and host cell metabolism is not yet clear, and how septins regulate the abundance of carbon sources in host cell will require further investigation.

5.6. Summary

In conclusion, this thesis demonstrates how *S. flexneri* is an important paradigm to investigate new links between septins, mitochondria, and autophagy. My thesis (Chapter 2, 3) has shown that septin-mitochondria interactions are important for septin cage assembly and for targeting *Shigella* to degradation by autophagy. Moreover, thesis (Chapter 4) has shown that septins modulate host cell metabolism crucial for the replication of intracellular *Shigella*.

In the future, *in vivo* studies will be required to test the role of these mechanisms in host defence at the whole animal level. In turn, this information can provide valuable tools and insights to fight infection and / or other septin-related diseases.

CHAPTER 6: Materials and Methods

6.1. Bacterial strains

All bacterial strains used in this work are listed in **Table 6.1**.

Table 6.1:List of bacterial strains used in this study

Bacterial strain	Antibiotic-resistance	Description	Source/Reference
Shigella			
M90T	Strepto *	BUG 2505 Serotype 5a	Mostowy *at al*., CHM, 2010
M90T GFP	Carb 50 µg/ml	BUG 1908. Stable mutant express GFP from chromosome	Mostowy *at al*., CHM, 2010
M90T mCherry	Carb 50 µg/ml	pFPV 25.1 mCherry construct	This study; Mostowy *et al.,* 2013
M90T AfaI	Carb 50 µg/ml; Kan 50 µg/ml	Hyper-invasive strain that expresses an adhesin from *Escherichia coli*	Mazon Moya *et al*,. 2014
M90T Crimson	Kan 50 µg/ml	E2-Crimson fluorescent protein contruct	Kind gift from Francois-Xavier Campbell
M90T x-light GFP/mCherry	Carb 50 µg/ml	Detect live/dead bacteria, Induce 0.5h with 0.1 mM IPTG	This study
∆IcsA	Carb 50 µg/ml	M90T, No actin tail polymerization	Mostowy *at al*., CHM, 2010
***E. coli* (DH5α)**			
pSEPT6-GFP	Kan 50 µg/ml	SEPT6-GFP expression	This study
pFPV 25.1 mCherry	Carb 50 µg/ml	mCherry expression	This study
pmito-BFP	Carb 50 µg/ml	mito-BFP expression	This study
pActA-SEPT7-mRFP	Kan 50 µg/ml	ActA-SEPT7-mRFP expression	This study
pYFP-Mito^{cb5}TM	Kan 50 µg/ml	YFP-Mitocb5TM expression	This study
pKB2689	Carb 50 µg/ml	x-light mCherry construct expression	This study
pSA11	Carb 50 µg/ml	x-light GFP construct expression	This study
*** all M90T derivates are streptomycin resistant**			

6.2. Eukaryotic cell lines

- HeLa (ATCC CCL-2), epithelial cell line derived from human cervix carcinoma, were used to study the mechanism of assembly of human septin cytoskeleton upon bacterial infection.
- HEK293FT, human embryonal kidney cell line transformed with the SV40 large T antigen, were used for lentiviral transfection and generate SEPT6-GFP stable cell line.

6.3. Transfection, molecular probes, pharmacological inhibition

All reagents, molecular probes and pharmacological inhibitors are listed in **Table 6.2.**

Table 6.2: List of reagents and pharmacological inhibitors used in this study.

Compound	Specificity/treatment	Concentration	Source
Oligofectamine	siRNA transfection in HeLa cells	3µl/ml	ThermoFisher
JetPei	DNA transfection in HeLa cells	4µl/ml	Polyplus
Cytochalasin D	Inhibition of actin polymeization	1µM	Sigma (C8273)
Bafilomycin A1	Inhibition of lysosome acidification	160nM	Sigma (B1793-10uG)
Dimethyl sulfoxide (DMSO) Hybri-Max	Polar aprotic solvent for cell culture	0.05%	Sigma (D2650)
Isopropyl β-D-1-thiogalactopyranoside IPTG	Mimic of allolactose for induction of x-light Shigella	0.1mM	Sigma (I6758)
Paraformaldehyde (PFA)	Fixation of cell cultures for microscopy	4%	Sigma (P6148)
Glutaraldehyde	Fixation of cell cultures for microscopy	0.50%	Sigma (G5882)
TritonX-100	cell membrane permeabilization	0.1%	Sigma (X100)

6.4. Plasmids

All plasmids used in this study are listed in **Table 6.3**. Colonies of transformed bacteria were grown in 4ml of antibiotic-containing LB medium, at 37°C with aeration for 14 – 16 h. Plasmids were purified using GenElute^{TM} Plasmid Miniprep Kit (Sigma) according to manufacturer instructions.

SEPT6-GFP (Mostowy et al., 2010) and pLVX-GFP-SEPT6 (Cancer Research UK) plasmids were used to make stably expressing HeLa cell lines. pFPV 25.1 mCherry plasmid (Valdivia et al., 1996) was used to make M90T mCherry *Shigella* strains. pSA11 and pKB268 plasmids (gift from Prof. Ilan Rosenshine) were used to make x-light *S. flexneri* M90T strains. ActA-SEPT7-mRFP (gift from Dr. Elias Spiliotis), mito-BFP (Addgene #49151), or YFP-Mito^{cb5}TM (gift from Dr. Dale Hailey) were used for quantitative and real-time confocal microscopy.

Table 6.3: List of plasmids used in this study

Plasmids	Vector Type	Application/Description	Source/Reference
SEPT6-GFP	Mammalian expression	Visualization of SEPT6 conjugated to green fluorescent protein (GFP)	Mostowy at al., CHM, 2010
mito-BFP	Mammalian expression	Visualization of mitochondria; expression of mitochondrial matrix protein conjugated to blue fluorescent protein (BFP)	Gift from Gia Voeltz (Addgene plasmid # 49151)
ActA-SEPT7-mRFP	Mammalian expression	Visualization of SEPT7localised to mitochondria; expression of SPET7 and the *Listeria monocytogenes* ActA mitochondria-targeting sequence conjugated to red fluorescent protein (RFP)	Gift from Elias Spiliotis
YFP-Mitocb5TM	Mammalian expression	Mammalian expression of mitochondrial cb5 transmembrane protein conjugated to yellow fluorescent protein	Gift from Dale Hailey
pLVX-GFP-SEPT6	Mammalian expression	Expression of lentiviral vector for SEPT6-GFP HeLa stable cell line	Cancer Research UK (Julia Pfanzelter)
N-FLAG-2xSTREP-SEPT6-pcDNA3	Mammalian expression	Used for tandem affinity purification (TAP) experiments. Expression of N-FLAG-2xSTREP-SEPT6 inserted in XhoI and ApaI sites.	This study (Stephen Buranyi)
pFPV 25.1 mCherry	Bacterial expression	Expression of mCherry protein	Valdivia et al., 1996
pSA11	Bacterial expression	Visualization of M90T x-light GFP under induction with IPTG	Schlosser-Silverman et al., 2000
pKB2689	Bacterial expression	Visualization of M90T x-light mCherry under induction with IPTG	Schlosser-Silverman et al., 2000

6.5. siRNA oligonucleotides

All siRNA used in this study are listed in **Table 6.4**. Small interfering RNA transfection was employed to induce gene knockdown in HeLa cells, by targeting to degradation specific mRNA. The negative universal control with medium G + C content (Ambion, AM4635) was used as control.

Table 6.4:List of siRNA oligonucleotides used in this study

Target gene symbol	siRNA ID	Seuqnce (5'->3')	Source/ Reference
SEPT2	14709	AUAAGCGACGUCCGCGUGGtt	Ambion
SEPT7-1	s2743	GCCUGUUAUCGACUACAUUtt	Ambion
SEPT7-1	s2741	GAAGGGAGCAUGUAGCUAAtt	Ambion
SEPT9	18228	GGGCUUCGAGUUCAACAUCtt	Ambion
SQSTM1 (p62)	s16962	CUUCCGAAUCUACAUUAAAtt	Ambion
NDP52	s19994	GUUGAAGCAGCUCUGUCUAtt	Ambion
DRP1	s19559	GGUUCAUCAGUAAUCCUAAtt	Ambion
MFN1	s31218	GAAAUUUGAUCUCAGUUAUtt	Ambion

6.6. Antibodies

The antibodies used in this study are listed in **Table 6.5.** Working dilutions for each individual application are also indicated. Secondary antibodies used for immunofluorescence (IF) microscopy were 405-conjugated goat anti-rabbit (Biotium), Alexa 488-, 555-, or 647-conjugated donkey anti-rabbit or donkey anti-mouse (Molecular Probes). F-actin was labelled with Alexa 488-, 555-, or 647-phalloidin (Molecular Probes). For immunoblotting, peroxidase-conjugated goat anti-mouse (Dako) or anti-rabbit antibodies (Santa Cruz) were used at a dilution of 1/2000 for western blot (WB) analysis.

Table 6.5: List of antibodies used for this study

Antibody	Species	Application/Dilution	Source/Reference
Primary antibodies			
SEPT2	Rabbit	IF 1/1000; WB 1/1000	Mostowy at al., CHM, 2010
SEPT6	Rabbit	WB 1/1000	Mostowy at al., CHM, 2010
SEPT7	Rabbit	IF 1/1000; WB 1/1000	IBL 18991
SEPT9	Rabbit	IF 1/1000; WB 1/1000	Mostowy at al., CHM, 2010
SEPT11	Rabbit	IF 1/1000; WB 1/1000	Mostowy at al., CHM, 2010
p62	Rabbit	WB 1/1000	MBL (PM045)
p62	Mouse	IF 1/100	BD (610832)
LC3	Rabbit	WB 1/1000	MBL (PM036)
Calcoco2 (NDP52)	Rabbit	WB 1/1000	Abcam (ab68588)
DRP1	Mouse	IF 1/200; WB 1/1000	Abcam (ab56788)
Phospho-DRP1 (Ser616)	Rabbit	IF 1/400; WB 1/1000	Cell Signaling (3455)
MFN1	Mouse	IF 1/100; WB 1/1000	Abcam (ab57602)
GFP	Mouse	WB 1/1000	Abcam (ab1218)
GFP 3E1	Mouse	WB 1/1000	Cancer Research UK
GAPDH	Mouse	WB 1/1000	Abcam (ab8245)
FLAG	Mouse	WB 1/1000	Sigma (F3165-2MG)
eIF2α	Rabbit	WB 1/1000	Cell Signaling (9722)
Phospho-eIF2α (Ser51)	Rabbit	WB 1/1000	Cell Signaling (3597)
Secondary antibodies			
Anti-rabbit 405	Goat	IF 1/500	Biotium (20082)
Anti-rabbit 488	Donkey	IF 1/500	Molecular Probes Alexa Fluor ®
Anti-mouse 488	Donkey	IF 1/500	Molecular Probes Alexa Fluor ®
Anti-rabbit 555	Donkey	IF 1/500	Molecular Probes Alexa Fluor ®
Anti-mouse 555	Donkey	IF 1/500	Molecular Probes Alexa Fluor ®
Anti-rabbit 647	Donkey	IF 1/500	Molecular Probes Alexa Fluor ®
Anti-mouse 647	Donkey	IF 1/500	Molecular Probes Alexa Fluor ®
Anti-Actin 488	Phalloidin	IF 1/200	Molecular Probes Alexa Fluor ®
Anti-Actin 555	Phalloidin	IF 1/200	Molecular Probes Alexa Fluor ®
Anti-Actin 647	Phalloidin	IF 1/200	Molecular Probes Alexa Fluor ®
Anti-rabbit IgG-HRP	Goat	WB 1/2000	Santa Cruz (sc2004)
Anti-mouse IgG-HRP	Goat	WB 1/2000	Dako (P0260)

6.7. Microbiology

6.7.1. Bacterial culture

Shigella flexneri strains were cultured overnight in trypticase soy (TCS) medium, at 37°C with aeration, diluted 50x in 5ml of fresh TCS, and sub-cultured until OD_{600nm} = 0.6 as previously described (Mazon Moya et al., 2014). *Escherichia coli* DH5α strains were grown in Luria Bertani (LB) medium, at 37°C with aeration. Solid bacterial cultures were also grown on solid medium: TCS supplemented with agar (1.5% w/v) and Congo Red (0.01%), or LB supplemented with agar (1.5% w/v). When appropriate, bacterial cultures or solid medium were supplemented with antibiotics: 50µg/ml for Kanamycin (kan) and carbenicillin (carb). *Shigella* strains were used for infection of non-phagocytic cells. *E.coli* strains were used for plasmid production.

6.7.2. Preparation and transformation of bacterial electrocompetent cells

Shigella or *E.coli* DH5α were grown overnight in 8ml of TCS or LB respectively, diluted 80x in 8ml of fresh medium, and cultured until OD_{600nm} = 0.4 – 0.6. Subcultures were incubated on ice for 30 min and subsequently centrifuged at 4000 rpm for 10 min at 4°C and the supernatant was discarded. The cell pellets were washed with 25 ml ice-cold sterile MilliQ water before further centrifugation under the same conditions. This step was repeated twice more. After the final centrifugation the supernatant was discarded and the

bacterial pellet was resuspended in 200µl ice-cold sterile 10% glycerol. Aliquots of 50µl were used immediately or stored at -80.

Electrocompetent bacteria (50µl of *Shigella* or *E.coli* DH5α) were transformed with 0.1 – 0.2 µg of plasmid. The mixture of bacterial and plasmid was incubated in a 0.2cm ice-cold electroporation cuvette (Molecular Bioproducts) for 5 min, thenelectroporation was performed at 2.5KV, 25µF, and 200Ω for 5 milliseconds using a GenePulser II (BioRad). Transformed bacteria were then grown for 1 h in S.O.C. (super optimal) medium (ThermoFisher) shaking at 37°C before plating them onto agar plates supplemented with appropriate antibiotic for selection.

6.8. Eukaryotic cell culture assays

6.8.1. Cell culture

Cells were cultured in Dulbecco's modified Eagle medium (DMEM, GIBCO) supplemented with 10% heat inactivated fetal bovine serum (FBS, Sigma) at 37°C in 5% CO_2. HeLa cells stably expressing GFP-SEPT6 (see section 4.6.2) were grown with a supplement of 1 µg/ml puromycin to maintain selectivity of the cell line.

6.8.2. Generation of GFP-SEPT6 stable cell line

The pLVX-GFP-SEPT6 lentiviral expression vector was created by inserting the human SEPT6_i3 (NP_665798) with a N-terminal GFPtag into the pLVX-puro vector (Takara Bio Inc.) (Barry et al., 2015). Lentivirus was produced in HEK293FT cells by co-transfection of pLVX-GFP-SEPT6 with psPAX2 and pMD2.g vectors at a ratio of 10:7:3 µg DNA, respectively (Trono laboratory second generation packaging system; Addgene). Supernatants from transfected HEK293FT cells containing the lentivirus were collected 24 and 48h after transfection, pooled, and filtered. HeLa cells were then infected with lentivirus for 48h, and cells stably expressing GFP-SEPT6 were selected by adding 1 µg/ml puromycin to the culturing media.

6.8.3. siRNA transfections

HeLa cells (0.8 - 2 × 10^5) were plated in 6-well plates (Thermo Scientific) in 2 ml of DMEM containing 10% FBS, and transfected the following day.

siRNA transfections were performed in DMEM with Oligofectamine

(Invitrogen) according to the manufacturer's instructions. HeLa cells were seeded at 0.8 × 10^5 cells per well for 18 h, and then transfection reactions containing 3µl Oligofectamine or 50nM of siRNA in in 100µl of DMEM were mixed after a previous incubation for 1 min. Following incubation for 20 min at room temperature, the transfection mixtures were added to the cells in a total volume of 1ml DMEM containing 10% FBS. Cells were tested 72 h after siRNA transfection.

6.8.4. qRT-PCR

HeLa cells (1 × 10^5) were grown in 6-well plates and transfected with siRNA as described in section 6.6.1. Following total RNA isolation from cells using an RNAeasy kit (QIAGEN), cDNA was obtained using M-MLV H- reverse-transcriptase (Promega) with a dT17 primer. Quantitative PCR was then performed on an ABI7300 thermocycler (Applied Biosystems) using SYBR green reaction power mix (Applied Biosystems). The primers used for qRT-PCR analysis are listed in **Table 6.6.**

Table 6.6: List of primers used for qRT-PCR analysis

Target gene	Target sequence
GAPDH	qFWD: AATCCCATCACCATCTTCCA
	qREV: TGGACTCCACGACGTACTCA
SEPT2	qFWD: CACCGAAAATCAGTGAAAAAAGG
	qREV: GCTGTTTATGAGAGTCGATTTTCCT
SEPT6	qFWD: GCCAGGGCTTCTGCTTCA
	qREV: AGGGTGGACTTGCCCAAAC
SEPT7	qFWD: TGTTGTTTATACTTCATTGCTCCTTCA
	qREV: CTTTTTCATGCAAACGCTTCAT
SEPT9	qFWD: CCATCGAGATCAAGTCCATCAC
	qREV: CGATATTGAGGAGAAAGGCGTCCGG

Published in (Sirianni et al., 2016).

6.8.5. DNA transfections

DNA plasmid transfections were performed in DMEM with JetPEI (Polyplus transfection) according to protocol from (Mazon Moya et al., 2014). Briefly, HeLa cells were seeded at 1 – 2 × 10^5 cells per well. Transfection reactions containing 4µl JetPei or 0.5 – 1 µg of DNA in 150 µl of NaCl were mixed after a previous incubation for 5 min. Following incubation for 30 min at room temperature, the transfection mixtures were added to the cells in a total volume of 1ml DMEM containing 10% FBS. Cells were tested 24 h after transfection.

6.8.6. Bacterial infection of HeLa cells

HeLa cells (1-2.5 × 10^5) were seeded in 6-well plates (Thermo Scientific) and grown for 24 – 72 h. *Shigella* was grown in TCS for 16 h at 37°C with aeration and sub-cultured as described in previous section. For quantification analysis, bacteria were diluted in warm DMEM and added to HeLa cells monolayers at a MOI of 100; for imaging analysis, 400 µl of growth (OD_{600nm} = 0.6) was diluted in DMEM and directly added to cells. Bacteria and cells were centrifuged at 110 g for 10 min at 21°C and were then placed at 37°C and 5% CO_2 for 30min to synchronise and allow invasion. After 30 min cells were washed with DMEM, and incubated with fresh gentamicin-containing media (50 µg/ml) for at least 1 h to kill extracellular bacteria and avoid re-infections from the extracellular space.

6.8.7. Pharmacological Inhibition of HeLa cells

For experiments involving pharmacological inhibition of actin polymerization,

HeLa cells were treated for 30 min with 0.05% DMSO or 1 µM cytochalasin D prior fixation for confocal microscopy. For the inhibition of *Shigella* activity, HeLa cells were infected and treated with 25 µg/ml Erythromycin for 2 h prior fixation. For inhibition of the acidification of the lysosome, HeLa cells were treated with 160nM Bafilomycin A1 for 6h prior cell harvest from culture dish. Cytochalasin D and Bafilomycin A1 were suspended in DMSO and handled as suggested by the manufacturer (Sigma). Erythromycin was dissolved in EtOH.

6.8.8. Gentamicin survival assay

Gentamicin survival assays were performed according to protocols previously described (Pizarro-Cerdá et al., 2002). HeLa cells (0.8×10^5) were seeded in 6-well plates (Thermo Scientific) in DMEM, infected with *Shigella* at MOI of 100, and centrifuged at 110 g for 10 minutes at 21°C. Cells were then placed at 37°C and 5% CO_2 for 30 minutes, washed with DMEM without antibiotic, and subsequently incubated for 1, 2, or 5 h in presence of gentamicin (50 µg/ml). At given time point, cells were washed twice with 1x sterile PBS and lysed with 1 ml of 0.1 % TritonX-100 in PBS for 1 min at room temperature, followed by vigorous pipetting. After performing serial dilutions (1:10, 1:100, 1:1000) of each time point, undiluted and diluted lysates were plated on LB plates for bacterial counting on the following day. Each experiment was done in three technical replicates, and triplicates were performed at least 3 times independently. Bacterial colonies from each time point were enumerated considering dilutions that only displayed a range of 10 - 80 colonies, and then multiplied by the respective dilution factors. Results from different time points were finally divided by 1 h post infection (p.i.) in order to quantify the difference in fold-change of bacterial intracellular growth over time.

6.8.9. Starvation assays in HeLa cells

Amino acid (AA) starvation experiments in mammalian cells were performed by treating HeLa cells with Earle's Balanced Salt Solution (EBSS) (Dooley et al., 2014) for 6 h at 37°C, 5% CO_2. To measure de efficiency of the treatment, the protein expression level of p62, NDP52 or LC3 was assessed by western blot (see below).

6.8.10. Autophagy flux assays

Autophagy flux assays were performed by treating HeLa cells with EBSS, which leads to a decrease in protein level of the autophagy markers p62, NDP52, and LC3 (Mizushima et al., 2010). Cells were treated with bafilomycin A1 to inhibit the acidification of autophagosomes. This allows an accumulation of the autophagy markers into autophagosomes, subsequently blocking the autophagic degradation (i.e. flux) (Klionsky et al., 2016, Dooley et al., 2014).

For autophagy flux assay in uninfected cells, HeLa cells (0.8 - 1 × 10^5) were grown in 6-well plates. When appropriate, cells were treated with CTRL or SEPT7 siRNA. Cells from different wells were incubated with EBSS, 160 nM Bafilomycin A1, or both for 6 h at 37 °C, 5% CO_2. A fourth well of cells was incubated with DMEM + 10% FBS as a control. After 6 h, protein cell extracts were prepared for western blot as described in section 6.8. Samples were then immunoblotted with specific antibodies to detect the protein levels of p62, NDP52, LC3. GAPDH was used as loading control, and SEPT7 was used to test the efficiency of SEPT7 siRNA treatment. Blots were processed with Fiji and protein expression level was quantified by densitometry.

For autophagy flux assay in infected cells, *Shigella* M90T Afa I was added to treated cells at an MOI of 10 for 4h.

6.8.11. Single population analysis using IPTG-inducible x-light *Shigella*

To test the precise role of septin cages in the restriction or promotion of bacterial replication, individual bacteria entrapped by septin cages were analysed. To allow single bacterial analysis, inducible fluorescent (x-light) *Shigella* strains based on isopropyl β-D-1-thiogalactopyranoside (IPTG) inducible plasmids were generated. X-Light *Shigella* carrying the inducible plasmid would express The inducible plasmids encode for GFP or mCherry, which were cloned downstream of a *tac* promoter under the control of the LacI repressor (Schlosser-Silverman et al., 2000). Binding of IPTG to LacI induces conformational change of the repressor and loss of contact with *tac.* As a consequence, IPTG induces expression of the fluorescent proteins only in x-light *Shigella* with an active metabolism.

6.9. Immunofluorescence microscopy assays

6.9.1. Sample preparation and antibody labelling

HeLa (0.8 - 2.5 × 10^5) were plated on glass coverslips in 6-well plates (Thermo Scientific) and used for experiments 24-72 h later. Cells on coverslips were fixed 15 min in 4% paraformaldehyde (PFA) and washed with 1 × PBS and processed for immunofluorescence. Remaining aldehyde was quenched by incubation with 0.05 M ammonium chloride (Nh_4Cl) for 10 min, and then cells were permeabilised 5-10 min with 0.1% Triton X-100. The antibodies were diluted to the appropriate concentration in 1% BSA and 0.1% Triton X-100 in PBS. Coverslips were washed twice with PBS and incubated with primary antibodies for 1 - 3 h at room temperature or overnight at 4°C. Following incubation coverslips were washed twice with PBS and incubated with secondary antibodies for 30 min. When appropriate, 1 µg Hoechst 33342 (Molecular Probes) was added to the secondary antibody solution. After incubation with secondary antibodies cells were washed 3 times in PBS and mounted on slide with Aqua polymount mounting medium (Polyscience Inc.) for 10 min at 37°C for immunofluorescence.

6.9.2. Image acquisition and image processing

Fixed samples images were acquired on fluorescence-inverted microscope Axiovert 200M (Carl Zeiss MicroImaging) driven by Volocity software (Parkin Elmer), Axiovert Z1 driven by ZEN software Carl Zeiss MicroImaging), or confocal microscope LSM 710 (Carl Zeiss MicroImaging) driven by ZEN 2010 software. For live microscopy, cells were grown on MatTek glass-bottom dishes (MatTek corporation), then supplied with Opti-MEM (GIBCO) medium

and acquired using an LSM 710 and temperature-controlled incubator (37°C). Images or movies were processed and false coloured using Fiji (ImageJ) or Icy (http://icy.bioimageanalysis.org).

6.9.3. Molecular probe labelling of mitochondria or live/dead cells

Where mentioned, mitochondria were stained with MitoTracker Red CMXRos (Invitrogen). HeLa cells were treated with 100nM MitoTracker Red CMXRos in 1ml of serum-free DMEM for 20-30 min at 37°C in 5% CO_2, prior to fixation. MitoTracker Red CMXRos was suspended in DMSO and handled as suggested by the manufacturer (Molecular Probes®).

The detection of live / dead cells was performed with SYTOX Orange® nucleic acid stain (Invitrogen), a marker for compromised cellular membrane characteristic of dead cells. HeLa and/or bacterial cells were treated with 0.4 µM SYTOX Orange in MOPS/$MgCl_2$, in the dark for 10 - 15 min at room temperature. Live image acquisition was then performed using confocal microscope LSM 710.

6.9.4. Quantitative confocal microscopy

For quantitative microscopy of septin cages, p62 punctae, or IPTG-responsive x-light *Shigella,* HeLa cells (0.8 - 2.5 × 10^5) were seeded on glass coverslips in 6-well plates for 24 - 48 h, and infected with *Shigella* at MOI of 100. When appropriate, cells were treated with siRNA for 72 h. Quantifications were performed using a Z stack image series and counting 300–800 bacteria per experiment. Images were processed with Fiji (ImageJ) or Icy (http://icy.bioimageanalysis.org). Where necessary, deconvolution was performed using Huygens deconvolution software or ZEN software.

Mitochondrial length was measured as described in (Korobova et al., 2013, Korobova et al., 2014). In brief, cells were grown on glass coverslip in 6 well plates, and stained with MitoTracker Red CMXRos prior fixation. Z stack image series with 0.2 µm increments for red channel (MitoTracker) were captured. The flat regions of cells with clearly resolved mitochondria were selected, and 25-30 mitochondria per cell were measured using the line tool in Fiji or Icy. For quantification of mitochondrial fission during infection, HeLa cells were infected with *Shigella* for 3 h 40 min, and only mitochondria surrounding *Shigella* were considered. For quantification of mitochondria length around septin cages, only mitochondria associated with a majority of the septin cage (i.e. at least three sides of the bacterial surface) was considered. For quantification of mitochondria associated to septins in cytochalasin D-treated cells, only mitochondria associated with septin rings were considered.

6.9.5. Quantification of IPTG-responsive x-light *Shigella*

For quantification of IPTG-responsive, intracellular *Shigella*, HeLa (0.8 - 1.5 × 10^5) cells were grown on glass coverslips in 6 well plates, infected with x-light *Shigella*, and then induced with 0.1 mM IPTG for 30 min at 37°C prior fixation. When indicated, HeLa cells were treated with siRNA for 72 h. Z stack image series with 0.3 µm increments were acquired with Widefield Axiovert 200M or confocal LSM 710 microscopes. Images were then quantified and analysed as described in previous sections.

6.9.6. Quantification of live/dead x-light *Shigella*

For live / dead stain experiments, x-light *Shigella* GFP/mCherry were grown in TCS overnight and sub-cultured to an OD_{600nm} = 0.6, The culture was split; half of the culture was treated with 70% isopropanol for 30 min at room temperature and the other half remained untreated. The two halves were centrifuged at 10000 g for 2 min 30 sec and washed with 1 ml 1 x PBS. This step was repeated once more. The cultures were then induced with 0.1 mM IPTG for 30 min at 37°C, washed twice with PBS, and then stained with SYTOX orange and Hoechst 33342 in solution with 0.03% saponin and MOPS/$MgCl_2$.

For live / dead stain in infected cells, HeLa cells were grown on MatTek glass-bottom dishes, infected with x-light *Shigella* GFP for 3 h, and then induced with IPTG for 30 min at 37°C. After washing twice with MOPS/$MgCl_2$, cells were stained with SYTOX orange® in solution with 0.03% saponin and MOPS/$MgCl_2$ for 15 min in the dark.

Live Z stack image series were acquired within 30-45 min in a temperature-controlled incubator (37°C).

6.9.7. Fluorescence mean intensity profiling of ActA-SEPT7-mRFP transfected cells

HeLa (1.0×10^5) cells were grown on glass coverslips in 6 well plates, transfected with ActA-SEPT7-mRFP construct for 24 h, then fixed and stained for endogenous SEPT7 and Drp1. Z stack image series with 0.2 µm increments were captured using a confocal microscope LSM 710. A region of interest (ROI) was created using the line tool in Icy, and then the fluorescence mean intensity profile was generated using Icy intensity profile plugin.

Overlapping peaks of fluorescence intensity indicate pattern of colocalization between specifically labelled proteins.

6.9.8. Pearson's correlation coefficient analysis

HeLa cells (0.8 - 1.5 × 10^5) were grown on glass coverslips in 6-well plates, fixed and labelled with specific antibodies. Z stack image series with 0.2 µm increments were captured using a confocal microscope LSM 710. Pearson's correlation coefficient was calculated using Icy colocalization studio plugin (http://icy.bioimageanalysis.org) on defined ROIs of at least 250 cells per biological replicate. For values close to "0", no correlation was considered; for values close to "1", maximum correlation was considered.

For colocalization analysis of P-Drp1 and Mfn1, HeLa cells were treated with CTRL or SEPT7 siRNA for 72 h, labelled with MitoTracker CMXRos prior fixation, and stained with endogenous antibody for P-Drp1 or Mfn1. The analysis was performed comparing the Pearson's correlation coefficient of MitoTracker / Drp1 and MitoTracker / Mfn1 in CTRL- versus SEPT7- treated cells.

For colocalization analysis of Drp1 on mitochondria in ActA-SEPT7-mRFP treated cells, HeLa cells were transfected with mito-BFP for 24 h to visualize mitochondria, fixed and then stained for endogenous Drp1. The analysis was performed comparing the Pearson's correlation coefficient of mito-BFP / Drp1 in untreated- versus ActA-SEPT7-mRFP-treated cells.

6.9.9. Live microscopy of SEPT7 cage assembly

HeLa cells (0.5 - 1 × 10^5) stably expressing SEPT6-GFP were grown on glass-bottom dishes, transfected with mito-BFP for 24 h, infected with *Shigella*-mCherry for 2h, and then live images were acquired using a confocal microscope LSM 710. For fast image acquisition, z stack image series with an increment of 0.4 µm were acquired every 2 min with a line averaging of 2, 512 by 512 pixel, and optimal 1 Airy Unit pinhole. A 63x objective was employed and digital zoom was applied on ROIs. To avoid phototoxicity of cells, time lapse imaging was performed at a low laser power, using 0.31W/cm^2 for mito-BFP imaging, 0.96W/cm^2 for MitoTracker Red CMXRos imaging and 0.52W/cm^2 for GFP imaging.

For **Figure 3.9A**, HeLa cells were treated with Drp1 siRNA for 72 h; infection and images acquisition followed as described above.

6.9.10. Correlative Light-Electron Microscopy (CLEM)

For Correlative Light-Electron Microscopy (CLEM), SEPT6-GFP HeLa cells (1 × 10^5) were grown on cell-locator glass-bottom dishes (MatTek Corporation), transfected with mito-BFP for 24 h, infected with *Shigella*-mCherry, and processed for CLEM. To preserve mitochondrial membrane cells were pre-fixed for confocal microscopy with 4% PFA/0.25 M Hepes at 4°C for 10 min, then with 8% PFA/0.25 M Hepes at room temperature. All the washing steps were performed in 0.25 M Hepes buffer. Specific locations were imaged and localised with high resolution on the cell-locator glass-bottom dishes by using a confocal microscope LSM 710. For subsequent transmission electron microscopy (TEM) analysis, the same samples were fixed with 0.05% Glutaraldehyde/0.2 M Sodium Cacodylate for 45 min at room temperature. All

the washing steps were performed in 0.2 M Sodium Cacodylate buffer. Samples were processed for TEM according to (Hollinshead et al., 2012, Mostowy et al., 2010), the same coordinates imaged with confocal microscopy were recovered, and then images were acquired.

For SEPT7 labelling, HeLa cells were fixed in 8% PFA / Hepes, then cells were permeabilised with 0.2% Saponin. Cells were labelled using the SEPT7 antibody (1:1000) followed by horseradish peroxidase (HRP) anti-Rabbit (1:1000) and then 5 min metal enhanced DAB. Samples were then embedded into Epon for EM.

6.9.11. Structured illumination microscopy (3D-SIM)

HeLa cells (1×10^5) were plated on high precision glass coverslips (Carl Roth) in 6-well plates (Thermo Scientific) and used for experiments 48 h later. Cells were infected with 400 µl of exponential growing *Shigella*-mCherry (OD_{600nm} = 0.6) for 4 h 40 min. Before fixation for 15 min in 4% PFA, infected cells were pre-extracted for 30sec with 0.2% Triton-X-100 in 1 × BRB80 and were washed three times in 1 × PBS. After quenching for 10 min in 50 mM ammonium chloride, cells were incubated with primary or secondary antibodies in 1 × PBS containing 0.1% Triton-X-100 and 5% horse serum and mounted in Vectashield for 3D-SIM. In brief, SIM generates high-resolution images by applying grid patterns of light on a sample, which are rotated and shifted at each focal plane. Fixed 3D-SIM samples were imaged with Elyra S.1 (Carl Zeiss MicroImaging) driven by ZEN 2012 software using 5 grid positions and 3 rotations, resulting in 15 images of each focal plane. The reconstructed, high-resolution 3D images were used to determine the SEPT7 cage architecture.

6.9.12. Super-resolution optical fluctuation imaging

A Super-resolution Optical Fluctuation Imaging (SOFI)-based method was used for imaging septins during mitochondrial fission in live cells, as SOFI allows for the generation of super resolution images acquired at low intensity laser illumination through the temporal analysis of fluorescence intensity fluctuations (Dertinger et al., 2009). For SOFI-based super resolution imaging, HeLa cells stably expressing SEPT6-GFP were grown on glass-bottom dishes (MatTek Corporation) and stained for 30 min with 20 nM MitoTracker Red CMXRos. Live cell imaging of MitoTracker Red CMXRos and Sept6-GFP was performed using an N-STORM inverted microscope (Nikon) in TIRF mode with incubation at 37ºC and 5% CO_2. 561nm and 488nm excitation lasers were angled through the back focal plane of a 60x objective (Nikon) for imaging of MitoTracker Red CMXRos and GFP respectively. A range of laser powers was tested for imaging the samples to determine an appropriate power where sufficient fluctuations for super resolution were achieved while maintaining cell viability. As a result, time lapse imaging was performed using 1.24W/cm^2 for MitoTracker Red CMXRos imaging and 0.82W/cm^2 for GFP imaging. For each super resolution image, 100 frames were acquired with the 561nm laser and 100 frames were acquired with the 488nm laser; this was repeated every 30 seconds with both lasers turned off between time points. Emitted signal from the excited MitoTracker Red CMXRos and GFP molecules was collected by an EMCCD camera (iXon Ultra 897, Andor) with an additional magnification of 1.5x, yielding a pixel size of 178 nm. Final super resolution reconstructions were generated in Fiji (Schindelin et al., 2012) through a custom made SOFI-based algorithm using 2^{nd}-order SOFI and generating images with a pixel size of 36 nm. Thanks to Sian Culley for helping with the text.

6.10. Biochemistry

6.10.1. Preparation of protein cell extracts

For detection of proteins expressed in mammalian cells, HeLa cells (0.5 - 1 × 10^5) were grown in 6 well plates and then the cytosolic content of cells was released to the supernatant by lysing cells with 1 x Laemmli buffer (10 mM Tris-Cl pH 6.8, 2% SDS, 10% glycerol, 5% β-mercaptoethanol, 0.01% bromophenol blue) solution. For the detection of phosphorylated proteins, 1 mM sodium orthovanadate was added to the samples before lysing cells. To reduce the sample viscosity, the cell extracts were subsequently sonicated on ice with mild cycle for 30 sec; proteins were then denaturated by heating samples at 90°C for 10 min.

6.10.2. Electrophoresis

Proteins were separated on an 8, 10 or 12 % Tris-Glycine acrylamide gels (BioRad) prepared as listed in **Table 6.7** and **Table 6.8** (Modified from Harlow and Lane, 1988). Depending on the size of protein of interest, gels were run in 1 x SDS running buffer at 200 V for 35 or 50 min. Gels were further processed for immunoblotting.

Table 6.7: Solutions for preparing resolving gels for Tris-glycine SDS-polyacrylamide gel electrophoresis.

	Volume (ml) of Components Required to Cast Gels of Indicated Volumes and Concentrations							
Components	**Gel Volume =>**	**5 ml**	**10 ml**	**15 ml**	**20 ml**	**25 ml**	**30 ml**	**40 ml**	**50 ml**
8% gel								
H2O		2.3	4.6	6.9	9.3	11.5	13.9	18.5	23.2
30% acrylamide mix		1.3	2.7	4	5.3	6.7	8	10.7	13.3
Tris-Cl (1.5 M, pH 8.8)		1.3	2.5	3.8	5	6.3	7.5	10	12.5
SDS (10%)		0.05	0.1	0.15	0.2	0.25	0.3	0.4	0.5
10% ammonium persulfate		0.05	0.1	0.15	0.2	0.25	0.3	0.4	0.5
TEMED		0.003	0.006	0.009	0.012	0.015	0.018	0.024	0.03
10% gel								
H2O		1.9	4	5.9	7.9	9.9	11.9	15.9	19.8
30% acrylamide mix		1.7	3.3	5	6.7	8.3	10	13.3	16.7
Tris-Cl (1.5 M, pH 8.8)		1.3	2.5	3.8	5	6.3	7.5	10	12.5
SDS (10%)		0.05	0.1	0.15	0.2	0.25	0.3	0.4	0.5
10% ammonium persulfate		0.05	0.1	0.15	0.2	0.25	0.3	0.4	0.5
TEMED		0.002	0.004	0.006	0.008	0.01	0.012	0.016	0.02
12% gel								
H2O		1.6	3.3	4.9	6.6	8.2	9.9	13.2	16.5
30% acrylamide mix		2	4	6	8	10	12	16	20
Tris-Cl (1.5 M, pH 8.8)		1.3	2.5	3.8	5	6.3	7.5	10	12.5
SDS (10%)		0.05	0.1	0.15	0.2	0.25	0.3	0.4	0.5
10% ammonium persulfate		0.05	0.1	0.15	0.2	0.25	0.3	0.4	0.5
TEMED		0.002	0.004	0.006	0.008	0.01	0.012	0.016	0.02

Table 6.8: Solutions for preparing 5% stacking gels for Tris-glycine SDS-polyacrylamide gel electrophoresis

	Volume (ml) of Components Required to Cast Gels of Indicated Volumes							
Components	**Gel Volume =>**	**1 ml**	**2 ml**	**3 ml**	**4 ml**	**5 ml**	**6 ml**	**8 ml**	**10 ml**
H2O		0.68	1.4	2.1	2.7	3.4	4.1	5.5	6.8
30% acrylamide mix		0.17	0.33	0.5	0.67	0.83	1	1.3	1.7
Tris-Cl (1.0 M, pH 6.8)		0.13	0.25	0.38	0.5	0.63	0.75	1	1.25
SDS (10%)		0.01	0.02	0.03	0.04	0.05	0.06	0.08	0.1
ammonium persulfate (10%)		0.01	0.02	0.03	0.04	0.05	0.06	0.08	0.1
TEMED		0.001	0.002	0.003	0.004	0.005	0.006	0.008	0.01

6.10.3. Immunoblotting

To detect specific proteins by immunoblot (western blot), proteins separated by electrophoresis were transferred to nitrocellulose PVDF membranes (Millipore) previously hydrated in 95% ethanol and equilibrated in transfer buffer (7.2 g Glycine, 1.5 g Tris base, 50 ml Ethanol, total volume of 400 ml), at 15 V, 2.5 mA for 15 min. After transfer, the membranes were blocked with 5 % non-fat dried milk in TBST (100 mM Tris-HCl, 150 mM NaCl and 0.1 % Tween-20) for 1 h at room temperature. After 3x washes with TBST, the membranes were incubated with the primary antibody diluted in 5 % milk/TBST for 1 – 2 h at room temperature, or at 4°C overnight. GAPDH was used throughout as a loading control. The membranes were washed 3x times for 5 min in TBST and further incubated with appropriate HRP-conjugated secondary antibody for 30 min at room temperature. After 3x washes in TBST, proteins were visualized on x-ray film (GE Healthcare) using ECL Plus (GE Healthcare) detection reagents and a film developer (AGFA).

Images were processed on Fiji and protein levels were quantified by using the densitometry tool in Fiji (http://fiji.sc/Fiji).

6.10.4. Tandem affinity purification for mass spectrometry

SEPT6 constructs for proteomic analysis of HeLa cells were used because overexpression of SEPT6 does not inhibit *Shigella* invasion, and SEPT6 is found with SEPT7 in septin filaments and cages. To maximise the number of cells infected with *Shigella*, cells were infected with *S. flexneri* M90T AfaI, a hyper-invasive strain that expresses an adhesin from *Escherichia coli* (Mazon Moya et al., 2014).

For tandem affinity purification HeLa cells (5×10^6) were plated in 15 cm plates. Plasmid transfections were performed the following day using 5 µg of N-FLAG-2xSTREP-SEPT6-pcDNA3 and 10 µl jetPEI (Polyplus) per plate. For infection *Shigella* AfaI was added at MOI of 10 and bacteria and cells placed at 37°C and 5% CO_2 for 30 min, washed with DMEM, and incubated with fresh gentamicin-containing media (50 µg/ml) for 4hr. 2 or 4 plates (4 or 8×10^7 cells) per condition were collected by centrifugation for 5 min at 1000 x g.

Cell pellets were lysed in 500 µl lysis buffer (10 mM Tris/Cl pH 7.5; 150 mM NaCl; 0.5 mM EDTA; 0.5% Triton X-100 1x cOmplete (Roche)) and passed through a syringe (23G) 5x. Lysates were centrifuged at 13,000 RPM for 20 min. Supernatants were applied to ANTI-FLAG M2 Magnetic Beads (Sigma) and incubated for 2 h at room temperature. Bound proteins were eluted using 3xFLAG peptide (Sigma) and eluents were applied directed to Strep-Tactin magnetic beads (IBA) and incubated for 2 h at room temperature. Bound proteins were eluted with 0.1 M Glycine HCl, pH 3.0. Final elutions were run on an SDS-PAGE gel and total protein in gel was sent for mass spectrometry service (http://mslab-ibb.pl/). The resulting MS/MS data were used as input for protein identification by MASCOT (www.matrixscience.com) search using the UniprotKB/Swiss-Prot database. The 'CRAPome' (www.crapome.org) database was used to manually remove commonly occurring results and Gene Ontology (http://geneontology.org/) was used to putatively annotate protein function. The use of buffers suitable for mass spectrometry might not prevent potential insolubility of septins, due to their association with lipids. As a consequence, the generation of peptide ions by electrospray would be affected, and important information could be lost. To overcome this, proteins

could be delipidated from membrane bilayers by chloroform extraction, increasing the quality of the resulting mass spectral data.

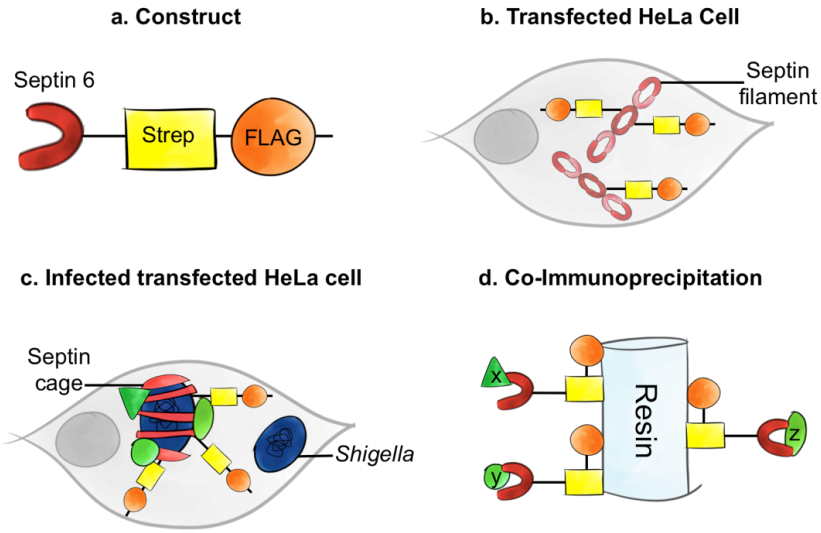

Figure 6.1: Schematic representation of the proteomic experiments used to isolate novel proteins enriched at the *Shigella*-septin cage.
(**a**) A SEPT6-STREP-FLAG construct was (**b**) transfected in HeLa cells for 24h. (**c**) Cells were infected with *S. flexneri* AfaI for 4 h, harvested, and (**d**) SEPT6-STREP-FLAG cage-associated proteins isolated through co-immunoprecipitation (Image from Sirianni *et al*, 2016).

6.10.5. Co-immunoprecipitations

For immunoprecipitation of SEPT6-GFP from infected HeLa cells, 1×10^7 cells were plated in 15 cm plates. For infection, *Shigella* AfaI was added at MOI of 10 and bacteria and cells placed at 37°C and 10% CO_2 for 30 min, washed with DMEM, and incubated with fresh gentamicin-containing media (50 µg/ml) for 4 h. Two plates (4×10^7 cells) per condition were collected by centrifugation for 5 min at 1000 x g. Cell pellets were lysed in 200µl lysis buffer (10 mM Tris/Cl pH 7.5; 150 mM NaCl; 0.5 mM EDTA; 0.5% NP-40, 1x cOmplete (Roche)). Lysates were centrifuged at 13,000 RPM for 20 min. Supernatants were applied to GFP-Trap agarose (Chromotek) and incubated for 1 h at room temperature. Bound proteins were eluted using Laemmli buffer (10 mM Tris-Cl pH 6.8, 2% SDS, 10% glycerol, 5% β-mercaptoethanol, 0.01% bromophenol blue).

For immunoprecipitations, HeLa cells stably expressing either GFP or GFP-SEPT6 were grown to 80% confluency in 15 cm dishes. After washing once with ice-cold PMSF (1mM) cells were scraped into 600 µl lysis buffer and incubated at 4°C for 10 min. Cell lysates were clarified at 13,000 rpm at 4°C for 5 min and the supernatant retained. Lysates were diluted with the addition of 400 µl of wash buffer. 30µl of the diluted lysate was retained as an input sample, to which 30 µl of 2x Laemmli buffer was added. 60 µl of pre-washed GFP-Trap beads (Chromotek) were added to cell lysates and the mixture rotated for 1 hr at 4°C. GFP-Trap beads were then washed 3x with ice-cold wash buffer, and finally resuspended in 60 µl of Laemmli buffer. GFP-Trap beads and input samples were boiled at 95°C for 10 min and samples resolved by SDS-PAGE.

6.10.6. Metabolomic analysis

For metabolomic studies liquid chromatography mass-spectrometry accurate mass retention time (LC-MS AMRT) was used in collaboration with Dr. Gerald Larrouy Maumus (Larrouy-Maumus et al., 2013). HeLa cells (0.8×10^5) were seeded in 6 well plates and treated with CTRL or SEPT7 siRNA respectively for 72 h in DMEM + 10 % FBS at 37°C. Cells were incubated with fresh medium for at least 2 h; for starvation experiments, cells were incubated with EBSS for 6 h at 37°C. After washing twice with PBS and incubation on dry ice for 5 min, cells were lysed into 1 mL acetonitrile/methanol/water (2 : 2 : 1, v/v/v) mixture at −40°C. For each condition, $1.5 – 2.5 \times 10^7$ cells were collected. The lysates were then transferred into a cryotube and after centrifugation at 13,000 x g for 10 min at 4°C, clear supernatants were directly analysed by LC-MS AMRT or stored at -80°C for future analysis.

An Agilent 1200 LC system equipped with a solvent degasser, binary pump, temperature-controlled auto-sampler and temperature-controlled column compartment containing a Cogent Diamond Hydride Type C silica column (150 mm × 2.1 mm; dead volume 315 µl) was used for liquid chromatography. The flow rate on Agilent 1200 LC was 0.4 ml/min. The gradient employed is based on the number 3, according to Pesek and colleagues (Pesek et al., 2008). Briefly, solvent A consists of deionized water, 0.2% acetic acid and solvent B consists in acetonitrile and 0.2% acetic acid and the gradient as follows: 0 min 85%B; 0-2 min 85% B; 2-3 min to 80%B; 3-5 min 80%B; 5-6 min to 75%B; 6-7 min 75%B; 7-8 min to 70%B; 8-9 min 70%B; 9-10 min to 50%B; 10-11 min 50%B; 11-11.1 min to 20%B; 11.1-14 min hold 20%B.

An Agilent Accurate Mass 6230 TOF apparatus was used. Dynamic mass axis

calibration was achieved by continuous infusion of a reference mass solution using an isocratic pump connected to a multimode ionization source, operated in the positive-ion mode. ESI capillary and fragmentor voltages were set at 3500 V and 100 V, respectively. The nebulizer pressure was set at 40 psi and the nitrogen drying gas flow rate was set at 10 L/min. The drying gas temperature was maintained at 250°C. The MS acquisition rate was 1.5 spectra/sec and *m*/*z* data ranging from 50-1200 were stored. This instrument routinely enabled accurate mass spectral measurements with an error of less than 5 parts-per-million (ppm), mass resolution ranging from 10,000-25,000 over the m/z range of 121-955 atomic mass units, and a 100,000-fold dynamic range with picomolar sensitivity. Data were collected in the centroid mode in the 4 GHz (extended dynamic range) mode. Detected *m*/*z* were deemed to be identified metabolites on the basis of unique accurate mass-retention time identifiers for masses exhibiting the expected distribution of accompanying isotopomers (de Carvalho et al., 2010). Variation in abundance for most of the metabolites stayed between 5 and 20% under these experimental conditions.

6.11. Statistics

Statistical analysis was performed in Excel (Microsoft) or Prism GraphPad. Pearson's correlation coefficient was calculated using Icy colocalisation studio plugin (http://icy.bioimageanalysis.org). Data are presented as mean ± standard error of the mean (s.e.m.) from at least 3 independent experiments per treatment. Student's t-test and two-way ANOVA were used to compare values, with $p<0.05$ considered as significant.

BIBLIOGRAPHY

AGUILERA, M. O., BERÓN, W. & COLOMBO, M. I. 2012. The actin cytoskeleton participates in the early events of autophagosome formation upon starvation induced autophagy. *Autophagy,* 8**,** 1590-1603.

ARAKI, Y., KU, W. C., AKIOKA, M., MAY, A. I., HAYASHI, Y., ARISAKA, F., ISHIHAMA, Y. & OHSUMI, Y. 2013. Atg38 is required for autophagy-specific phosphatidylinositol 3-kinase complex integrity. *J Cell Biol,* 203**,** 299-313.

ARCHER, S. L. 2014. Mitochondrial fission and fusion in human diseases. *N Engl J Med,* 370**,** 1074.

AXE, E. L., WALKER, S. A., MANIFAVA, M., CHANDRA, P., RODERICK, H. L., HABERMANN, A., GRIFFITHS, G. & KTISTAKIS, N. T. 2008. Autophagosome formation from membrane compartments enriched in phosphatidylinositol 3-phosphate and dynamically connected to the endoplasmic reticulum. *The Journal of cell biology,* 182**,** 685-701.

BARRY, D. J., DURKIN, C. H., ABELLA, J. V. & WAY, M. 2015. Open source software for quantification of cell migration, protrusions, and fluorescence intensities. *J Cell Biol,* 209**,** 163-180.

BARVE, G., SRIDHAR, S., AHER, A., SINGH, S., K.N., L. & MANJITHAYA, R. 2016. Septins are involved at the early stages of macroautophagy. *bioRxiv*.

BAXT, L. A. & GOLDBERG, M. B. 2014. Host and bacterial proteins that repress recruitment of LC3 to Shigella early during infection. *PloS one,* 9.

BERTIN, A., MCMURRAY, M. A., PIERSON, J., THAI, L., MCDONALD, K. L., ZEHR, E. A., GARCIA, G., PETERS, P., THORNER, J. & NOGALES, E. 2012. Three-dimensional ultrastructure of the septin filament network in Saccharomyces cerevisiae. *Molecular Biology of the Cell,* 23**,** 423-432.

BESTEBROER, J., V'KOVSKI, P., MAUTHE, M. & REGGIORI, F. 2013. Hidden Behind Autophagy: The Unconventional Roles of ATG Proteins. *Traffic,* 14**,** 1029-1041.

BIRGISDOTTIR, Å. B., LAMARK, T. & JOHANSEN, T. 2013. The LIR motif – crucial for selective autophagy. *Journal of Cell Science,* 126**,** 3237-3247.

BIRMINGHAM, C. L., CANADIEN, V., KANIUK, N. A., STEINBERG, B. E., HIGGINS, D. E. & BRUMELL, J. H. 2008. Listeriolysin O allows

Listeria monocytogenes replication in macrophage vacuoles. *Nature,* 451**,** 350-4.
BIRSOY, K., WANG, T., CHEN, W. W., FREINKMAN, E., ABU-REMAILEH, M. & SABATINI, D. M. 2015. An Essential Role of the Mitochondrial Electron Transport Chain in Cell Proliferation Is to Enable Aspartate Synthesis. *Cell,* 162**,** 540-51.
BLANCHOIN, L., BOUJEMAA-PATERSKI, R., SYKES, C. & PLASTINO, J. 2014. Actin dynamics, architecture, and mechanics in cell motility. *Physiol Rev,* 94**,** 235-63.
BLEAZARD, W., MCCAFFERY, J. M., KING, E. J., BALE, S., MOZDY, A., TIEU, Q., NUNNARI, J. & SHAW, J. M. 1999. The dynamin-related GTPase Dnm1 regulates mitochondrial fission in yeast. *Nature cell biology,* 1**,** 298-304.
BOYLE, K. B. & RANDOW, F. 2013. The role of 'eat-me'signals and autophagy cargo receptors in innate immunity. *Current opinion in microbiology*.
BRIDGES, A. A. & GLADFELTER, A. S. 2015. Septin form and function at the cell cortex. *J Biol Chem,* 290**,** 17173-17180.
BRIDGES, A. A., JENTZSCH, M. S., OAKES, P. W., OCCHIPINTI, P. & GLADFELTER, A. S. 2016. Micron-scale plasma membrane curvature is recognized by the septin cytoskeleton. *The Journal of cell biology,* 213**,** 23-32.
BRUMELL, J. H., GOOSNEY, D. L. & FINLAY, B. B. 2002. SifA, a type III secreted effector of *Salmonella typhimurium*, directs *Salmonella*-induced filament (Sif) formation along microtubules. *Traffic,* 3**,** 407-415.
BUI, H. T. & SHAW, J. M. 2013. Dynamin assembly strategies and adaptor proteins in mitochondrial fission. *Current biology : CB,* 23**,** 9.
CAMPBELL-VALOIS, F.-X. X., SACHSE, M., SANSONETTI, P. J. & PARSOT, C. 2015. Escape of Actively Secreting Shigella flexneri from ATG8/LC3-Positive Vacuoles Formed during Cell-To-Cell Spread Is Facilitated by IcsB and VirA. *mBio,* 6**,** 14.
CAO, L., DING, X., YU, W., YANG, X., SHEN, S. & YU, L. 2007. Phylogenetic and evolutionary analysis of the septin protein family in metazoan. *FEBS letters,* 581**,** 5526-5532.
CARNEIRO, L. A. M., TRAVASSOS, L. H., SOARES, F., TATTOLI, I., MAGALHAES, J. G., BOZZA, M. T., PLOTKOWSKI, M. C., SANSONETTI, P. J., MOLKENTIN, J. D., PHILPOTT, D. J. & GIRARDIN, S. E. 2009. *Shigella* induces mitochondrial dysfunction and cell death in nonmyleoid cells. *Cell Host Microbe,* 5**,** 123-136.
CAUDRON, F. & BARRAL, Y. 2009. Septins and the lateral compartmentalization of eukaryotic membranes. *Dev Cell,* 16**,** 493-506.
CEMMA, M. & BRUMELL, J. H. 2012. Interactions of pathogenic bacteria with autophagy systems. *Curr Biol,* 22**,** R540-5.
CHAN, D. C. 2012. Fusion and fission: interlinked processes critical for mitochondrial health. *Annual review of genetics,* 46**,** 265-287.

CHANG, C.-R. & BLACKSTONE, C. 2010. Dynamic regulation of mitochondrial fission through modification of the dynamin-related protein Drp1. *Ann New York Acad Sci,* 1201**,** 34-39.
CHANG, C. R. & BLACKSTONE, C. 2007. Drp1 phosphorylation and mitochondrial regulation. *EMBO Rep,* 8**,** 1088-9; author reply 1089-90.
CHEN, D., FAN, W., LU, Y., DING, X., CHEN, S. & ZHONG, Q. 2012a. A mammalian autophagosome maturation mechanism mediated by TECPR1 and the Atg12-Atg5 conjugate. *Mol Cell,* 45**,** 629-41.
CHEN, D., FAN, W., LU, Y., DING, X., CHEN, S. & ZHONG, Q. 2012b. A mammalian autophagosome maturation mechanism mediated by TECPR1 and the Atg12-Atg5 conjugate. *Molecular cell,* 45**,** 629-641.
CHONG, A., WEHRLY, T. D., CHILD, R., HANSEN, B., HWANG, S., VIRGIN, H. W. & CELLI, J. 2012. Cytosolic clearance of replication-deficient mutants reveals Francisella tularensis interactions with the autophagic pathway. *Autophagy,* 8**,** 1342-56.
CHOY, A. & ROY, C. R. 2013. Autophagy and bacterial infection: an evolving arms race. *Trends in Microbiology,* 21**,** 451-456.
CLAY, L., CAUDRON, F., DENOTH-LIPPUNER, A., BOETTCHER, B., BUVELOT FREI, S., SNAPP, E. L. & BARRAL, Y. 2014. A sphingolipid-dependent diffusion barrier confines ER stress to the yeast mother cell. *eLife,* 3.
COLES, C. H. & BRADKE, F. 2015. Coordinating neuronal actin-microtubule dynamics. *Curr Biol,* 25**,** R677-91.
COSSART, P. 2011. Illuminating the landscape of host-pathogen interactions with the bacterium Listeria monocytogenes. *Proc Natl Acad Sci U S A,* 108**,** 19484-91.
DE BRITO, O. M. & SCORRANO, L. 2008. Mitofusin 2 tethers endoplasmic reticulum to mitochondria. *Nature,* 456**,** 605-610.
DE CARVALHO, L. P. S., FISCHER, S. M., MARRERO, J., NATHAN, C., EHRT, S. & RHEE, K. Y. 2010. Metabolomics of Mycobacterium tuberculosis Reveals Compartmentalized Co-Catabolism of Carbon Substrates. *Chemistry & Biology,* 17**,** 1122-1131.
DE VOS, K. J., ALLAN, V. J., GRIERSON, A. J. & SHEETZ, M. P. 2005. Mitochondrial function and actin regulate dynamin-related protein 1-dependent mitochondrial fission. *Curr Biol,* 15**,** 678-683.
DERETIC, V. 2012. Autophagy as an innate immunity paradigm: expanding the scope and repertoire of pattern recognition receptors. *Current opinion in immunology,* 24**,** 21-31.
DERETIC, V. & LEVINE, B. 2009. Autophagy, immunity, and microbial adaptations. *Cell Host Microbe,* 5**,** 527-49.
DERETIC, V., SAITOH, T. & AKIRA, S. 2013. Autophagy in infection, inflammation and immunity. *Nature reviews. Immunology,* 13**,** 722-737.
DERTINGER, T., COLYER, R., IYER, G., WEISS, S. & ENDERLEIN, J. 2009. Fast, background-free, 3D super-resolution optical fluctuation imaging (SOFI). *Proceedings of the National Academy of Sciences,* 106**,** 22287-22292.

DESAI, A. & MITCHISON, T. J. 1997. Microtubule polymerization dynamics. *Annu Rev Cell Dev Biol,* 13**,** 83-117.
DIAO, J., LIU, R., RONG, Y., ZHAO, M., ZHANG, J., LAI, Y., ZHOU, Q., WILZ, L. M., LI, J., VIVONA, S., PFUETZNER, R. A., BRUNGER, A. T. & ZHONG, Q. 2015. ATG14 promotes membrane tethering and fusion of autophagosomes to endolysosomes. *Nature,* 520**,** 563-566.
DONG, N., ZHU, Y., LU, Q., HU, L., ZHENG, Y. & SHAO, F. 2012. Structurally distinct bacterial TBC-like GAPs link Arf GTPase to Rab1 inactivation to counteract host defenses. *Cell,* 150**,** 1029-41.
DOOLEY, H. C., RAZI, M., POLSON, H. E., GIRARDIN, S. E., WILSON, M. I. & TOOZE, S. A. 2014. WIPI2 links LC3 conjugation with PI3P, autophagosome formation, and pathogen clearance by recruiting Atg12-5-16L1. *Mol Cell,* 55**,** 238-52.
DORTET, L., MOSTOWY, S., SAMBA-LOUAKA, A., LOUAKA, A., GOUIN, E., NAHORI, M.-A., WIEMER, E., DUSSURGET, O. & COSSART, P. 2011. Recruitment of the major vault protein by InlK: a Listeria monocytogenes strategy to avoid autophagy. *PLoS pathogens,* 7.
DUPONT, N., LACAS-GERVAIS, S., BERTOUT, J., PAZ, I., FRECHE, B., VAN NHIEU, G. T., VAN DER GOOT, F. G., SANSONETTI, P. J. & LAFONT, F. 2009. Shigella phagocytic vacuolar membrane remnants participate in the cellular response to pathogen invasion and are regulated by autophagy. *Cell Host Microbe,* 6**,** 137-49.
ESTEY, M., DI CIANO-OLIVEIRA, C., FROESE, C., BEJIDE, M. & TRIMBLE, W. 2010. Distinct roles of septins in cytokinesis: SEPT9 mediates midbody abscission. *The Journal of cell biology,* 191**,** 741-749.
ESTEY, M. P., DI CIANO-OLIVEIRA, C., FROESE, C. D., FUNG, K. Y., STEELS, J. D., LITCHFIELD, D. W. & TRIMBLE, W. S. 2013. Mitotic regulation of SEPT9 protein by cyclin-dependent kinase 1 (Cdk1) and Pin1 protein is important for the completion of cytokinesis. *J Biol Chem,* 288**,** 30075-86.
FENG, Y., HE, D., YAO, Z. & KLIONSKY, D. J. 2014. The machinery of macroautophagy. *Cell research,* 24**,** 24-41.
FENGSRUD, M., ERICHSEN, E. S., BERG, T. O., RAIBORG, C. & SEGLEN, P. O. 2000. Ultrastructural characterization of the delimiting membranes of isolated autophagosomes and amphisomes by freeze-fracture electron microscopy. *European journal of cell biology,* 79**,** 871-882.
FLOREY, O., KIM, S. E., SANDOVAL, C. P., HAYNES, C. M. & OVERHOLTZER, M. 2011. Autophagy machinery mediates macroendocytic processing and entotic cell death by targeting single membranes. *Nat Cell Biol,* 13**,** 1335-43.
FLOREY, O. & OVERHOLTZER, M. 2012. Autophagy proteins in macroendocytic engulfment. *Trends Cell Biol,* 22**,** 374-80.
FRIEDMAN, J. R., LACKNER, L. L., WEST, M., DIBENEDETTO, J. R., NUNNARI, J. & VOELTZ, G. K. 2011. ER tubules mark sites of mitochondrial division. *Science (New York, N.Y.),* 334**,** 358-362.
FRIEDMAN, J. R. & NUNNARI, J. 2014. Mitochondrial form and function. *Nature,* 505**,** 335-343.

FRÖHLICH, C., GRABIGER, S., SCHWEFEL, D., FAELBER, K., ROSENBAUM, E., MEARS, J., ROCKS, O. & DAUMKE, O. 2013. Structural insights into oligomerization and mitochondrial remodelling of dynamin 1-like protein. *The EMBO journal,* 32**,** 1280-1292.

FUJITA, N., HAYASHI-NISHINO, M., FUKUMOTO, H., OMORI, H., YAMAMOTO, A., NODA, T. & YOSHIMORI, T. 2008. An Atg4B mutant hampers the lipidation of LC3 paralogues and causes defects in autophagosome closure. *Molecular biology of the cell,* 19**,** 4651-4659.

FUNG, K. Y., DAI, L. & TRIMBLE, W. S. 2014. Cell and molecular biology of septins. *Int Rev Cell Mol Biol,* 310**,** 289-339.

GANLEY, I. G., LAM DU, H., WANG, J., DING, X., CHEN, S. & JIANG, X. 2009. ULK1.ATG13.FIP200 complex mediates mTOR signaling and is essential for autophagy. *J Biol Chem,* 284**,** 12297-305.

GEERAERT, C., RATIER, A., PFISTERER, S., PERDIZ, D., CANTALOUBE, I., ROUAULT, A., PATTINGRE, S., PROIKAS-CEZANNE, T., CODOGNO, P. & POÜS, C. 2010. Starvation-induced hyperacetylation of tubulin is required for the stimulation of autophagy by nutrient deprivation. *The Journal of biological chemistry,* 285**,** 24184-24194.

GLOTZER, M. 2005. The molecular requirements for cytokinesis. *Science (New York, N.Y.),* 307**,** 1735-1739.

GOLDBERG, M. B. & THERIOT, J. A. 1995. Shigella flexneri surface protein IcsA is sufficient to direct actin-based motility. *Proc Natl Acad Sci U S A,* 92**,** 6572-6.

GUSTAFSSON, N., CULLEY, S., ASHDOWN, G., OWEN, D. M., PEREIRA, P. M. & HENRIQUES, R. 2016. Fast live-cell conventional fluorophore nanoscopy with ImageJ through super-resolution radial fluctuations. *Nat Commun,* 7**,** 12471.

HAAS, A. 2007. The phagosome: compartment with a license to kill. *Traffic,* 8**,** 311-30.

HAGIWARA, A., TANAKA, Y., HIKAWA, R., MORONE, N., KUSUMI, A., KIMURA, H. & KINOSHITA, M. 2011. Submembranous septins as relatively stable components of actin-based membrane skeleton. *Cytoskeleton (Hoboken),* 68**,** 512-25.

HAGLUND, C. & WELCH, M. 2011. Pathogens and polymers: microbe-host interactions illuminate the cytoskeleton. *The Journal of cell biology,* 195**,** 7-17.

HAILEY, D. W., RAMBOLD, A. S., SATPUTE-KRISHNAN, P., MITRA, K., SOUGRAT, R., KIM, P. K. & LIPPINCOTT-SCHWARTZ, J. 2010. Mitochondria supply membranes for autophagosome biogenesis during starvation. *Cell,* 141**,** 656-667.

HARRIS, H. & RUBINSZTEIN, D. C. 2012. Control of autophagy as a therapy for neurodegenerative disease. *Nature reviews. Neurology,* 8**,** 108-117.

HARTWELL, L. H. 1971. Genetic control of the cell division cycle in yeast. IV. Genes controlling bud emergence and cytokinesis. *Exp Cell Res,* 69**,** 265-76.

HATCH, A. L., GUREL, P. S. & HIGGS, H. N. 2014. Novel roles for actin in mitochondrial fission. *J Cell Sci,* 127**,** 4549-4560.
HAYASHI-NISHINO, M., FUJITA, N., NODA, T., YAMAGUCHI, A., YOSHIMORI, T. & YAMAMOTO, A. 2009. A subdomain of the endoplasmic reticulum forms a cradle for autophagosome formation. *Nature cell biology,* 11**,** 1433-1437.
HEO, J. M., ORDUREAU, A., PAULO, J. A., RINEHART, J. & HARPER, J. W. 2015. The PINK1-PARKIN Mitochondrial Ubiquitylation Pathway Drives a Program of OPTN/NDP52 Recruitment and TBK1 Activation to Promote Mitophagy. *Mol Cell,* 60**,** 7-20.
HERRMANN, H., BAR, H., KREPLAK, L., STRELKOV, S. V. & AEBI, U. 2007. Intermediate filaments: from cell architecture to nanomechanics. *Nat Rev Mol Cell Biol,* 8**,** 562-73.
HERRMANN, H., STRELKOV, S. V., BURKHARD, P. & AEBI, U. 2009. Intermediate filaments: primary determinants of cell architecture and plasticity. *J Clin Invest,* 119**,** 1772-83.
HIRD, S. J., LAU, B. P. Y., SCHUHMACHER, R. & KRSKA, R. 2014. Liquid chromatography-mass spectrometry for the determination of chemical contaminants in food. *TrAC Trends in Analytical Chemistry,* 59**,** 59-72.
HOHFELD, J. 2016. Autophagy: Press and Push for Destruction. *Curr Biol,* 26**,** R703-5.
HOLLINSHEAD, M., JOHNS, H. L., SAYERS, C. L., GONZALEZ‐LOPEZ, C., SMITH, G. L. & ELLIOTT, G. 2012. Endocytic tubules regulated by Rab GTPases 5 and 11 are used for envelopment of herpes simplex virus. *EMBO J,* 31**,** 4204-4220.
HOSOKAWA, N., HARA, T., KAIZUKA, T., KISHI, C., TAKAMURA, A., MIURA, Y., IEMURA, S., NATSUME, T., TAKEHANA, K., YAMADA, N., GUAN, J. L., OSHIRO, N. & MIZUSHIMA, N. 2009. Nutrient-dependent mTORC1 association with the ULK1-Atg13-FIP200 complex required for autophagy. *Mol Biol Cell,* 20**,** 1981-91.
HU, Q., NELSON, W. J. & SPILIOTIS, E. T. 2008. Forchlorfenuron alters mammalian septin assembly, organization, and dynamics. *J Biol Chem,* 283**,** 29563-71.
HUANG, J. & BRUMELL, J. H. 2014. Bacteria-autophagy interplay: a battle for survival. *Nature Reviews Microbiology,* 12.
HUETT, A., HEATH, R. J., BEGUN, J., SASSI, S. O., BAXT, L. A., VYAS, J. M., GOLDBERG, M. B. & XAVIER, R. J. 2012. The LRR and RING domain protein LRSAM1 is an E3 ligase crucial for ubiquitin-dependent autophagy of intracellular Salmonella Typhimurium. *Cell host & microbe,* 12**,** 778-790.
ICHIMURA, Y., KIRISAKO, T., TAKAO, T., SATOMI, Y., SHIMONISHI, Y., ISHIHARA, N., MIZUSHIMA, N., TANIDA, I., KOMINAMI, E., OHSUMI, M., NODA, T. & OHSUMI, Y. 2000. A ubiquitin-like system mediates protein lipidation. *Nature,* 408**,** 488-92.

ISHIHARA, N., EURA, Y. & MIHARA, K. 2004. Mitofusin 1 and 2 play distinct roles in mitochondrial fusion reactions via GTPase activity. *J Cell Sci,* 117**,** 6535-46.
ISHIHARA, N., NOMURA, M., JOFUKU, A., KATO, H., SUZUKI, S. O., MASUDA, K., OTERA, H., NAKANISHI, Y., NONAKA, I., GOTO, Y.-I., TAGUCHI, N., MORINAGA, H., MAEDA, M., TAKAYANAGI, R., YOKOTA, S. & MIHARA, K. 2009. Mitochondrial fission factor Drp1 is essential for embryonic development and synapse formation in mice. *Nature Cell Biology,* 11**,** 958-966.
ITAKURA, E., KISHI-ITAKURA, C. & MIZUSHIMA, N. 2012. The hairpin-type tail-anchored SNARE syntaxin 17 targets to autophagosomes for fusion with endosomes/lysosomes. *Cell,* 151**,** 1256-1269.
ITAKURA, E. & MIZUSHIMA, N. 2010. Characterization of autophagosome formation site by a hierarchical analysis of mammalian Atg proteins. *Autophagy,* 6**,** 764-76.
JOHANSEN, T. & LAMARK, T. 2011. Selective autophagy mediated by autophagic adapter proteins. *Autophagy,* 7**,** 279-296.
JUNG, C. H., JUN, C. B., RO, S. H., KIM, Y. M., OTTO, N. M., CAO, J., KUNDU, M. & KIM, D. H. 2009. ULK-Atg13-FIP200 complexes mediate mTOR signaling to the autophagy machinery. *Mol Biol Cell,* 20**,** 1992-2003.
KABEYA, Y., MIZUSHIMA, N., UENO, T., YAMAMOTO, A., KIRISAKO, T., NODA, T., KOMINAMI, E., OHSUMI, Y. & YOSHIMORI, T. 2000. LC3, a mammalian homologue of yeast Apg8p, is localized in autophagosome membranes after processing. *EMBO J,* 19**,** 5720-8.
KABEYA, Y., MIZUSHIMA, N., YAMAMOTO, A., OSHITANI-OKAMOTO, S., OHSUMI, Y. & YOSHIMORI, T. 2004. LC3, GABARAP and GATE16 localize to autophagosomal membrane depending on form-II formation. *J Cell Sci,* 117**,** 2805-12.
KENTNER, D., MARTANO, G., CALLON, M., CHIQUET, P., BRODMANN, M., BURTON, O., WAHLANDER, A., NANNI, P., DELMOTTE, N., GROSSMANN, J., LIMENITAKIS, J., SCHLAPBACH, R., KIEFER, P., VORHOLT, J. A., HILLER, S. & BUMANN, D. 2014. Shigella reroutes host cell central metabolism to obtain high-flux nutrient supply for vigorous intracellular growth. *Proceedings of the National Academy of Sciences of the United States of America*.
KHAMINETS, A., BEHL, C. & DIKIC, I. 2016. Ubiquitin-Dependent And Independent Signals In Selective Autophagy. *Trends in cell biology,* 26**,** 6-16.
KILLACKEY, S. A., SORBARA, M. T. & GIRARDIN, S. E. 2016. Cellular Aspects of Shigella Pathogenesis: Focus on the Manipulation of Host Cell Processes. *Frontiers in cellular and infection microbiology,* 6**,** 38.
KIM, M., FROESE, C., ESTEY, M. & TRIMBLE, W. 2011. SEPT9 occupies the terminal positions in septin octamers and mediates polymerization-dependent functions in abscission. *The Journal of cell biology,* 195**,** 815-826.
KINOSHITA, M. 2003. The septins. *Genome Biol,* 4**,** 236.

KINOSHITA, M., FIELD, C., COUGHLIN, M., STRAIGHT, A. & MITCHISON, T. 2002. Self- and actin-templated assembly of Mammalian septins. *Developmental cell,* 3**,** 791-802.
KIRISAKO, T., ICHIMURA, Y., OKADA, H., KABEYA, Y., MIZUSHIMA, N., YOSHIMORI, T., OHSUMI, M., TAKAO, T., NODA, T. & OHSUMI, Y. 2000. The reversible modification regulates the membrane-binding state of Apg8/Aut7 essential for autophagy and the cytoplasm to vacuole targeting pathway. *J Cell Biol,* 151**,** 263-76.
KISSEL, H., GEORGESCU, M.-M. M., LARISCH, S., MANOVA, K., HUNNICUTT, G. R. & STELLER, H. 2005. The Sept4 septin locus is required for sperm terminal differentiation in mice. *Developmental cell,* 8**,** 353-364.
KLIONSKY, D. J., ABDELMOHSEN, K., ABE, A., ABEDIN, M. J., ABELIOVICH, H., ACEVEDO AROZENA, A., ADACHI, H., ADAMS, C. M., ADAMS, P. D., ADELI, K., ADHIHETTY, P. J., ADLER, S. G., AGAM, G., AGARWAL, R., AGHI, M. K., AGNELLO, M., AGOSTINIS, P., AGUILAR, P. V., AGUIRRE-GHISO, J., AIROLDI, E. M., AIT-SI-ALI, S., AKEMATSU, T., AKPORIAYE, E. T., AL-RUBEAI, M., ALBAICETA, G. M., ALBANESE, C., ALBANI, D., ALBERT, M. L., ALDUDO, J., ALGÜL, H., ALIREZAEI, M., ALLOZA, I., ALMASAN, A., ALMONTE-BECERIL, M., ALNEMRI, E. S., ALONSO, C., ALTAN-BONNET, N., ALTIERI, D. C., ALVAREZ, S., ALVAREZ-ERVITI, L., ALVES, S., AMADORO, G., AMANO, A., AMANTINI, C., AMBROSIO, S., AMELIO, I., AMER, A. O., AMESSOU, M., AMON, A., AN, Z., ANANIA, F. A., ANDERSEN, S. U., ANDLEY, U. P., ANDREADI, C. K., ANDRIEU-ABADIE, N., ANEL, A., ANN, D. K., ANOOPKUMAR-DUKIE, S., ANTONIOLI, M., AOKI, H., APOSTOLOVA, N., AQUILA, S., AQUILANO, K., ARAKI, K., ARAMA, E., ARANDA, A., ARAYA, J., ARCARO, A., ARIAS, E., ARIMOTO, H., ARIOSA, A. R., ARMSTRONG, J. L., ARNOULD, T., ARSOV, I., ASANUMA, K., ASKANAS, V., ASSELIN, E., ATARASHI, R., ATHERTON, S. S., ATKIN, J. D., ATTARDI, L. D., AUBERGER, P., AUBURGER, G., AURELIAN, L., AUTELLI, R., AVAGLIANO, L., AVANTAGGIATI, M. L., AVRAHAMI, L., AWALE, S., AZAD, N., BACHETTI, T., BACKER, J. M., BAE, D.-H. H., BAE, J.-S. S., BAE, O.-N. N., BAE, S. H., BAEHRECKE, E. H., BAEK, S.-H. H., BAGHDIGUIAN, S. & BAGNIEWSKA-ZADWORNA, A. 2016. Guidelines for the use and interpretation of assays for monitoring autophagy (3rd edition). *Autophagy,* 12**,** 1-222.
KOIRALA, S., GUO, Q., KALIA, R. & BUI, H. T. 2013. Interchangeable adaptors regulate mitochondrial dynamin assembly for membrane scission. *Proceedings of the ….*
KORNREICH, M., AVINERY, R., MALKA-GIBOR, E., LASER-AZOGUI, A. & BECK, R. 2015. Order and disorder in intermediate filament proteins. *FEBS Lett,* 589**,** 2464-76.
KOROBOVA, F., GAUVIN, T. J. & HIGGS, H. N. 2014. A role for myosin II in mammalian mitochondrial fission. *Current biology : CB,* 24**,** 409-414.

KOROBOVA, F., RAMABHADRAN, V. & HIGGS, H. N. 2013. An actin-dependent step in mitochondrial fission mediated by the ER-associated formin INF2. *Science (New York, N.Y.),* 339**,** 464-467.
KOROLCHUK, V. I., SAIKI, S., LICHTENBERG, M., SIDDIQI, F. H., ROBERTS, E. A., IMARISIO, S., JAHREISS, L., SARKAR, S., FUTTER, M., MENZIES, F. M., O'KANE, C. J., DERETIC, V. & RUBINSZTEIN, D. C. 2011. Lysosomal positioning coordinates cellular nutrient responses. *Nature Cell Biology,* 13**,** 453-460.
KUMAR, Y. & VALDIVIA, R. H. 2008. Actin and Intermediate Filaments Stabilize the Chlamydia trachomatis Vacuole by Forming Dynamic Structural Scaffolds. *Cell Host & Microbe,* 4**,** 159-169.
LACKNER, L. L. & NUNNARI, J. M. 2009. The molecular mechanism and cellular functions of mitochondrial division. *Biochim Biophys Acta,* 1792**,** 1138-44.
LAM, G. Y., CEMMA, M., MUISE, A. M., HIGGINS, D. E. & BRUMELL, J. H. 2013. Host and bacterial factors that regulate LC3 recruitment to Listeria monocytogenes during the early stages of macrophage infection. *Autophagy,* 9**,** 985-95.
LARROUY-MAUMUS, G., BISWAS, T., HUNT, D. M., KELLY, G., TSODIKOV, O. V. & DE CARVALHO, L. P. S. 2013. Discovery of a glycerol 3-phosphate phosphatase reveals glycerophospholipid polar head recycling in Mycobacterium tuberculosis. *Proceedings of the National Academy of Sciences,* 110**,** 11320-11325.
LAZAROU, M., SLITER, D. A., KANE, L. A., SARRAF, S. A., WANG, C., BURMAN, J. L., SIDERIS, D. P., FOGEL, A. I. & YOULE, R. J. 2015. The ubiquitin kinase PINK1 recruits autophagy receptors to induce mitophagy. *Nature,* 524**,** 309-314.
LEE, I. J. J., COFFMAN, V. C. & WU, J.-Q. Q. 2012. Contractile-ring assembly in fission yeast cytokinesis: Recent advances and new perspectives. *Cytoskeleton (Hoboken, N.J.),* 69**,** 751-763.
LEE, J.-Y., KOGA, H., KAWAGUCHI, Y., TANG, W., WONG, E., GAO, Y.-S., PANDEY, U. B., KAUSHIK, S., TRESSE, E., LU, J., TAYLOR, P. J., CUERVO, A. & YAO, T.-P. 2010. HDAC6 controls autophagosome maturation essential for ubiquitin-selective quality-control autophagy. *The EMBO Journal,* 29**,** 969-980.
LEUNG, Y., ALLY, S. & GOLDBERG, M. B. 2008. Bacterial actin assembly requires toca-1 to relieve N-wasp autoinhibition. *Cell Host Microbe,* 3**,** 39-47.
LEVINE, B., MIZUSHIMA, N. & VIRGIN, H. 2011a. Autophagy in immunity and inflammation. *Nature,* 469**,** 323-335.
LEVINE, B., MIZUSHIMA, N. & VIRGIN, H. W. 2011b. Autophagy in immunity and inflammation. *Nature,* 469**,** 323-335.
LIMA, I. F., HAVT, A. & LIMA, A. A. 2015. Update on molecular epidemiology of Shigella infection. *Curr Opin Gastroenterol,* 31**,** 30-7.
LOBATO-MARQUEZ, D. & MOSTOWY, S. 2016. Septins recognize micron-scale membrane curvature. *J Cell Biol,* 213**,** 5-6.

LOBET, E., LETESSON, J. J. & ARNOULD, T. 2015. Mitochondria: a target for bacteria. *Biochem Pharmacol,* 94**,** 173-85.
LUM, M. & MORONA, R. 2014. Dynamin-related protein Drp1 and mitochondria are important for Shigella flexneri infection. *International journal of medical microbiology : IJMM,* 304**,** 530-541.
LYDIA, L. & BENJAMIN, F. 2013. Mitochondria: Metabolic regulators of innate immune responses to pathogens and cell stress. *The International Journal of Biochemistry & Cell Biology,* 45**,** 2052-2056.
MACDONALD, P. J., STEPANYANTS, N. & MEHROTRA, N. 2014. A dimeric equilibrium intermediate nucleates Drp1 reassembly on mitochondrial membranes for fission. *Molecular biology of ….*
MANOR, U., BARTHOLOMEW, S., GOLANI, G., CHRISTENSON, E., KOZLOV, M., HIGGS, H., SPUDICH, J. & LIPPINCOTT-SCHWARTZ, J. 2015. A mitochondria-anchored isoform of the actin-nucleating Spire protein regulates mitochondrial division. *eLife,* 10.7554**,** eLife.08828.
MANZANILLO, P. S., AYRES, J. S., WATSON, R. O., COLLINS, A. C., SOUZA, G., RAE, C. S., SCHNEIDER, D. S., NAKAMURA, K., SHILOH, M. U. & COX, J. S. 2013. The ubiquitin ligase parkin mediates resistance to intracellular pathogens. *Nature,* advance online publication.
MARGIOTTA, A. & BUCCI, C. 2016. Role of Intermediate Filaments in Vesicular Traffic. *Cells,* 5.
MARTINEZ, J., MALIREDDI, R. K., LU, Q., CUNHA, L. D., PELLETIER, S., GINGRAS, S., ORCHARD, R., GUAN, J. L., TAN, H., PENG, J., KANNEGANTI, T. D., VIRGIN, H. W. & GREEN, D. R. 2015. Molecular characterization of LC3-associated phagocytosis reveals distinct roles for Rubicon, NOX2 and autophagy proteins. *Nat Cell Biol,* 17**,** 893-906.
MAZON MOYA, M. J., COLUCCI-GUYON, E. & MOSTOWY, S. 2014. Use of *Shigella flexneri* to study autophagy-cytoskeleton interactions. *J Vis Exp***,** e51601.
MCCONVILLE, M. 2014. Open questions: microbes, metabolism and host-pathogen interactions. *BMC Biology,* 12**,** 1-2.
MEARS, J. A., LACKNER, L. L., FANG, S., INGERMAN, E., NUNNARI, J. & HINSHAW, J. E. 2011. Conformational changes in Dnm1 support a contractile mechanism for mitochondrial fission. *Nature structural & molecular biology,* 18**,** 20-26.
MEEUSEN, S., DEVAY, R., BLOCK, J., CASSIDY-STONE, A., WAYSON, S., MCCAFFERY, J. M. & NUNNARI, J. 2006. Mitochondrial inner-membrane fusion and crista maintenance requires the dynamin-related GTPase Mgm1. *Cell,* 127**,** 383-395.
MELLACHERUVU, D., WRIGHT, Z., COUZENS, A. L., LAMBERT, J.-P. P., ST-DENIS, N. A., LI, T., MITEVA, Y. V., HAURI, S., SARDIU, M. E., LOW, T. Y., HALIM, V. A., BAGSHAW, R. D., HUBNER, N. C., AL-HAKIM, A., BOUCHARD, A., FAUBERT, D., FERMIN, D., DUNHAM, W. H., GOUDREAULT, M., LIN, Z.-Y. Y., BADILLO, B. G., PAWSON, T.,

DUROCHER, D., COULOMBE, B., AEBERSOLD, R., SUPERTI-FURGA, G., COLINGE, J., HECK, A. J., CHOI, H., GSTAIGER, M., MOHAMMED, S., CRISTEA, I. M., BENNETT, K. L., WASHBURN, M. P., RAUGHT, B., EWING, R. M., GINGRAS, A.-C. C. & NESVIZHSKII, A. I. 2013. The CRAPome: a contaminant repository for affinity purification-mass spectrometry data. *Nature methods,* 10**,** 730-736.

MENDES PINTO, I., RUBINSTEIN, B., KUCHARAVY, A., UNRUH, JAY R. & LI, R. 2012. Actin Depolymerization Drives Actomyosin Ring Contraction during Budding Yeast Cytokinesis. *Developmental Cell,* 22**,** 1247-1260.

MESQUITA, F., THOMAS, M., SACHSE, M., SANTOS, A., FIGUEIRA, R. & HOLDEN, D. 2012. The Salmonella deubiquitinase SseL inhibits selective autophagy of cytosolic aggregates. *PLoS pathogens,* 8.

MESTRE, M. B., FADER, C. M., SOLA, C. & COLOMBO, M. I. 2010. Alpha-hemolysin is required for the activation of the autophagic pathway in Staphylococcus aureus-infected cells. *Autophagy,* 6**,** 110-25.

MEYER-MORSE, N., ROBBINS, J. R., RAE, C. S., MOCHEGOVA, S. N., SWANSON, M. S., ZHAO, Z., VIRGIN, H. W. & PORTNOY, D. 2010. Listeriolysin O is necessary and sufficient to induce autophagy during Listeria monocytogenes infection. *PLoS One,* 5**,** e8610.

MILLER, W. L. 2013. Steroid hormone synthesis in mitochondria. *Mol Cell Endocrinol,* 379**,** 62-73.

MISHRA, P. & CHAN, D. C. 2014. Mitochondrial dynamics and inheritance during cell division, development and disease. *Nature Reviews Molecular Cell Biology,* 15**,** 634-646.

MIZUSHIMA, N. & KOMATSU, M. 2011. Autophagy: Renovation of Cells and Tissues. *Cell,* 147**,** 728-741.

MIZUSHIMA, N., KUMA, A., KOBAYASHI, Y., YAMAMOTO, A., MATSUBAE, M., TAKAO, T., NATSUME, T., OHSUMI, Y. & YOSHIMORI, T. 2003. Mouse Apg16L, a novel WD-repeat protein, targets to the autophagic isolation membrane with the Apg12-Apg5 conjugate. *J Cell Sci,* 116**,** 1679-88.

MIZUSHIMA, N., LEVINE, B., CUERVO, A. M. & KLIONSKY, D. J. 2008. Autophagy fights disease through cellular self-digestion. *Nature,* 451**,** 1069-75.

MIZUSHIMA, N., YAMAMOTO, A., HATANO, M., KOBAYASHI, Y., KABEYA, Y., SUZUKI, K., TOKUHISA, T., OHSUMI, Y. & YOSHIMORI, T. 2001. Dissection of autophagosome formation using Apg5-deficient mouse embryonic stem cells. *J Cell Biol,* 152**,** 657-68.

MIZUSHIMA, N., YOSHIMORI, T. & LEVINE, B. 2010. Methods in mammalian autophagy research. *Cell,* 140**,** 313-26.

MIZUSHIMA, N., YOSHIMORI, T. & OHSUMI, Y. 2011. The role of Atg proteins in autophagosome formation. *Annual review of cell and developmental biology,* 27**,** 107-132.

MOOREN, O. L., GALLETTA, B. J. & COOPER, J. A. 2012. Roles for actin assembly in endocytosis. *Annu Rev Biochem,* 81**,** 661-86.

MOREAU, K., RAVIKUMAR, B., RENNA, M., PURI, C. & RUBINSZTEIN, D. 2011. Autophagosome precursor maturation requires homotypic fusion. *Cell,* 146**,** 303-317.
MOREAU, K., RENNA, M. & RUBINSZTEIN, D. 2013. Connections between SNAREs and autophagy. *Trends in biochemical sciences,* 38**,** 57-63.
MORIMOTO, D., WALINDA, E., FUKADA, H., SOU, Y. S., KAGEYAMA, S., HOSHINO, M., FUJII, T., TSUCHIYA, H., SAEKI, Y., ARITA, K., ARIYOSHI, M., TOCHIO, H., IWAI, K., NAMBA, K., KOMATSU, M., TANAKA, K. & SHIRAKAWA, M. 2015. The unexpected role of polyubiquitin chains in the formation of fibrillar aggregates. *Nat Commun,* 6**,** 6116.
MOSTOWY, S. 2013. Autophagy and bacterial clearance: a not so clear picture. *Cellular microbiology,* 15**,** 395-402.
MOSTOWY, S. 2014. Multiple roles of the cytoskeleton in bacterial autophagy. *PLoS Pathog,* 10**,** e1004409.
MOSTOWY, S., BONAZZI, M., HAMON, M. A., THAM, T. N., MALLET, A., LELEK, M., GOUIN, E., DEMANGEL, C., BROSCH, R., ZIMMER, C., SARTORI, A., KINOSHITA, M., LECUIT, M. & COSSART, P. 2010. Entrapment of intracytosolic bacteria by septin cage-like structures. *Cell Host Microbe,* 8**,** 433-444.
MOSTOWY, S., BOUCONTET, L., MAZON MOYA, M. J., SIRIANNI, A., BOUDINOT, P., HOLLINSHEAD, M., COSSART, P., HERBOMEL, P., LEVRAUD, J.-P. & COLUCCI-GUYON, E. 2013. The zebrafish as a new model for the *in vivo* study of *Shigella flexneri* interaction with phagocytes and bacterial autophagy. *PLoS Pathog,* 9**,** e1003588.
MOSTOWY, S. & COSSART, P. 2009. Cytoskeleton rearrangements during Listeria infection: clathrin and septins as new players in the game. *Cell motility and the cytoskeleton*.
MOSTOWY, S. & COSSART, P. 2011a. Autophagy and the cytoskeleton: new links revealed by intracellular pathogens. *Autophagy,* 7**,** 780-2.
MOSTOWY, S. & COSSART, P. 2011b. Septins as key regulators of actin based processes in bacterial infection. *Biol Chem,* 392**,** 831-5.
MOSTOWY, S. & COSSART, P. 2012a. Bacterial autophagy: restriction or promotion of bacterial replication? *Trends in Cell Biology,* 22**,** 283-291.
MOSTOWY, S. & COSSART, P. 2012b. Septins: the fourth component of the cytoskeleton. *Nat Rev Mol Cell Biol,* 13**,** 183-94.
MOSTOWY, S., DANCKAERT, A., THAM, T., MACHU, C., GUADAGNINI, S., PIZARRO-CERDÁ, J. & COSSART, P. 2009a. Septin 11 restricts InlB-mediated invasion by Listeria. *Journal of Biological Chemistry,* 284**,** 11613-11621.
MOSTOWY, S., JANEL, S., FORESTIER, C., RODUIT, C., KASAS, S., PIZARRO-CERDÁ, J., COSSART, P. & LAFONT, F. 2011a. A role for septins in the interaction between the Listeria monocytogenes INVASION PROTEIN InlB and the Met receptor. *Biophysical journal,* 100**,** 1949-1959.

MOSTOWY, S., NAM THAM, T., DANCKAERT, A., GUADAGNINI, S., BOISSON-DUPUIS, S., PIZARRO-CERDÁ, J. & COSSART, P. 2009b. Septins regulate bacterial entry into host cells. *PloS one,* 4.
MOSTOWY, S., SANCHO-SHIMIZU, V., HAMON, M. A., SIMEONE, R., BROSCH, R., JOHANSEN, T. & COSSART, P. 2011b. p62 and NDP52 Proteins Target Intracytosolic Shigella and Listeria to Different Autophagy Pathways. *Journal of Biological Chemistry,* 286**,** 26987-26995.
MOSTOWY, S. & SHENOY, A. R. 2015. The cytoskeleton in cell-autonomous immunity: structural determinants of host defence. *Nature reviews. Immunology,* 15**,** 559-573.
MURLEY, A., LACKNER, L. L., OSMAN, C., WEST, M., VOELTZ, G. K., WALTER, P. & NUNNARI, J. 2013. ER-associated mitochondrial division links the distribution of mitochondria and mitochondrial DNA in yeast. *Elife,* 2**,** e00422.
NISHIHAMA, R., ONISHI, M. & PRINGLE, J. R. 2011. New insights into the phylogenetic distribution and evolutionary origins of the septins. *Biological chemistry*.
NIU, H., XIONG, Q., YAMAMOTO, A., HAYASHI-NISHINO, M. & RIKIHISA, Y. 2012. Autophagosomes induced by a bacterial Beclin 1 binding protein facilitate obligatory intracellular infection. *Proceedings of the National Academy of Sciences of the United States of America,* 109**,** 20800-20807.
NUNNARI, J. & SUOMALAINEN, A. 2012. Mitochondria: in sickness and in health. *Cell,* 148**,** 1145-1159.
OGAWA, M., YOSHIKAWA, Y., KOBAYASHI, T., MIMURO, H., FUKUMATSU, M., KIGA, K., PIAO, Z., ASHIDA, H., YOSHIDA, M., KAKUTA, S., KOYAMA, T., GOTO, Y., NAGATAKE, T., NAGAI, S., KIYONO, H., KAWALEC, M., REICHHART, J.-M. M. & SASAKAWA, C. 2011. A Tecpr1-dependent selective autophagy pathway targets bacterial pathogens. *Cell host & microbe,* 9**,** 376-389.
OGAWA, M., YOSHIMORI, T., SUZUKI, T., SAGARA, H., MIZUSHIMA, N. & SASAKAWA, C. 2005. Escape of intracellular Shigella from autophagy. *Science,* 307**,** 727-31.
OHSUMI, Y. 2001. Molecular dissection of autophagy: two ubiquitin-like systems. *Nat Rev Mol Cell Biol,* 2**,** 211-6.
ORSI, A., POLSON, H. E. & TOOZE, S. A. 2010. Membrane trafficking events that partake in autophagy. *Curr Opin Cell Biol,* 22**,** 150-6.
PALIKARAS, K., LIONAKI, E. & TAVERNARAKIS, N. 2015. Interfacing mitochondrial biogenesis and elimination to enhance host pathogen defense and longevity. *Worm,* 4**,** e1071763.
PAN, F., MALMBERG, R. L. & MOMANY, M. 2007. Analysis of septins across kingdoms reveals orthology and new motifs. *BMC evolutionary biology,* 7**,** 103.
PATZIG, J., ERWIG, M. S., TENZER, S., KUSCH, K., DIBAJ, P., MOBIUS, W., GOEBBELS, S., SCHAEREN-WIEMERS, N., NAVE, K. A. & WERNER, H. B. 2016. Septin/anillin filaments scaffold central nervous system myelin to accelerate nerve conduction. *Elife,* 5.

PELLEGRINI, L., WETZEL, A., GRANNO, S., HEATON, G. & HARVEY, K. 2016. Back to the tubule: microtubule dynamics in Parkinson's disease. *Cell Mol Life Sci*.
PERRIN, A. J., JIANG, X., BIRMINGHAM, C. L., SO, N. S. Y. & BRUMELL, J. H. 2004. Recognition of bacteria in the cytosol of mammalian cells by the ubiquitin system. *Curr Biol,* 14**,** 806-811.
PESEK, J. J., MATYSKA, M. T., FISCHER, S. M. & SANA, T. R. 2008. Analysis of hydrophilic metabolites by high-performance liquid chromatography-mass spectrometry using a silica hydride-based stationary phase. *J Chromatogr A,* 1204**,** 48-55.
PHALIPON, A. & SANSONETTI, P. J. 2007. Shigella's ways of manipulating the host intestinal innate and adaptive immune system: a tool box for survival? *Immunol Cell Biol,* 85**,** 119-29.
PHAN, Q. T., ENG, D. K., MOSTOWY, S., PARK, H., COSSART, P. & FILLER, S. G. 2013. Role of endothelial cell septin 7 in the endocytosis of Candida albicans. *MBio,* 4**,** e00542-13.
PHILPOTT, D. J., SORBARA, M. T., ROBERTSON, S. J., CROITORU, K. & GIRARDIN, S. E. 2014. NOD proteins: regulators of inflammation in health and disease. *Nat Rev Immunol,* 14**,** 9-23.
PIEPER, R., FISHER, C. R., SUH, M.-J. J., HUANG, S. T. T., PARMAR, P. & PAYNE, S. M. 2013. Analysis of the proteome of intracellular Shigella flexneri reveals pathways important for intracellular growth. *Infection and immunity,* 81**,** 4635-4648.
PILLI, M., ARKO-MENSAH, J., PONPUAK, M., ROBERTS, E., MASTER, S., MANDELL, M. A., DUPONT, N., ORNATOWSKI, W., JIANG, S., BRADFUTE, S. B., BRUUN, J. A., HANSEN, T. E., JOHANSEN, T. & DERETIC, V. 2012. TBK-1 promotes autophagy-mediated antimicrobial defense by controlling autophagosome maturation. *Immunity,* 37**,** 223-234.
PISTOR, S., CHAKRABORTY, T., NIEBUHR, K., DOMANN, E. & WEHLAND, J. 1994. The ActA protein of Listeria monocytogenes acts as a nucleator inducing reorganization of the actin cytoskeleton. *The EMBO journal,* 13**,** 758-763.
PIZARRO-CERDA, J., CHARBIT, A., ENNINGA, J., LAFONT, F. & COSSART, P. 2016. Manipulation of host membranes by the bacterial pathogens Listeria, Francisella, Shigella and Yersinia. *Semin Cell Dev Biol*.
PIZARRO-CERDÁ, J., LECUIT, M. & COSSART, P. 2002. 8 Measuring and analysing invasion of mammalian cells by bacterial pathogens: The Listeria monocytogenes system. *Methods in Microbiology.* Academic Press.
POLLARD, T. D. 2010. Mechanics of cytokinesis in eukaryotes. *Current opinion in cell biology,* 22**,** 50-56.
POLLARD, T. D. & COOPER, J. A. 2009. Actin, a central player in cell shape and movement. *Science,* 326**,** 1208-12.
POLSON, H. E., DE LARTIGUE, J., RIGDEN, D. J., REEDIJK, M., URBE, S., CLAGUE, M. J. & TOOZE, S. A. 2010. Mammalian Atg18 (WIPI2)

localizes to omegasome-anchored phagophores and positively regulates LC3 lipidation. *Autophagy,* 6**,** 506-22.
POPP, J., NOSTER, J., BUSCH, K., KEHL, A., ZUR HELLEN, G. & HENSEL, M. 2015. Role of Host Cell-Derived Amino Acids in Nutrition of Intracellular Salmonella enterica. *Infection and Immunity,* 83**,** 4466-4475.
PRAEFCKE, G. J. K. & MCMAHON, H. T. 2004. The dynamin superfamily: universal membrane tubulation and fission molecules? *Nat Rev Mol Cell Biol,* 5**,** 133-147.
PRENTICE, A. M., GHATTAS, H. & COX, S. E. 2007. Host-Pathogen Interactions: Can Micronutrients Tip the Balance? *The Journal of Nutrition,* 137**,** 1334-1337.
PROCTOR, S. A., MINC, N., BOUDAOUD, A. & CHANG, F. 2012. Contributions of turgor pressure, the contractile ring, and septum assembly to forces in cytokinesis in fission yeast. *Current biology : CB,* 22**,** 1601-1608.
PRUNEDA, J. N., DURKIN, C. H., GEURINK, P. P., OVAA, H., SANTHANAM, B., HOLDEN, D. W. & KOMANDER, D. 2016. The Molecular Basis for Ubiquitin and Ubiquitin-like Specificities in Bacterial Effector Proteases. *Mol Cell,* 63**,** 261-76.
RADHAKRISHNAN, G. K. & SPLITTER, G. A. 2012. Modulation of host microtubule dynamics by pathogenic bacteria. *Biomol Concepts,* 3**,** 571-580.
RAMBOLD, A. S., KOSTELECKY, B., ELIA, N. & LIPPINCOTT-SCHWARTZ, J. 2011. Tubular network formation protects mitochondria from autophagosomal degradation during nutrient starvation. *Proc Natl Acad Sci USA,* 108**,** 10190-10195.
RANDOW, F. 2011. How cells deploy ubiquitin and autophagy to defend their cytosol from bacterial invasion. *Autophagy,* 7**,** 304-9.
RANDOW, F., MACMICKING, J. D. & JAMES, L. C. 2013. Cellular self-defense: how cell-autonomous immunity protects against pathogens. *Science,* 340**,** 701-706.
RANDOW, F. & MÜNZ, C. 2012. Autophagy in the regulation of pathogen replication and adaptive immunity. *Trends in immunology,* 33**,** 475-487.
RANDOW, F. & YOULE, RICHARD J. 2014. Self and nonself: how autophagy targets mitochondria and bacteria. *Cell Host Microbe,* 15**,** 403-411.
RAVIKUMAR, B., MOREAU, K., JAHREISS, L., PURI, C. & RUBINSZTEIN, D. C. 2010. Plasma membrane contributes to the formation of pre-autophagosomal structures. *Nature cell biology,* 12**,** 747-757.
RAVIKUMAR, B., VACHER, C., BERGER, Z., DAVIES, J. E., LUO, S., OROZ, L. G., SCARAVILLI, F., EASTON, D. F., DUDEN, R., O'KANE, C. J. & RUBINSZTEIN, D. C. 2004. Inhibition of mTOR induces autophagy and reduces toxicity of polyglutamine expansions in fly and mouse models of Huntington disease. *Nat Genet,* 36**,** 585-95.

RAY, K., MARTEYN, B., SANSONETTI, P. J. & TANG, C. M. 2009. Life on the inside: the intracellular lifestyle of cytosolic bacteria. *Nat Rev Microbiol,* 7**,** 333-40.
RENSHAW, M. J., LIU, J., LAVOIE, B. D. & WILDE, A. 2014. Anillin-dependent organization of septin filaments promotes intercellular bridge elongation and Chmp4B targeting to the abscission site. *Open biology,* 4**,** 130190.
RUBINSZTEIN, D. C., MARIÑO, G. & KROEMER, G. 2011. Autophagy and aging. *Cell,* 146**,** 682-695.
SAIER, M. H., JR., WENTZEL, D. L., FEUCHT, B. U. & JUDICE, J. J. 1975. A transport system for phosphoenolpyruvate, 2-phosphoglycerate, and 3-phosphoglycerate in Salmonella typhimurium. *J Biol Chem,* 250**,** 5089-96.
SAINT-GEORGES-CHAUMET, Y. & EDEAS, M. 2016. Microbiota-mitochondria inter-talk: consequence for microbiota-host interaction. *Pathog Dis,* 74**,** ftv096.
SANCAK, Y., BAR-PELED, L., ZONCU, R., MARKHARD, A. L., NADA, S. & SABATINI, D. M. 2010. Ragulator-Rag complex targets mTORC1 to the lysosomal surface and is necessary for its activation by amino acids. *Cell,* 141**,** 290-303.
SANCAK, Y., PETERSON, T. R., SHAUL, Y. D., LINDQUIST, R. A., THOREEN, C. C., BAR-PELED, L. & SABATINI, D. M. 2008. The Rag GTPases bind raptor and mediate amino acid signaling to mTORC1. *Science,* 320**,** 1496-501.
SANJUAN, M. A., DILLON, C. P., TAIT, S. W., MOSHIACH, S., DORSEY, F., CONNELL, S., KOMATSU, M., TANAKA, K., CLEVELAND, J. L., WITHOFF, S. & GREEN, D. R. 2007. Toll-like receptor signalling in macrophages links the autophagy pathway to phagocytosis. *Nature,* 450**,** 1253-7.
SANSONETTI, P. J. 2006. Rupture, invasion and inflammatory destruction of the intestinal barrier by Shigella: the yin and yang of innate immunity. *Can J Infect Dis Med Microbiol,* 17**,** 117-9.
SCHINDELIN, J., ARGANDA-CARRERAS, I., FRISE, E., KAYNIG, V., LONGAIR, M., PIETZSCH, T., PREIBISCH, S., RUEDEN, C., SAALFELD, S., SCHMID, B., TINEVEZ, J. Y., WHITE, D. J., HARTENSTEIN, V., ELICEIRI, K., TOMANCAK, P. & CARDONA, A. 2012. Fiji: an open-source platform for biological-image analysis. *Nat Methods,* 9**,** 676-82.
SCHLOSSER-SILVERMAN, E., ELGRABLY-WEISS, M., ROSENSHINE, I., KOHEN, R. & ALTUVIA, S. 2000. Characterization of Escherichia coli DNA lesions generated within J774 macrophages. *Journal of bacteriology,* 182**,** 5225-5230.
SELLIN, M., SANDBLAD, L., STENMARK, S. & GULLBERG, M. 2011. Deciphering the rules governing assembly order of mammalian septin complexes. *Molecular biology of the cell,* 22**,** 3152-3164.
SHAHNAZARI, S., YEN, W.-L., BIRMINGHAM, C. L., SHIU, J., NAMOLOVAN, A., ZHENG, Y. T., NAKAYAMA, K., KLIONSKY, D. J. & BRUMELL, J. H.

2010. A diacylglycerol-dependent signaling pathway contributes to regulation of antibacterial autophagy. *Cell Host Microbe,* 8**,** 137-146.
SHCHEPROVA, Z., BALDI, S., FREI, S. B., GONNET, G. & BARRAL, Y. 2008. A mechanism for asymmetric segregation of age during yeast budding. *Nature,* 454**,** 728-734.
SIRAJUDDIN, M., FARKASOVSKY, M., HAUER, F., KÜHLMANN, D., MACARA, I. G., WEYAND, M., STARK, H. & WITTINGHOFER, A. 2007. Structural insight into filament formation by mammalian septins. *Nature,* 449**,** 311-315.
SIRAJUDDIN, M., FARKASOVSKY, M., ZENT, E. & WITTINGHOFER, A. 2009. GTP-induced conformational changes in septins and implications for function. *Proceedings of the National Academy of Sciences,* 106**,** 16592-16597.
SIRIANNI, A., KROKOWSKI, S., LOBATO-MARQUEZ, D., BURANYI, S., PFANZELTER, J., GALEA, D., WILLIS, A., CULLEY, S., HENRIQUES, R., LARROUY-MAUMUS, G., HOLLINSHEAD, M., SANCHO-SHIMIZU, V., WAY, M. & MOSTOWY, S. 2016. Mitochondria mediate septin cage assembly to promote autophagy of Shigella. *EMBO Rep*.
SIRIANNI, A. & MOSTOWY, S. 2014. Autophagy in the Infected Cell: Insights from Pathogenic Bacteria. *Autophagy, Infection, and the Immune Response.* John Wiley & Sons, Inc.
SKAU, C. T. & WATERMAN, C. M. 2015. Specification of Architecture and Function of Actin Structures by Actin Nucleation Factors. *Annu Rev Biophys,* 44**,** 285-310.
SMIRNOVA, E., GRIPARIC, L., SHURLAND, D. L. & VAN DER BLIEK, A. M. 2001. Dynamin-related protein Drp1 is required for mitochondrial division in mammalian cells. *Molecular biology of the cell,* 12**,** 2245-2256.
SONG, Z., GHOCHANI, M., MCCAFFERY, J. M., FREY, T. G. & CHAN, D. C. 2009. Mitofusins and OPA1 mediate sequential steps in mitochondrial membrane fusion. *Molecular biology of the cell,* 20**,** 3525-3532.
SORBARA, M. T., ELLISON, L. K., RAMJEET, M., TRAVASSOS, L. H., JONES, N. L., GIRARDIN, S. E. & PHILPOTT, D. J. 2013. The protein ATG16L1 suppresses inflammatory cytokines induced by the intracellular sensors Nod1 and Nod2 in an autophagy-independent manner. *Immunity,* 39**,** 858-73.
SPILIOTIS, E. T., KINOSHITA, M. & NELSON, W. J. 2005. A mitotic septin scaffold required for Mammalian chromosome congression and segregation. *Science,* 307**,** 1781-5.
STARR, T., CHILD, R., WEHRLY, T. D., HANSEN, B., HWANG, S., LOPEZ-OTIN, C., VIRGIN, H. W. & CELLI, J. 2012. Selective subversion of autophagy complexes facilitates completion of the Brucella intracellular cycle. *Cell Host Microbe,* 11**,** 33-45.
STAVRU, F., BOUILLAUD, F., SARTORI, A., RICQUIER, D. & COSSART, P. 2011. Listeria monocytogenes transiently alters mitochondrial dynamics during infection. *Proc Natl Acad Sci U S A,* 108**,** 3612-7.

STEEB, B., CLAUDI, B., BURTON, N. A., TIENZ, P., SCHMIDT, A., FARHAN, H., MAZÈ, A. & BUMANN, D. 2013. Parallel Exploitation of Diverse Host Nutrients Enhances <italic>Salmonella</italic> Virulence. *PLoS Pathog,* 9**,** e1003301.

STEELE, S., BRUNTON, J. & KAWULA, T. 2015. The role of autophagy in intracellular pathogen nutrient acquisition. *Frontiers in Cellular and Infection Microbiology,* 5**,** 51.

STEELE, S., BRUNTON, J., ZIEHR, B., TAFT-BENZ, S., MOORMAN, N. & KAWULA, T. 2013. Francisella tularensis Harvests Nutrients Derived via ATG5-Independent Autophagy to Support Intracellular Growth. *PLoS Pathogens,* 9**,** e1003562.

STEHLING, O., WILBRECHT, C. & LILL, R. 2014. Mitochondrial iron-sulfur protein biogenesis and human disease. *Biochimie,* 100**,** 61-77.

SUZUKI, T., FRANCHI, L., TOMA, C., ASHIDA, H., OGAWA, M., YOSHIKAWA, Y., MIMURO, H., INOHARA, N., SASAKAWA, C. & NUÑEZ, G. 2007. Differential regulation of caspase-1 activation, pyroptosis, and autophagy via Ipaf and ASC in Shigella-infected macrophages. *PLoS pathogens,* 3.

TAKÁTS, S., PIRCS, K., NAGY, P., VARGA, Á., KÁRPÁTI, M., HEGEDŰS, K., KRAMER, H., KOVÁCS, A. L., SASS, M. & JUHÁSZ, G. 2014. Interaction of the HOPS complex with Syntaxin 17 mediates autophagosome clearance in Drosophila. *Molecular biology of the cell,* 25**,** 1338-1354.

TANAKA K, W. M., COATES PJ, FARTHING MJ, WALKER-SMITH JA, TABAQCHALI S. 1991. Mycobacterium paratuberculosis and Crohn's disease. *Gut* 32: 43-45.

TANAKA-TAKIGUCHI, Y., KINOSHITA, M. & TAKIGUCHI, K. 2009. Septin-mediated uniform bracing of phospholipid membranes. *Curr Biol,* 19**,** 140-145.

TATTOLI, I., SORBARA, M. T., VUCKOVIC, D., LING, A., SOARES, F., CARNEIRO, L. A., YANG, C., EMILI, A., PHILPOTT, D. J. & GIRARDIN, S. E. 2012. Amino acid starvation induced by invasive bacterial pathogens triggers an innate host defense program. *Cell host & microbe,* 11**,** 563-575.

THURSTON, T., WANDEL, M., VON MUHLINEN, N., FOEGLEIN, A. & RANDOW, F. 2012. Galectin 8 targets damaged vesicles for autophagy to defend cells against bacterial invasion. *Nature,* 482**,** 414-418.

THURSTON, T. L., BOYLE, K. B., ALLEN, M., RAVENHILL, B. J., KARPIYEVICH, M., BLOOR, S., KAUL, A., NOAD, J., FOEGLEIN, A., MATTHEWS, S. A., KOMANDER, D., BYCROFT, M. & RANDOW, F. 2016. Recruitment of TBK1 to cytosol-invading Salmonella induces WIPI2-dependent antibacterial autophagy. *EMBO J*.

THURSTON, T. L. M., RYZHAKOV, G. & BLOOR, S. 2009. The TBK1 adaptor and autophagy receptor NDP52 restricts the proliferation of ubiquitin-coated bacteria. *Nature ….*

TOOLEY, A., GILDEN, J., JACOBELLI, J., BEEMILLER, P., TRIMBLE, W., KINOSHITA, M. & KRUMMEL, M. 2009. Amoeboid T lymphocytes require the septin cytoskeleton for cortical integrity and persistent motility. *Nature cell biology,* 11**,** 17-26.

TOOZE, S. A. & YOSHIMORI, T. 2010. The origin of the autophagosomal membrane. *Nat Cell Biol,* 12**,** 831-5.

TRAVASSOS, L. H., CARNEIRO, L. A., RAMJEET, M., HUSSEY, S., KIM, Y. G., MAGALHAES, J. G., YUAN, L., SOARES, F., CHEA, E., LE BOURHIS, L., BONECA, I. G., ALLAOUI, A., JONES, N. L., NUNEZ, G., GIRARDIN, S. E. & PHILPOTT, D. J. 2010. Nod1 and Nod2 direct autophagy by recruiting ATG16L1 to the plasma membrane at the site of bacterial entry. *Nat Immunol,* 11**,** 55-62.

VALDIVIA, R. H., HROMOCKYJ, A. E., MONACK, D., RAMAKRISHNAN, L. & FALKOW, S. 1996. Applications for green fluorescent protein (GFP) in the study of host-pathogen interactions. *Gene,* 173**,** 47-52.

VAN TROYS, M., LAMBRECHTS, A., DAVID, V., DEMOL, H., PUYPE, M., PIZARRO-CERDA, J., GEVAERT, K., COSSART, P. & VANDEKERCKHOVE, J. 2008. The actin propulsive machinery: the proteome of Listeria monocytogenes tails. *Biochem Biophys Res Commun,* 375**,** 194-9.

VOLCEANOV, L., HERBST, K., BINIOSSEK, M., SCHILLING, O., HALLER, D., NOLKE, T., SUBBARAYAL, P., RUDEL, T., ZIEGER, B. & HACKER, G. 2014. Septins arrange F-actin-containing fibers on the Chlamydia trachomatis inclusion and are required for normal release of the inclusion by extrusion. *MBio,* 5**,** e01802-14.

VON MUHLINEN, N., AKUTSU, M., RAVENHILL, B. J., FOEGLEIN, Á., BLOOR, S., RUTHERFORD, T. J., FREUND, S. M., KOMANDER, D. & RANDOW, F. 2012. LC3C, bound selectively by a noncanonical LIR motif in NDP52, is required for antibacterial autophagy. *Molecular cell,* 48**,** 329-342.

WAI, T. & LANGER, T. 2016. Mitochondrial Dynamics and Metabolic Regulation. *Trends Endocrinol Metab,* 27**,** 105-17.

WALKER, M. A., VOLPI, S., SIMS, K. B., WALTER, J. E. & TRAGGIAI, E. 2014. Powering the immune system: mitochondria in immune function and deficiency. *J Immunol Res,* 2014**,** 164309.

WANG, R., WEI, Y., AN, Z., ZOU, Z., XIAO, G., BHAGAT, G., WHITE, M., REICHELT, J. & LEVINE, B. 2012. Akt-mediated regulation of autophagy and tumorigenesis through Beclin 1 phosphorylation. *Science (New York, N.Y.),* 338**,** 956-959.

WANG, Y., WEISS, L. M. & ORLOFSKY, A. 2009. Host Cell Autophagy Is Induced by Toxoplasma gondii and Contributes to Parasite Growth. *The Journal of Biological Chemistry,* 284**,** 1694-1701.

WEI, Y. & MURPHY, E. R. 2016. Shigella Iron Acquisition Systems and their Regulation. *Frontiers in cellular and infection microbiology,* 6**,** 18.

WEK, R. C., JIANG, H. Y. & ANTHONY, T. G. 2006. Coping with stress: eIF2 kinases and translational control. *Biochem Soc Trans,* 34**,** 7-11.

WELCH, M. D. & WAY, M. 2013. Arp2/3-mediated actin-based motility: a tail of pathogen abuse. *Cell Host Microbe,* 14**,** 242-255.
WEN, X. & KLIONSKY, D. J. 2016. An overview of macroautophagy in yeast. *Journal of molecular biology*.
WILD, P., FARHAN, H., MCEWAN, D. G. & WAGNER, S. 2011. Phosphorylation of the autophagy receptor optineurin restricts Salmonella growth. ….
WILLINGHAM, S. B., BERGSTRALH, D. T., O'CONNOR, W., MORRISON, A. C., TAXMAN, D. J., DUNCAN, J. A., BARNOY, S., VENKATESAN, M. M., FLAVELL, R. A., DESHMUKH, M., HOFFMAN, H. M. & TING, J. P. 2007. Microbial pathogen-induced necrotic cell death mediated by the inflammasome components CIAS1/cryopyrin/NLRP3 and ASC. *Cell host & microbe,* 2**,** 147-159.
WONG, P. M., FENG, Y., WANG, J., SHI, R. & JIANG, X. 2015. Regulation of autophagy by coordinated action of mTORC1 and protein phosphatase 2A. *Nat Commun,* 6**,** 8048.
XIE, Y., KANG, R., SUN, X., ZHONG, M., HUANG, J., KLIONSKY, D. J. & TANG, D. 2015. Posttranslational modification of autophagy-related proteins in macroautophagy. *Autophagy,* 11**,** 28-45.
YANG, Z. & KLIONSKY, D. 2010. Eaten alive: a history of macroautophagy. *Nature cell biology,* 12**,** 814-822.
YANO, T., MITA, S., OHMORI, H., OSHIMA, Y., FUJIMOTO, Y., UEDA, R., TAKADA, H., GOLDMAN, W. E., FUKASE, K., SILVERMAN, N., YOSHIMORI, T. & KURATA, S. 2008. Autophagic control of listeria through intracellular innate immune recognition in drosophila. *Nat Immunol,* 9**,** 908-16.
YOSHIKAWA, Y., OGAWA, M., HAIN, T., YOSHIDA, M., FUKUMATSU, M., KIM, M., MIMURO, H., NAKAGAWA, I., YANAGAWA, T., ISHII, T., KAKIZUKA, A., SZTUL, E., CHAKRABORTY, T. & SASAKAWA, C. 2009. Listeria monocytogenes ActA-mediated escape from autophagic recognition. *Nature cell biology,* 11**,** 1233-1240.
YU, H. B., CROXEN, M. A., MARCHIANDO, A. M., FERREIRA, R. B., CADWELL, K., FOSTER, L. J. & FINLAY, B. B. 2014. Autophagy facilitates Salmonella replication in HeLa cells. *mBio,* 5**,** 14.
ZAVODSZKY, E., SEAMAN, M., MOREAU, K., JIMENEZ-SANCHEZ, M., BREUSEGEM, S. Y., HARBOUR, M. E. & RUBINSZTEIN, D. C. 2014. Mutation in VPS35 associated with Parkinson's disease impairs WASH complex association and inhibits autophagy. *Nature Communications,* 5.
ZHENG, Y. T., SHAHNAZARI, S., BRECH, A., LAMARK, T., JOHANSEN, T. & BRUMELL, J. H. 2009. The adaptor protein p62/SQSTM1 targets invading bacteria to the autophagy pathway. *J Immunol,* 183**,** 5909-16.
ZHONG, Y., WANG, Q. J., LI, X., YAN, Y., BACKER, J. M., CHAIT, B. T., HEINTZ, N. & YUE, Z. 2009. Distinct regulation of autophagic activity by Atg14L and Rubicon associated with Beclin 1-phosphatidylinositol-3-kinase complex. *Nat Cell Biol,* 11**,** 468-76.

ZHONG, Z., UMEMURA, A., SANCHEZ-LOPEZ, E., LIANG, S., SHALAPOUR, S., WONG, J., HE, F., BOASSA, D., PERKINS, G., ALI, S. R., MCGEOUGH, M. D., ELLISMAN, M. H., SEKI, E., GUSTAFSSON, A. B., HOFFMAN, H. M., DIAZ-MECO, M. T., MOSCAT, J. & KARIN, M. 2016. NF-kappaB Restricts Inflammasome Activation via Elimination of Damaged Mitochondria. *Cell,* 164**,** 896-910.

ZHU, Z. J., SCHULTZ, A. W., WANG, J., JOHNSON, C. H., YANNONE, S. M., PATTI, G. J. & SIUZDAK, G. 2013. Liquid chromatography quadrupole time-of-flight mass spectrometry characterization of metabolites guided by the METLIN database. *Nat Protoc,* 8**,** 451-60.

APPENDIX

Table A.1: Classification of the human septins

Septin	Septin group
SEPT1	SEPT2
SEPT2	SEPT2
SEPT3	SEPT3
SEPT4	SEPT2
SEPT5	SEPT2
SEPT6	SEPT6
SEPT7	SEPT7
SEPT8	SEPT6
SEPT9	SEPT3
SEPT10	SEPT6
SEPT11	SEPT6
SEPT12	SEPT3
SEPT14	SEPT6

Table A.2: Proteins enriched at the septin cytoskeleton in non-infected cells.

Accession	Score	Mass (Da)	Num. of matches	Description	GO classification
O75881	42	58632	2	25-hydroxycholesterol 7-alpha-hydroxylase (CYP7B1)	Plasma Membrane
P62266	57	15936	2	40S ribosomal protein S23 (RPS23)	Cytoplasmic
P62851	124	13780	2	40S ribosomal protein S25 (RPS25)	Cytoplasmic
Q01813	376	86277	9	6-phosphofructokinase type C (PFKP)	Cytoplasmic
Q01813	73	86454	2	6-phosphofructokinase type C (PFKP)	Cytoplasmic
P08237	115	85818	3	6-phosphofructokinase, muscle type (PFKM)	Cytoplasmic
P05388	91	34390	2	60S acidic ribosomal protein P0(RPLP0)	Cytoplasmic
P62913	183	20424	4	60S ribosomal protein L11 (RPL11)	Cytoplasmic
P40429	84	23608	2	60S ribosomal protein L13a (RPL13A)	Cytoplasmic
P36578	208	47897	4	60S ribosomal protein L4 (GN=RPL4)	Cytoplasmic
P18124	192	29253	2	60S ribosomal protein L7 (RPL7)	Cytoplasmic
P68032	533	42334	13	Actin, alpha cardiac muscle 1 (ACTC1)	Cytoplasmic
P68032	4670	42268	106	Actin, alpha cardiac muscle 1 (ACTC1)	Cytoplasmic
O14561	43	17544	3	Acyl carrier protein (NDUFAB1)	Mitochondrial
Q15109	1717	43052	19	Advanced glycosylation end product-specific receptor (AGER)	Plasma Membrane
P01023	641	164338	13	Alpha-2-macroglobulin (A2M)	Extracellular
P01008	162	52937	2	Antithrombin-III (SERPINC1)	Extracellular
Q9Y2X7	45	84887	2	ARF GTPase-activating protein GIT1 (GIT1)	Cytoplasmic
P17174	199	46402	2	Aspartate aminotransferase (GOT1)	Cytoplasmic
P24539	77	28936	2	ATP synthase F(0) complex subunit B1, mitochondrial (ATP5F1)	Mitochondrial
O75964	187	11421	2	ATP synthase subunit g, mitochondrial (ATP5L)	Mitochondrial
Q5T9A4	149	72987	2	ATPase family AAA domain-containing protein 3B (ATAD3B)	Mitochondrial
Q13410	59	59383	5	Butyrophilin subfamily 1 member A1 (BTN1A1)	Plasma membrane
P62158	183	16827	3	Calmodulin (CALM1)	Cytoplasmic
Q9UMQ6	65	85224	2	Calpain-11 (CAPN11)	Cytoplasmic
Q8NEV1	81	45305	3	Casein kinase II subunit alpha 3 (CSNK2A3)	Cytoplasmic
Q9HC77	91	153872	9	Centromere protein J (CENPJ)	Cytoplasmic
P00450	87	122817	3	Ceruloplasmin (CP)	Extracellular
Q8N0X4	35	37520	3	Citrate lyase subunit beta-like protein (CLYBL)	Mitochondrial
Q00610	324	192918	7	Clathrin heavy chain 1 (CLTC)	Plasma membrane

P53618	143	107994	3	Coatomer subunit beta (COPB1)	Cytoplasmic
A6NGH7	69	38345	2	Coiled-coil domain-containing protein 160 (CCDC160)	Unknown
Q8IWP9	49	30486	8	Coiled-coil domain-containing protein 28A (CCDC28A)	Extracellular
P01024	148	188272	2	Complement C3 (C3)	Extracellular
Q04656	113	164752	6	Copper-transporting ATPase 1 (ATP7A)	Plasma membrane
P52701	82	154160	2	DNA mismatch repair protein Msh6 (MSH6)	Nuclear
P78527	89	472789	3	DNA-dependent protein kinase catalytic subunit (PRKDC)	Cytoplasmic
Q13049	262	73230	4	E3 ubiquitin-protein ligase TRIM32 (TRIM32)	Nuclear
P58107	259	557210	5	Epiplakin (EPPK1)	Cytoplasmic
P05413	115	14895	2	Fatty acid-binding protein (FABP3)	Cytoplasmic
O60547	66	42199	2	GDP-mannose 4,6 dehydratase (GMDS)	Cytoplasmic
O60318	51	220199	4	Germinal-center associated nuclear protein (MCM3AP)	Nuclear
P00390	160	56681	2	Glutathione reductase, mitochondrial (GSR)	Cytoplasmic
Q5JWF2	165	111553	2	Guanine nucleotide-binding protein G(s) subunit alpha isoforms XLas (GNAS)	Cytoplasmic
Q5JWF2	74	111697	2	Guanine nucleotide-binding protein G(s) subunit alpha isoforms XLas (GNAS)	Cytoplasmic
P69905	372	15294	10	Hemoglobin subunit alpha (HBA1)	Cytoplasmic
P0C0S5	98	13545	2	Histone H2A.Z (H2AFZ)	Nuclear
Q5QNW6	135	13912	2	Histone H2B type 2-F (HIST2H2BF)	Nuclear
P01857	256	36497	5	Ig gamma-1 chain C (IGHG1)	Extracellular
P29218	118	30491	2	Inositol monophosphatase 1 (IMPA1)	Cytoplasmic
Q9H293	32	20777	3	Interleukin-25 (IL25)	Extracellular
P48735	309	51245	4	Isocitrate dehydrogenase (IDH2)	Mitochondrial
P51553	129	43089	2	Isocitrate dehydrogenase (IDH3G)	Mitochondrial
O43837	115	42387	3	Isocitrate dehydrogenase subunit beta (IDH3B)	Mitochondrial
Q01650	207	55526	3	Large neutral amino acids transporter small subunit 1 (SLC7A5)	Plasma membrane
O95490	177	165038	3	Latrophilin-2 (LPHN2)	Plasma Membrane
Q9UHB6	348	85541	10	LIM domain and actin-binding protein 1 (LIMA1)	Cytoplasmic
P14174	86	12606	3	Macrophage migration inhibitory factor (MIF)	Extracellular
Q9UBX3	78	31630	2	Mitochondrial dicarboxylate carrier (SLC25A10)	Mitochondrial
P60201	313	30701	8	Myelin proteolipid protein (PLP1)	Plasma Membrane
P35580	124	229640	2	Myosin-10 (MYH)	Cytoplasmic

O75694	157	156388	2	Nuclear pore complex protein Nup155 (NUP155)	Nuclear
Q15645	83	48796	2	Pachytene checkpoint protein 2 homolog (RIP13)	Nuclear
P23284	81	23774	2	Peptidyl-prolyl cis-trans isomerase B (PPIB)	Cytoplasmic
Q13162	96	30705	2	Peroxiredoxin-4 (PRDX4)	Cytoplasmic
Q16822	56	71328	2	Phosphoenolpyruvate carboxykinase (PCK2)	Mitochondrial
Q8TC59	48	110836	3	Piwi-like protein 2 (PIWIL2)	Cytoplasmic
Q9Y446	191	87397	5	Plakophilin-3 (PKP3)	Nuclear
P01127	56	27893	2	Platelet-derived growth factor subunit B (PDGFB)	Extracellular
Q15149	343	533076	10	Plectin (PLEC)	Plasma membrane
P17844	70	69519	2	Probable ATP-dependent RNA helicase DDX5 (DDX5)	Nuclear
P30101	88	57146	2	Protein disulfide-isomerase A3 (PDIA3)	Cytoplasmic
A6NE01	32	262917	2	Protein FAM186A (FAM186A)	Unknown
Q14207	41	155253	2	Protein NPAT (NPAT)	Nuclear
P22061	71	24759	2	Protein-L-isoaspartate(D-aspartate) O-methyltransferase (PCMT1)	Cytoplasmic
P61106	185	24110	3	Ras-related protein Rab-14 (RAB14)	Cytoplasmic
P63208	44	18784	2	S-phase kinase-associated protein 1 (SKP1)	Cytoplasmic
Q9P0V9	769	52927	26	Septin-10 (SEPT10)	Cytoplasmic
Q9NVA2	4459	49597	96	Septin-11 (SEPT11)	Cytoplasmic
Q15019	2927	41645	51	Septin-2 (SEPT2)	Cytoplasmic
Q14141	14417	50007	223	Septin-6 (SEPT6)	Cytoplasmic
Q16181	2259	50878	35	Septin-7 (SEPT7)	Cytoplasmic
Q9UHD8	2835	65591	52	Septin-9 (SEPT9)	Cytoplasmic
Q6S5L8	41	69615	3	SHC-transforming protein 4 (SHC4)	Plasma Membrane
Q9H9B4	146	35826	3	Sideroflexin-1 (SFXN1)	Mitochondrial
P05023	123	113882	3	Sodium/potassium-transporting ATPase subunit alpha-1 (ATP1A1)	Plasma membrane
P19447	41	90019	2	TFIIH basal transcription factor complex helicase XPB subunit (ERCC3)	Nuclear
Q86V81	83	26872	2	THO complex subunit 4 (ALYREF)	Nuclear
P49755	72	25098	2	Transmembrane emp24 domain-containing protein 10 (TMED10)	Cytoplasmic
Q13885	2201	50197	43	Tubulin beta-2A chain (TUBB2A)	Cytoplasmic
P68371	2877	50167	51	Tubulin beta-4B chain (TUBB4B)	Cytoplasmic
Q9HCI6	44	90586	2	Uncharacterized protein KIAA1586 (KIAA1586)	Cytoplasmic

O00159	943	122296	21	Unconventional myosin-Ic (MYO1C)	Cytoplasmic
Q12965	723	127442	15	Unconventional myosin-Ie (MYO1E)	Cytoplasmic
Q9UM54	142	150700	3	Unconventional myosin-VI (MYO6)	Cytoplasmic
Q9P202	48	96711	4	Whirlin (DFNB31)	Cytoplasmic
Q5T200	102	197071	15	Zinc finger CCCH domain-containing protein 13 (ZC3H13)	Nuclear
Q96H79	67	33768	2	Zinc finger CCCH-type antiviral protein 1-like (ZC3HAV1L)	Unknown

Table A.3: Proteins enriched at the *Shigella*-septin cage

Accession	Score	Mass (Da)	Num. of matches	Description	GO classification
O75881	42	58632	2	25-hydroxycholesterol 7-alpha-hydroxylase (CYP7B1)	Plasma Membrane
P08195	86	68180	3	4F2 cell-surface antigen heavy chain (SLC3A2)	Plasma Membrane
O14561	43	17544	3	Acyl carrier protein (NDUFAB1)	Mitochondrial
Q15109	17	43052	19	Advanced glycosylation end product-specific receptor (AGER)	Plasma Membrane
P01023	641	164338	13	Alpha-2-macroglobulin (A2M)	Extracellular
P04083	147	38918	2	Annexin A1 (ANXA1)	Cytoplasmic
P01008	162	52937	2	Antithrombin-III (SERPINC1)	Extracellular
P02647	2112	30759	41	Apolipoprotein A-I (APOA1)	Extracellular
P02652	123	11260	2	Apolipoprotein A-II (APOA2)	Extracellular
P02649	596	36224	7	Apolipoprotein E (APOE)	Extracellular
P17174	199	46402	2	Aspartate aminotransferase (GOT1)	Cytoplasmic
P31327	158	165975	5	Carbamoyl-phosphate synthase (CPS1)	Mitochondrial
Q8N3K9	104	450407	6	Cardiomyopathy-associated protein 5 (CMYA5)	Cytoplasmic
P07339	150	45037	2	Cathepsin D (CTSD)	Mitochondrial
Q9HC77	91	153872	9	Centromere protein J (CENPJ)	Cytoplasmic
Q8N0X4	35	37520	3	Citrate lyase subunit beta-like protein (CLYBL)	Mitochondrial
P10909	79	53031	2	Clusterin (CLU)	Cytoplasmic
Q8IWP9	49	30486	8	Coiled-coil domain-containing protein 28A (CCDC28A)	Extracellular
P00156	61	42781	2	Cytochrome b (MT-CYB)	Mitochondrial
Q08554	226	101406	3	Desmocollin-1 (DSC1)	Plasma Membrane
Q6ZR08	68	359792	3	Dynein heavy chain 12 (DNAH12)	Cytoplasmic
O75822	92	29159	2	Eukaryotic translation initiation factor 3 subunit J (EIF3J)	Cytoplasmic
P05413	115	14895	2	Fatty acid-binding protein (FABP3)	Cytoplasmic
P69905	372	15294	10	Hemoglobin subunit alpha (HBA1)	Cytoplasmic
P51858	84	26886	3	Hepatoma-derived growth factor (HDGF)	Nuclear
P01857	256	36497	5	Ig gamma-1 chain C (IGHG1)	Extracellular
P29218	118	30491	2	Inositol monophosphatase 1 (IMPA1)	Cytoplasmic
Q9H293	32	20777	3	Interleukin-25 (IL25)	Extracellular
P48735	309	51245	4	Isocitrate dehydrogenase (IDH2)	Mitochondrial
P51553	129	43089	2	Isocitrate dehydrogenase (IDH3G)	Mitochondrial

O43837	115	42387	3	Isocitrate dehydrogenase [NAD] subunit beta (IDH3B)	Mitochondrial
Q5VZ66	32	98607	2	Janus kinase and microtubule-interacting protein 3 (JAKMIP3)	Cytoplasmic
O95490	177	165038	3	Latrophilin-2 (LPHN2)	Plasma Membrane
P31025	150	19409	4	Lipocalin-1 (LCN1)	Extracellular
P11310	90	47015	2	Medium-chain specific acyl-CoA dehydrogenase (ACADM)	Mitochondrial
A6NCE7	99	14676	4	Microtubule-associated proteins 1A/1B light chain 3 beta 2 (MAP1LC3B2)	Cytoplasmic
P60201	313	30701	8	Myelin proteolipid protein (PLP1)	Plasma Membrane
P62942	68	11989	2	Peptidyl-prolyl cis-trans isomerase (FKBP1A)	Cytoplasmic
Q16822	56	71328	2	Phosphoenolpyruvate carboxykinase (PCK2)	Mitochondrial
A6NE01	32	262917	2	Protein FAM186A (FAM186A)	Unknown
Q14207	41	155253	2	Protein NPAT (NPAT)	Nuclear
Q9BRJ7	139	23461	2	Protein syndesmos (NUDT16L1)	Cytoplasmic
Q5T4F4	62	46840	3	Protrudin (ZFYVE27)	Plasma Membrane
P52565	143	23250	2	Rho GDP-dissociation inhibitor 1 (ARHGDIA)	Cytoplasmic
Q9NVA2	4459	49597	96	Septin-11 (SEPT11)	Cytoplasmic
Q15019	2927	41645	51	Septin-2 (SEPT2)	Cytoplasmic
Q14141	14417	50007	223	Septin-6 (SEPT6)	Cytoplasmic
Q16181	2259	50878	35	Septin-7 (SEPT7)	Cytoplasmic
Q9UHD8	2835	65591	52	Septin-9 (SEPT9)	Cytoplasmic
Q13501	201	48455	2	Sequestosome-1 (SQSTM1)	Cytoplasmic
P02787	72	78853	2	Serotransferrin (TF)	Extracellular
P0DJI8	141	13570	2	Serum amyloid A-1 protein (SAA1)	Extracellular
Q6S5L8	41	69615	3	SHC-transforming protein 4 (SHC4)	Plasma Membrane
Q9H9B4	146	35826	3	Sideroflexin-1 (SFXN1)	Mitochondrial
Q5T200	102	197071	15	Zinc finger CCCH domain-containing protein 13 (ZC3H13)	Nuclear
P25311	248	34465	6	Zinc-alpha-2-glycoprotein (AZGP1)	Extracellular